THE UNIVERSITY
of EDINBURGH

Gravitational Geomicrobiology: Biofilms and their Mineral Interactions under Terrestrial and Altered Gravity

Natasha Elizabeth Nicholson

Doctor of Philosophy
School of Physics and Astronomy
The University of Edinburgh
July 2018

Lay Summary

Biofilms are communities of bacteria that attach to a surface and work cooperatively to create a microenvironment that benefits all the cells. The cells in a biofilm will express different genes from their single-cell state, and begin to take on different functions within the community in order to benefit the whole. Biofilms have a structure, although the architecture of this structure will vary dependent on the microorganisms involved, the surface upon which attachment takes place, and the environmental conditions around the surface and the microorganisms.

Geomicrobial biofilms are formed by bacteria that attach to a rock or mineral surface, and they can contribute to the weathering of that rock, altering the surface and releasing elements from the mineral matrix. This can have benefits for human interests; bacterial biomining, or bioleaching, is already used on the Earth for extracting copper, gold, and cobalt from raw ores. Biomining could also be adapted for mining asteroids in space, or for acquiring resources in-situ on the moon or Mars, without having to transport them the great distances involved from Earth. Biomining and processing requires less heavy equipment, making it more suitable for launch and space-flight than other methods, it is also more energy efficient and does not require toxic chemicals. The same process of elemental extraction could also be used to provide nutrients for astronauts in life support systems, and similar processes could be of use for creating soil from regolith, and filtering dust from air circulation systems.

Understanding which properties of minerals affect biofilm formation can help inform the scientific community about geomicrobiological interactions and the processes happening on the micron scale. Bacteria have to attach to the surface of the mineral before they can adhere irreversibly to it, and learning which forces and factors are of the most relevance to this process will increase our understanding, and also potentially provide some insights that could help with applications. The work in this thesis indicates that the forces that most strongly influence interactions at that scale with simple surfaces are less relevant with complex and/or living surfaces.

By exposing microorganisms and their biofilms to different gravity conditions, it is possible to gain a better understanding into the role gravity has played in the evolution of life on this planet, as well as understanding how these organisms could be put to use in humanity's expansion into space.

The work in this thesis lays the groundwork for an International Space Station micro- and Martian gravity geomicrobial experiment due to fly in 2019. It also addresses the knowledge gap in how biofilms - general and geomicrobial - respond to higher than normal gravity conditions. The findings show that there is an altered growth response, with increased gravity leading to an increase in biofilm growth.

Abstract

Experiments with microbial biofilms in microgravity and simulated microgravity have revealed altered growth kinetics, but geomicrobial biofilms have not yet been studied in low gravity environments. No characterisation of biofilms, geomicrobial or otherwise, have been conducted at hypergravity. This thesis explores factors affecting microbe-mineral interactions under terrestrial conditions, lays the groundwork for a scheduled microgravity experiment, and provides the first data on biofilms grown at hypergravity.

As a first step in understanding microbe-mineral interactions in altered gravity environments, experiments were undertaken to identify factors that constrain attachment in a terrestrial environment. The model organism *Sphingomonas desiccabilis* and basaltic rock from Iceland were selected, and the minerals that make up the basalt were identified and procured in their pure form. The relative significance of physical factors such as hydrophobicity, surface charge, porosity and nutritional value were examined in relationship to the success with which biofilms colonised the mineral surfaces. Growth was measured by the quantity of biofilm biomass after a fixed time period, using Crystal Violet stain, in order to draw conclusions about the most influential physical conditions on biofilm attachment to a substrate. It was found that mineral attachment is influenced more by porosity and nutritional value than by hydrophobicity or surface charge.

To explore how reduced gravity affects biofilm formation and weathering rates, a European Space Agency experiment, BioRock, is underway. Samples of basalt, with monocultures of three different organisms, will be sent to the International Space Station in 2019 for long-term exposure to Martian and micro-gravity. Research testing proof of concepts, material compatibility, and experimental procedure and equipment is described. Confocal laser scanning microscopy (CLSM) was used to image the biofilms, and inductively coupled plasma mass spectroscopy (ICP-MS) experiments were conducted to compare biotic and abiotic elemental release rates from basalt. Both of these methods will be employed for post-flight analysis of BioRock. Preliminary terrestrial ICP-MS experiments indicated that rare Earth elements (REEs) showed the most reliable reflection of leaching patterns overall, as a consequence of their high molecular weight and low volatility during the ashing procedure.

To fully understand gravity's effect on microbiological processes it is important to investigate what occurs when its influences are removed, but also to establish what occurs when extra gravitational force is applied. Using simulated hypergravity, achieved through hyper-acceleration on a geotechnical centrifuge, the effects of 10 x g on biofilm development and the leaching of basalt were investigated. As this was the first time that biofilms had been studied under hypergravity, additional substrates were included with the basalt, to enable characterisation of the more general response of biofilms to hypergravity. In contrast to previous experiments

conducted on planktonic bacteria, which found decreased population sizes, the biofilms grown at 10 x g showed greater biomass than the 1 x g samples. ICP-MS showed no difference in the average weathering rates, but greater variability in the higher gravity samples.

The data collected here advances our understanding of microbial interactions with geologically important substrates, with implications for an ISS microgravity experiment and future human space exploration. It also presents new intelligence on the previously unstudied effects of hypergravity on biofilms and rock weathering.

Declaration

This thesis has been solely composed by the candidate. Unless clearly stated, this work is the candidate's own. Where results have been obtained through collaborations with other researchers, their precise contributions are made clear in the text as appropriate. Parts of this thesis have been published in a co-authored peer-reviewed paper. This publication is listed below and is referenced at the back of the thesis.
Loudon, C.M., Nicholson, N., Finster, K., Leys, N., Byloos, B., Van Houdt, R., Rettberg, P., Moeller, R., Fuchs, F.M., Demets, R. and Krause, J., (2017). 'BioRock: new experiments and hardware to investigate microbe–mineral interactions in space'. *International Journal of Astrobiology*, Jul:1-11.

This work has not been submitted for any other degree or professional qualification.

Candidate's signature.....

Date.....

Acknowledgements

"The working Planetologist has access to many resources, data, and projections. However, his most important tools are human beings." - Frank Herbert

Many thanks to all of those who have helped and facilitated this thesis.
First and foremost, my thanks goes to Charles S. Cockell, to whom I owe some significant gratitude.
A big thank you to the UK Space Agency for funding this research and my PhD, and for all the other opportunities that have come with it.
Thank you also to our lab group -its current and former members - who have guided me through protocols and new approaches to thinking scientifically: Toby Samuels, Jennifer 'Jenkins' Wadsworth, Mark Fox-Powell, Samuel Payler, Petra Schwendner, Claire Marie Loudon, Delma Childers, Adam Stevens, Claire Cousins, Casey Bryce, Hanna Landenmark, Rosie Cane, Liam Perera, Andy Dickinson, Scott McLaughlin, Susana Direito, and Angela Dawson.
The staff and fellow PhD students of the School of Physics and Astronomy, in particular: Paul Clegg, Job Thijssen, Wilson Poon, Aiden Brown, Andrew Schofield, Martina Foglino, Joshua Hellier, Alexander Slowman, Giulio De Magistris, Jochen Arlt, Oliver Entwisle, Ben Guy, Andy and Mike and the physics workshop, Liz Patterson and the support staff at JCMB.
Faculty members from other departments within Edinburgh University, in particular: Lorna Eades, Nick Odling, Mike Hall, Bryne Ngwenya.
The BioRock team: Rene Demet, ESA, Kayser Italia, Kai Finster, Bo Byloos, Felix Fuchs, Natalie Leys, Ralf Moeler, Petra Rettberg.
Academics and professionals from outside of Edinburgh University: Andrew Brennan of the University of Dundee, Novespace, and the European Space Agency.
Outside of academia, my parents, Oliver J. Nicholson and Marianne S. Villiers-Stuart who have each in their own way guided me to and through this process. My lovely family, Natalie, Titus, and Alexander, my grandmother Bridget M. V-S. I would also like to acknowledge the support of Veronica Newson, Jamie and Fiona Grant, Charlie and Jules Grant, Mike and Cally V-S, my cousins the three As, and my god-son Tom Grant.
All of my wonderful friends - especially Eleanor Pratt, who has been a steadfast friend and supporter throughout this whole process, and the afore-mentioned Jenkins, my lab and office mate, and my partner in scientific silliness.
And I mustn't forget Captain Tardigrade, and the Astrobiology Aardvark.

Contents

List of Figures

List of Tables

Glossary of Acronyms and Abbreviation

ANOVA: ANalysis Of Variance (Statistics)
BLAST: Basic Local Alignment Search Tool (Genomics)
BMR: BioMining Reactor
BSC: Biological Soil Crust
CFU: Colony Forming Unit
CLSM: Confocal Laser Scanning Microscopy
CV: Crystal Violet
DLVO: Derjaguin, Landau, Verwey, and Overbeek theory. (The balance between electrostatic repulsion and van der Waals attraction)
ELIPS: European Programme for Life and Physical Science (European Space Agency)
EPS: Extracellular Polysaccharide
ESA: European Space Agency
ESR: Experiment Scientific Requirement
EU: Experimental Unit
FASTA: FAST-All, a DNA and protein sequence alignment software package (genomics)
FIJI: FIJI Is Just Image J (image processing package)
FWHM: Full Width Half Maximum
GMV: Grey Mean Value
GSL: GlycoSphingoLipid
ICPMS: Inductively Coupled Plasma Mass Spectroscopy
ISS: International Space Station
LOI: Loss On Ignition
LSMMG: Low-Shear Modelled MicroGravity
LSS: Life Support System
M9: Minimal nutrient media
MaGe: Microbial Annotation and Analysis Platform (genomics)
MERLIN: Microgravity Experiment Research Locker/INcubator (cold stowage)
MFC: Microbial Fuel Cell
mRNA: messenger RiboNucleic Acid
NCBI: National Centre for Biotechnology Information (genomics)
OD: Optical Density
PBS: Phosphate Buffered Saline
PI: Principle Investigator
PPB: Parts Per Billion PPM: Parts Per Million R2A: A nutrient media, recipe in Appendix A
REE: Rare Earth Element
RNAlater: A fixative to arrest microbial growth
SEM: Scanning Electron Microscope

SNC: shergottite, nakhlite, and chassigny, (classes of Martian meteorite)
TSS: Two Syringe System
WGS: Whole Gene Sequence
XDLVO: eXtended Derjaguin, Landau, Verwey, and Overbeek theory. (Incorporates acid base interactions and hydrophobicity effects)
XRD: X-Ray Diffraction
XRF: X-Ray Fluorescence

1 Introduction

Bacteria are present throughout the biosphere at every level, and in every habitable environment, with are estimated to number 4-6x10^{30} cells at any one time [1].
Biofilms, as both the most common form in which to find bacteria outside of the laboratory, and the most resilient form to the majority of stresses, have received a lot of attention from the scientific community over the last few decades. In medicine, food science, the oil and gas industry, biofilms can be a hazard or a help, depending on which species they are composed of, and the context in which you find them. This thesis examines microbe-mineral interaction on the micron-scale, before examining how lower and then higher gravities change the dynamics of biofilm growth and mineral alteration.
Geomicrobial biofilms play an important part in the natural cycling of nutrients and soil stabilisation, and can provide useful anthropogenic services, such as bio-mining and soil enrichment for agriculture. The processes and products of geomicrobial biofilms would benefit anthropogenic activities off-world, where the ability to extract elements in-situ and transform regolith into soil could contribute to a successful human mission on the moon or Mars. Conversely, the additional stress-resistance afforded to bacteria in biofilms is compounded by microgravity, which can also increase the virulence of pathogenic bacteria. This, coupled with the proliferation of bacterial biofilms in life support systems, has led to concerns over the impact of gravitational microbiology on human health. Gaining a better understanding of gravity's effects can serve to improve our efficiency beyond the Earth, and give us fundamental insights into gravity's role in biological systems. On the other side of terrestrial gravity, gravities above 1 x g have not been investigated in regards to the effects on biofilm formation and subsequent processes. It is proposed that hypergravity is an untapped resource for the investigation into gravitational microbiology.

Thesis Layout

Astrobiology is not so much a branch of science unto itself, but rather an interdisciplinary approach to answering questions that pertain to life in the cosmic context. As a result, the research in this thesis brings together methodologies and scientific perspectives from physics, geochemistry, and biology.

Each chapter has a different focus, and consequently, a different layout. The background chapter endeavours to furnish the reader with the relevant knowledge to appreciate the research conducted here in the context of the current literature. It begins with an exploration of general biofilms, their formation and structure, and the benefits they provide for the organisms involved. The chapter goes on to

look at geomicrobial biofilms, with some mention of the techniques microbes use to interact with mineral surfaces, and the implications and applications of these interchanges. The chapter then proceeds with an exploration of the research that has been conducted thus far on microbial growth in reduced gravity and heightened gravitational environments, and concludes with some information on the model organism that has been used in the majority of the experiments in this thesis.

The methodology chapter is designed to introduce the reader to the methods that were most commonly employed throughout these investigations. While shorter explanations of the methodologies will still be present in the results chapters, the purposes, protocols, and principles of the techniques will be highlighted here so as not to disrupt the flow of the results.

The first results chapter, *The Properties of Basaltic Minerals and their Effects on Microbial Attachment*, deals with the physical properties of the different minerals that make up basalt, and how this affects microbial growth. The chapter will begin with an analysis of the basaltic minerals and how the physical and chemical differences between them determine the forces at their surfaces. The second part of the chapter will investigate the preferential bacterial growth on the different minerals, and link the growth patterns to the physical properties that have been measured. The chapter will finish with a discussion that compares the biological attachment findings to the physical properties of the minerals, and conclude with an attempt to rank the physical properties in order of their importance to microbial attachment.

The second results chapter, *Model Organism and Hardware Characterisation in Preparation for Reduced Gravity ISS Experiments* consists of many smaller tests and experiments, which fall into two main categories: experiments on the model organism, and experiments on the hardware. After the introduction, the first section (5.2) describes the ISS experiment 'BioRock' in detail. The next section is the longest of the chapter, and combines all of the tests on the model organism. The subsequent sections all deal with the test organism's responses to the materials and methods of the BioRock experiment. Each experiment described in this chapter was conducted in an effort to lay the groundwork for the main ISS experiment which is attempting to answer a fundamental scientific question, but this chapter in itself cannot provide such an answer. The conclusion of the chapter relates how the different tests have shaped the final experiment.

The third results chapter, *The Effects of Hypergravity on Biofilms and Biomining*, is laid out in a more traditional way, describing a series of experiments that were conducted in parallel to answer fundamental questions about the model organism's stress responses to hypergravity, and how that affects biofilm formation on general and geological surfaces. As a consequence, the chapter has describes the purpose behind each strand of the experiment, then the methodology, followed

by a results section and a discussion section.

The final chapter in the thesis is the conclusions chapter, which brings together the research in all of the different chapters. Due to the different focuses of each chapter, the limitations and future work sections are kept within the conclusions sections of the relevant results chapter, rather than being discussed in the final conclusions chapter.

2 Background

This thesis examines bacterial biofilms and their relationship to basaltic mineral surfaces. It considers the effects of different surface characteristics on the initiation of biofilm formation at terrestrial gravity, and the effects of reduced and exaggerated gravity on biofilm success and mineral weathering rates. In this chapter, background literature will be reviewed concerning: biofilms, basalt, geomicrobial weathering, microgravity microbiology, hypergravity microbiology, the model organism, *Sphingomonas desiccabilis*, and the relevance of these investigations for human endeavours.

2.1 Biofilms

Bacteria attached in communities to solid substrates behave very differently to their planktonic counterparts. They undergo phenotypic changes, up- and down-regulating different gene and protein expression, and work cooperatively in order to take full advantage of the microniche they occupy[2]. The cooperative communities are called biofilms. In the wild they are typically composed of more than one species of bacteria - unless found in an extreme environment where no other bacteria can co-exist. In the laboratory experiments conducted in this thesis, all of the biofilms were single species, so that differences in biofilm formation and weathering rates could be of more directly attributed to the variables. Biofilms are ubiquitous, and as varied as they are numerous. Their formation and structure are important to characterise in order to help develop an understanding of the environmental and genetic influences that lead to their specific architecture and functions. Microbial biofilms can confer advantages to human endeavours, or they can hinder our progress; this appears to be especially true in space, where microgravity alters microbes and their biofilms, causing yet more changes gene expression, and making them more resistant to stress and antibiotics.
A 1998 paper by Whitman *et al.* estimated the number of total global prokaryotic cells as being in the region of 4-6 x 10^{30} cells [1], the authors do not discuss the relative abundance of archaea versus eubacteria, but it can be inferred that there is a great number and diversity of bacteria in the natural environment. Costerton *et al.* claim that direct observation has demonstrated beyond any doubt that in nutrient-sufficient environments, biofilm bacteria are greater numerically and in terms of metabolical capabilites, to planktonic bacteria[3]. It is reasonable to assume, in line with evolutionary theory, that this is because of the advantages conferred by biofilms.
Biofilms have their differences in species and structure, but the fundamental characteristics remain consistent; biofilms are attached to a solid substrate, and numerous cells of multiple or single species are physically cohered together through physical appendages and a matrix of extracellular polymeric substance (EPS) [4].

2.1.1 Formation

Biofilm formation is a genetically programmed event that involves a change in gene expression [5]. Formation begins with a single planktonic cell attaching to a surface through adsorption or deposition, the cell then attaches and begins to divide. The original cell and its daughter cells will begin to exude exopolysaccharides (EPS), along with extra-cellular DNA, polysaccharides, and proteins [6]. This EPS matrix may then catch and incorporate additional particulate matter, and other cells of the same or a different species. The biofilm will continue to grow until it reaches the optimum size for the environment, and then growth will be slowed or arrested through methods such as quorum sensing[7].
This description is a broad generalisation, and will not apply to all biofilm forming species; some authors have also broken the steps down into further detail, which include more information on the physical and chemical requirements. Characklis and Marshal [8], and later Palmer and White [9], Hall-Stoodley and Stoodley [10], and Garrett *et al.*, [4], see distinct stages to the formation and development of biofilms.

Stage 1 — The Conditioning Layer:
This first stage is primarily abiotic, with the emphasis on the substrate upon which the attachment will occur. An ideal surface will be enriched by nutrients that, for example, settle out of the bulk liquid, although the surface itself may be composed of minerals that are themselves nutritionally valuable to heterotrophic and lithotrophic organisms. In addition, particles that are deposited on the surface may alter the substrate to make it more amenable to attachment and colonisation by altering the surface charges, potentials and tensions.

Stage 2 — Reversible Adhesion:
Only a fraction of the cells that reach the surface will actually attach, using bacterial appendages or through physical forces. Along with local environmental variables, this is determined predominantly by: available energy; temperature and pressure conditions; the ionic charges of the cell membrane, surrounding solution, and solid substrate; available -OH groups; and the specific stereochemistry (structure and chemistry) of the substrate. In colloidal physics, the forces associated with bacterial adhesion are grouped and collectively referred to as the extended DLVO theory – Derjaguin, Landau, Verwey, and Overbeek [11][12] [13]. It can be described in the following equation:

$$\Delta G^{TOT} = \Delta G^{LW} + \Delta GAB + \Delta G^{DL} + \Delta G^{BR} \tag{1}$$

Where ΔG^{TOT} is the total free energy of the interaction between the bacteria and the substrate in an aqueous medium, ΔG^{LW} represents the Lifshitz-van der Waals forces, ΔG^{AB} is the Lewis Acid-Base interactions, or polar forces, ΔG^{DL} is the electrical double layer charge, and ΔG^{BR} represents Brownian motion[14].

How effective this model is at describing microbe mineral interactions has been the cause of much debate, and is investigated further in Chapter 4.

Stage 3 — Irreversible Adhesion:
As the activation energy for desorption of bacteria is low, repulsive forces may be greater than the attractive forces, leading to the detachment of the bacterium before true biofilm formation can begin. Hoffman *et al.* showed that cells are likely to make contact with a surface multiple times before transitioning from reversible to irreversible adhesion [15].
On a successful transition to irreversible adhesion, chemical reactions such as oxidation and hydration consolidate the bacteria-substrate bond and then polysaccharide adhesives (EPS) bind the cell in place. It is during this stage that changes in genetic expression begin to occur, and polysaccharide production is up-regulated. As with stage 2, this stage has some dependency on the forces described in the extended DLVO theory. Much of the research on this stage has been done using colloids, but some researchers emphasise that the presence of structural cell surface appendages play a large and crucial role in the success of irreversible adhesion [16] [15].

Stage 4 — Population Growth:
The now sessile cell divides, and growth occurs in three dimensions as the daughter cells form clusters. Certain cells in these clusters will double faster and produce more EPS, leading to the formation of taller stacks of clusters, or microcolonies (see Fig. 1) - which have been described as the building blocks of biofilms[3]. Growth at this point follows the classic lag-log pattern, and the physical and chemical dependencies that affect initial attachment give way to the dominating metabolic processes.
Sauer *et al.*[17] catalogued the phenotypic differences between planktonic and biofilm bacteria with the species *Pseudomonas aeruginosa*, and found more than 800 proteins were shown to have a six-fold or greater change in expression level, which represented over half of the proteome. Research done on *E.coli* by Prigent-Combaret *et al.*[18] found that 38% of genes were differently expressed, with high levels of differentiation in genes relating to high osmolarity, oxygen limitation, and high cell density.
As the population grows, each cell in a microcolony will adapt to a particular microniche and begin to take on a function that benefits itself and the whole. Cell appendages are no longer formed, EPS continues to reinforce attachment and inter-cellular cohesion, and foreign cells, nutrients and particulates begin to get caught in the matrix. Additional proteins are produced, which support the structure of the biofilm and help with transport into and out of the cell. When it reaches this point, the biofilm is of a size and structure that it can be described as having primitive homeostasis and metabolic cooperativity [3], and many biofilms are capable of forming water channels which have branching anastomoses to allow the flow and exchange of nutrients, water, oxygen, and waste products.

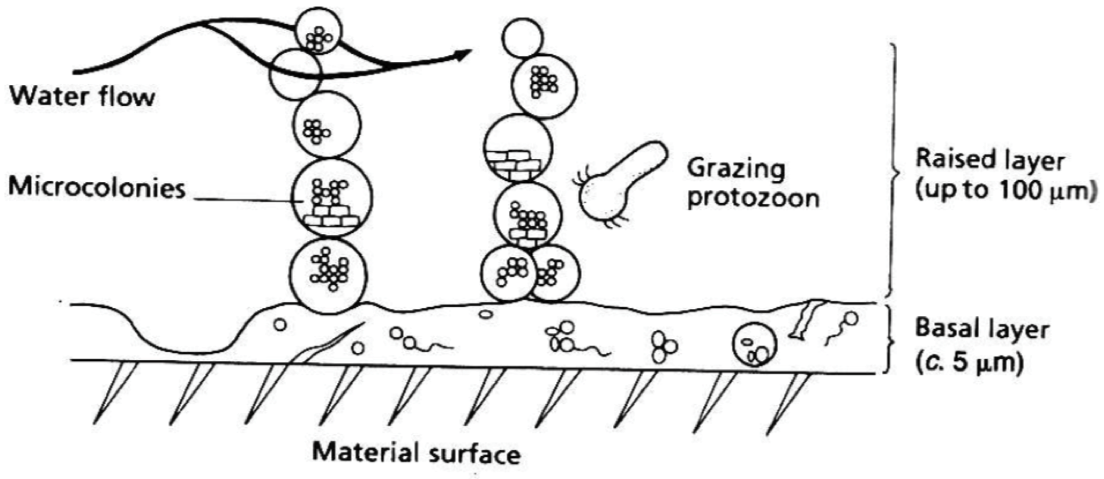

Figure 1: Representation of a biofilm growing on bitumen steel. In a thin layer on the mineral surface is a film of bacteria, with some higher conglomerations of microcolonies. Taken from Rogers *et al.*[19]

Stage 5 — Dispersion:
This stage incorporates the stationary and death phases of bacterial growth. When the cell concentration reaches an optimal size for the environment, quorum sensing and cell signalling triggers a change throughout the biofilm [20]. Little is known about the biological mechanisms of this stage[21], but Boyd and Chakrabarty[22] found that a lyase for the principle component of *Pseudomonas aeruginos* EPS, alginate, was produced during the latter stages of biofilm maturity, and the greater the amounts of this lyase, the greater the cell detachment. Another theory posits that dispersal can be seen as ejection of the hydrophilic daughter cells compared to older cells in a biofilm, which grow more hydrophobic or 'stickier'[23] as they age.

2.1.2 Composition and structure

In a 1998 study by Zhang *et al.*, who investigated the spatial distribution of proteins and polysaccharides through the biofilm of three different *Sphingomonas* sp, found that on average, 97% of the biofilm were composed of water, regardless of sampling position, depth, or age of the biofilm[6]. Horan and Eccles isolated biofilms from activated sludge, and found the dry weight of biofilm biomass was predominantly polysaccharide; of which 65.7% was carbohydrates, 23.6% nucleic acids, 10.5% proteins, and the remaining 0.2% was lipids[24].

Biofilms are diverse, as are the conditions they can grow in, and much like snowflakes, no two will ever be the same structurally. The architectural details of any single biofilm formed under any specific set of parameters are unique to the combination of the environment and the microflora involved [3][25][26]. Environmental conditions that can affect the architecture include type of carbon source, the properties of the substrate, oxygen availability, flow rate, level of shear forces, and nutrient availability. Species relevant conditions include the presence or absence of motile appendages, growth rate, physiological cooperativity, the type and amount of EPS that is produced, a range of genetic factors, and the number of different species involved [3][27]. However, when reviewing biofilm structure, including some research they had done on dental biofilms, Wimpenny and Colasanti proposed three different conceptual models for the structural tendencies of biofilms [28]. The first, the 'Water Channel Model', defines this type of biofilm structure as a collection of mushroom-shaped colonies, some of which fuse together leaving vertical shafts for water that penetrate to the base of the film. The second, the 'Heterogeneous Mosaic Biofilm' is a more extreme version of the first, where columns and stacks form, but with less fusion between them, leaving larger channels between the areas of the biofilm. The third, the 'Dense Biofilm Models' have no water channels or porous structures at all, and examples given are related to oral and indwelling catheter biofilms.

In the first two models described above, water channels void spaces and channels form. Using confocal scanning laser microscopy (CSLM) to track fluorescent beads down these void spaces, Stoodley *et al* [29] tracked 0.28μm beads through a multispecies biofilm. The biofilm was growing in a tube (2mm x 2mm x 30mm) packed with 500μm glass beads, and the flow velocity was 0/0025 m s^{-1} (See Fig. 2). They found that bacteria formed reproducible stable structures of microcolonies and water channels, and determined this allowed the distribution of water and fresh nutrients, as well as the removal of waste products. Some researchers have likened these void systems to primitive circulatory systems, as it provides this necessary distribution throughout the whole biofilm to keep the larger cooperative community healthy, and could provide an interesting insight into the emergence of multicellularity. [3] [28] [30].

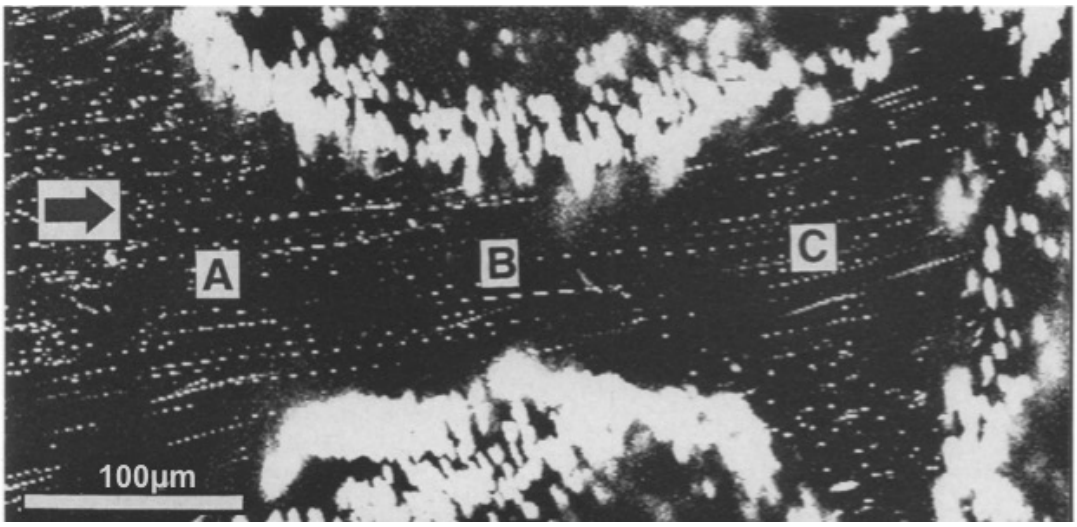

Figure 2: Flow channel within a 3 day old multispecies biofilm, flow velocity of 0/0025 m s^{-1} (*Pseudomonas aeruginosa, Pseudomonas fluorescens*, and *Kiebsiella pneumonia*) .The water is moving in the direction of the arrow, 'A' marks the entrance to the flow channel, 'B' its throat, 'C' the direction of channel exit.

DeBeer *et al.* [31] used integrated CSLM and microelectrode techniques to establish that the voids supplied approximately 50% of the consumed oxygen to the internal cells of the biofilm.
Stacks have been reported in a variety of shapes, with different researchers picking different terminology for qualitative descriptions: 'Ball-shaped' and 'coral reef' [26], 'mushroom shape' [32], 'conical'[3]. Stacks and voids will generally only occur in some parts of the biofilm coverage, while there will be areas of thinner but more dense microbial mat (5μm) in the areas surrounding and in between the taller structures[27] (see Figs. 1 and 3).

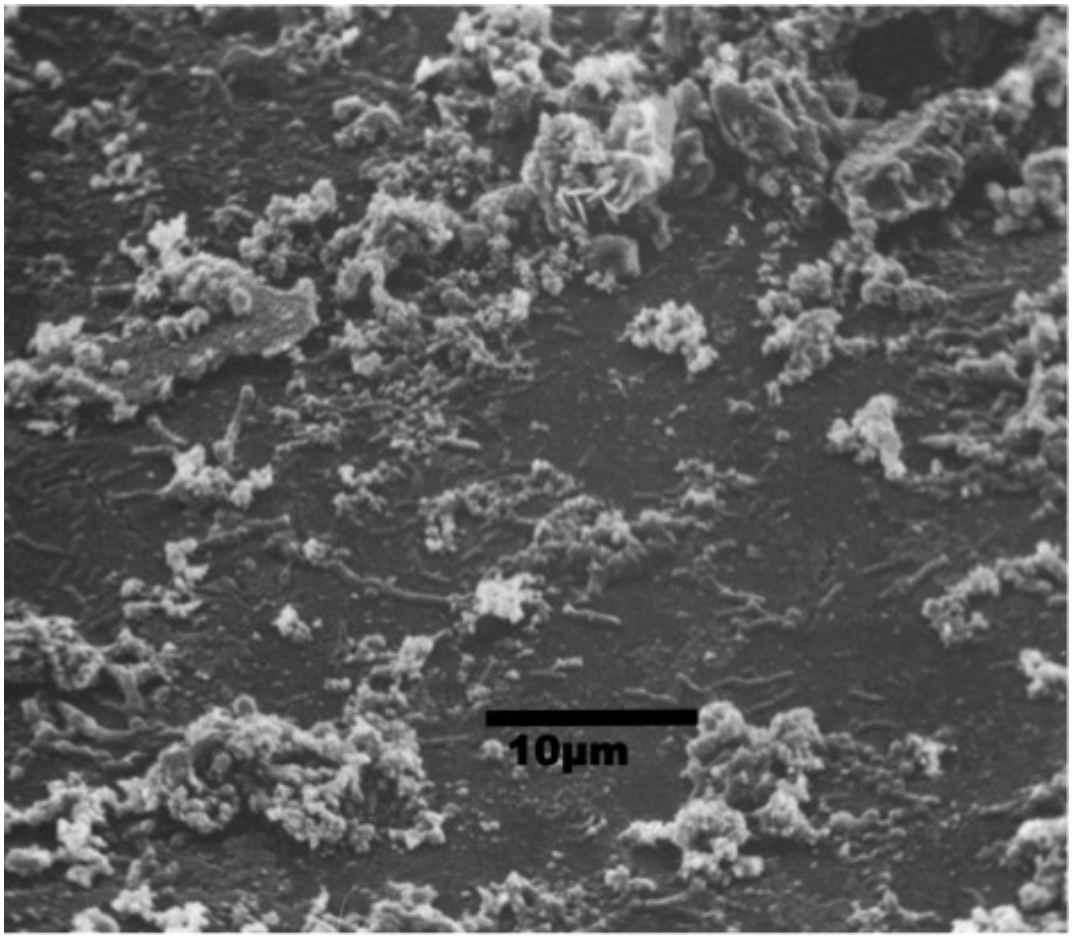

Figure 3: SEM image of the distribution of microbial biofilm across a solid substrate. Photo taken from Walter et al. [33]

2.2 Basalt

Basalt is the most common rock in the Earth's crust[34]. New terrestrial basalt is formed when volcanic eruptions channel magma from the Earth's mantle onto its surface, which solidifies, creating new habitable lithosphere[35]. New crustal production mainly takes place in the oceananic constructive boundaries[36]. Bach and Edwards estimated a seafloor production rate of 3.0 ± 0.5 km2/yr, with a basalt density of 2950 ± 50 kg/m3 [37] . Chemically, it is defined by the International Union of Geologists as having between 45 and 52 wt.% SiO, and less than 5% wt. (Na,O +K,O)[38] .

The surfaces of the other rocky bodies in the solar system are even more basaltic in their composition[39], which is why basalt was selected as the substrate for the experiments in Ch 5, investigating geomicrobiological interaction in reduced

gravitational environments. Orbital thermal emission spectra by the Mars Global Surveyor and the Mars Odyssey[40][41] indicate that the surface of Mars in predominantly basaltic to andesitic basaltic composition[40][41]. This IR spectral analysis is backed up by in situ analysis from the Viking Landers and the Mars rovers, as well as studies performed on the Shergottite, Nakhlite, and Chassigny (SNC) classes of Martian meteorites[42][43].

Considering the potential application of bacteria for extracting useful minerals from Martian rocks it is worth briefly considering the composition of Martian basalts. According to data acquired from SNC meterorites, Martian basalt - at least in the Northern hemisphere - contains similar or higher levels of ferromagnesian elements, and comparable levels of siderophile elements[44] (see Fig. 4). Consequently, it reasonable to confidently say that if bacteria can still successfully leach elements in reduced gravity, the metal resources would be available for them to do so.

2.3 Geomicrobial Weathering

Abiotic weathering falls into two main categories, physical and chemical. Geochemical weathering processes occur when minerals are exposed to acidic and/or oxidative conditions; geophysical weathering can be attributed to temperature, exfoliation (a lessening of pressure), or abrasion. Usually abiotic weathering is a combination of more than one of these actions.
Biotic weathering works to enhance and expedite the process of geochemical weathering, altering the texture and composition of the exposed mineral surface, leading to dissolution and crystallisation; the breakdown of existing minerals, and the creation of new ones [45]. Microbes have a number of mechanisms that can accelerate erosion and leaching by driving alterations in the geochemical environment, creating microenvironments to promote change at the microscopic level. Microbially induced weathering can be a direct or indirect result of bactieral behaviour: directly, microbes can extract elements that they require from a mineral surface; and indirectly, through metabolic activity resulting in the production of organic or inorganic acids[46].As basalt is primarily composed of silicate minerals, this section on weathering will explore the processes that alter this class of minerals.

Variation in pH

At either a microscopic or bulk-solution scale, pH alteration is one of the main microbial contributions to mineral and rock weathering[47]. When metabolic activity leads to alkaline products, or takes place in an environment of greater than pH 8, hydroxyl atoms act a catalyst, increasing the solubility of the mineral surface in aqueous environments. If the environment or microenvironment formed by bacterial products falls below pH 5, the concentration of protons begins to

	Terrestrial basalts[b]	Shergottites
Refractory incompatible elements		
Ba μg/g	~250 [1–3000] (323)	16.4 ± 11.8 (5)
La μg/g	~24 [0.7–238] (249)	0.785 ± 0.649 (8)
Nd μg/g	~23 [0.1–176] (175)	2.13 ± 1.11 (7)
U ng/g	~1000 [8–5700] (96)	51.7 ± 43.9 (6)
Ferromagnesian elements		
Cr μg/g	~270 [1–1660] (276)	3680 ± 2390 (8)
V μg/g	260 ± 66 (180)	206 ± 62 (8)
MnO mg/g	1.83 ± 0.34 (333)	4.74 ± 0.29 (8)
FeO wt%[c]	10.7 ± 1.6 (336)	18.8 ± 0.8 (8)
MgO wt%	7.55 ± 2.32 (383)	16.1 ± 8.5 (8)
Siderophile elements		
Ni μg/g	~110 [1–950] (317)	133 ± 107 (7)
Co μg/g	42.7 ± 10.0 (154)	48.3 ± 18.0 (8)
Ga μg/g	20.3 ± 3.4 (141)	14.3 ± 6.5 (8)
Ge ng/g	1480 ± 130 (8)	653 ± 106 (4)
Re pg/g	911 ± 357 (8)	~372 [44–1020] (4)
Ir pg/g	~94 [0.4–734] (65)	2100 ± 1520 (5)
Volatile incompatible elements		
Na mg/g	18.2 ± 5.1 (330)	7.59 ± 3.70 (8)
K mg/g	~5.4 [0.08–40.4] (399)	0.579 ± 0.442 (8)
Rb μg/g	~17 [0.11–105] (327)	2.77 ± 2.32 (6)
Cs ng/g	~840 [1–12000] (85)	185 ± 156 (6)
Tl ng/g	~47 [6–280] (23)	7.6 ± 3.8 (6)

Figure 4: Major and trace element mean abundances for selected elements in terrestrial basalts and basalts in the Martian shergottites from the SNC parent body. Chemical variability ranges are given in square brackets, numbers in parentheses refer to the number of rock samples. Modified from Ruzicka *et al.*, 2001.

corrode the mineral surface [48][49]. Quartz is an exception to this general rule, where as a result of its stable structure and chemistry, dissolution is independent of pH until after pH8, when dissolution rates rise with alkalinity ([50][51]. Other minerals that are found in basalt, such as the feldspars albite, anorthite, microcline and orthoclase (which comprise a large portion of the non-quartz content of basalt - see 4.2.1), have more reactive ions, and is at greater risk of pH driven dissolution.

Organic Ligands

The bacterial production of ligand molecules accelerates the removal of elements - particularly heavy metals - by weakening the metal-oxygen bonds and binding to metal ions within a mineral matrix. This complexing is faster still with multidentate ligands, known as chelates, which have more than one site for binding to

the metal ions ([52]. Ligands and chelates can also expedite weathering by lowering the saturation state of the surrounding solution by binding with ions in the bulk fluid[53]. Ligands that specifically bind to iron are known as siderophores, and can also transport the iron across the cell membrane[54]. Organic ligands have been shown to greatly increase weathering rates of aluminium and silicon relative to inorganic acids alone[55].

Redox Reactions

Redox reactions are another mechanism for biogeochemical weathering, involving a specific element being oxidized or reduced at the exposed mineral surface, losing or receiving an electron respectively. Redox weathering generally results in a mineral transformation, with the primary mineral containing the redox element being dissolved and the constituent elements or compounds forming new mineral products [48][56](See Fig. 5).

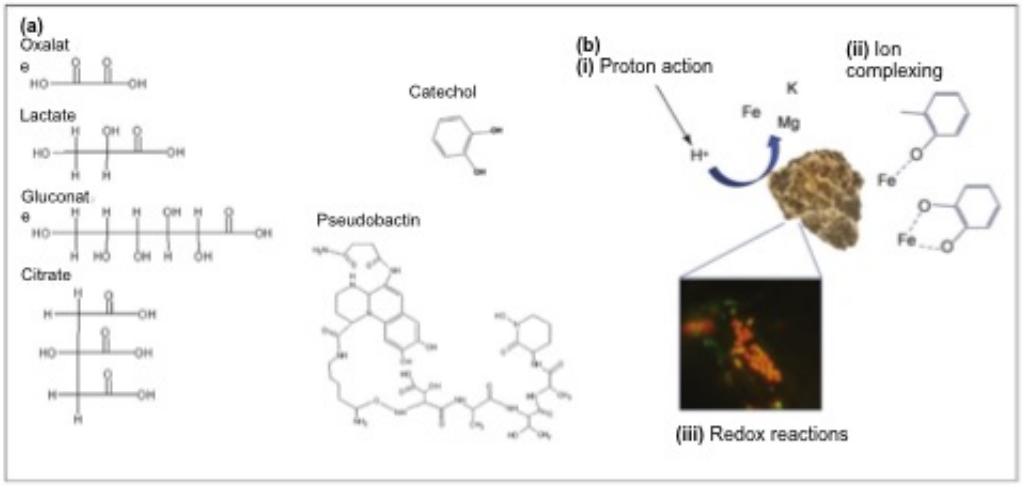

Figure 5: a) Common organic molecules involved in geomicrobial weathering. b) the actions of such molecules on minerals - here Biotite, which *Sphingomonads* can weather [45]. i) proton action - from a decrease in pH, ii) ion complexing, from ligand binding (iii) redox-reactions through electron exchange. Image modified from Gadd (2010)[56].

Polysaccharides, which make up the bulk weight of biofilm EPS, can also contribute to mineral weathering. They contain ligands and chelates, maintain diffusion pathways which delay solution saturation in the vicinity, and provide nucleation sites for mineral re-crystallisation. In addition, they prolong the time-frame of weathering in natural environments by creating a barrier against desiccation and other stressors [48]. How much acceleration EPS can contribute to the geomicrobial weathering process is difficult to qualify, with some research indicating a synergistic effect of ligands and EPS[**?**] with the EPS helping to concentrate the ligands at the mineral surface[57], and other research showing that EPS can inhibit ligands by occupying available reaction sites[58]. Ultimately, it seems that

biofilms do promote geomicrobial weathering compared to planktonic bacteria, by decreasing the pH of the bulk solution (3.3:4.0, biofilm to planktonic) and having a higher overall production of siderophores[59].

2.4 Bacteria Studies Under Microgravity

Microgravity experiments performed in Low Earth Orbit free-fall (1g x 10^{-6}), and simulated microgravity experiments performed by creating low shear environments, have shown that both planktonic bacteria and bacterial biofilms grow and behave differently when the action of the force of gravity is reduced or removed[60][61]. Results have revealed that bacteria express different genes, reproduce faster to higher population numbers, form different architectural biofilm structures, and acquire improved resistance to a number of stresses[62].

2.4.1 Altered Growth Dynamics

Bacteria, which have an average length of 2μm, are too small to directly sense gravity[63], and so too its lack. Due to the attraction between objects with mass, matter in a gravitational field experiences a force that draws it towards the centre of gravity. When an object meets an obstruction that prevents it from moving closer to the centre of gravity, the object experiences a counterforce based on its mass, and the strength of and distance to the gravitational field. This counterforce is called 'weight'. Thermodynamically, warmer objects have more energy, and are displaced in a liquid medium by the 'colder' objects that have less energy to counteract the pull of gravity. The behaviour of liquids in the presence of a gravitational field is dominated by these density driven thermodynamic considerations, along with Brownian motion - or diffusion - a slower process involving the random unpredictable movement of atoms. In the absence of gravity, denser particles do not sediment in any direction as objects with mass are not compelled to move, and the extra molecular energy afforded by 'heat' does not translate into convection. Consequently, the liquid environment, from the perspective of a bacterium - especially one without the benefit of motility, would be almost entirely quiescent without the associated shear forces, and only random Brownian motion to act as a mixing force[64].
Consequently, the mixing of waste and nutrients in a liquid environment is drastically reduced in microgravity, by four orders of magnitude. In an experiment onboard the Skylab, this was demonstrated by introducing concentrated tea to the surface of water in a tube (1.27 x 15.24 cm). The diffusion front advanced only 1.96 cm in 51.5 hr[65].

In a vacuum at 1x g bacteria would be subject to the inertial acceleration of gravity to the same extent as a tennis ball, feather, or bowling ball. In a gas or a liquid, however, other forces start coming into play, each of which has an effect that cannot easily be separated out. These forces can be classed in two main ways, liquid forces, and electrochemical forces.
Given the size of a bacterium, the liquid environment is very different. They have roughly the same density as water, and their size compared to the molecules in the water is a less extreme ratio than between a macro-scaled object and the water molecules. A bacterium has an average Reynolds number of $1x10^{-6}$, whereas a human has a Reynolds number of $1x10^{6}$ [66]. This means that the water is not an easy medium to transverse, and would appear to have a more viscous consistency. In addition, as a result of Brownian motion in the thicker substance of the water, the bacteria at that scale would be subject to the 'violent jerking' of random thermal fluctuations. In terrestrial gravity there would also be density driven convection, providing shear forces in the flow of water, at both macro and micro scales, which would act as currents, transporting the bacteria and providing additional turbulence. Also worth mentioning in this grouping is surface tension, the force of which is Albrecht-Buehler (1991) calculated to be 400,000 times stronger than the force of gravity acting on a single bacterium[67].
Beyond the physical aspects of the behaviour of the liquid, there are also the other forces which dominate at the micron scale. These forces are mainly electrochemical. Speaking in these terms, gravity exerts 5kcal/mole of energy on a cell. By contrast, typical energies for a hydrogen bond is 4kcal/mole, 80kcal for an ionic bond, and 90kcal for a covalent bond. The ionic force in a solution, then, has the potential to vastly overpower the gravitational force acting upon it, depending on the average electric charge of the bacterium and the ionic strength of the liquid. Within the cell, too, there are electric and chemical bonds, upon which gravity has little influence. Also in this category is polymerisation, whereby molecular subunits are held together by ionic and Van der Waals forces at a range of 6-30kcal/mole. For example, the electric repulsion between the macromolecules in a large protein such as myosin would require acceleration of $100{,}000g$ before the occurrence of sedimentation[67].

It is most likely that the gravitational trigger that causes the indirect effect upon the cell is this quiescence of the fluid. When this is considered in terms of the liquid dynamics and the forces described above, it is possible to gain insight into the reliance of nutrients on the behaviour of water for their distribution. From the trigger of quiescent liquid, one can chart the chain of events that leads to altered cellular behaviour[68]. For ease of characterisation and understanding, the chain can be broken into four fundamental steps:
• An altered physical force, in this case the inertia of water, acts upon the cell under microgravity.

• This altered force leads to a reduction in the availability and exchange of nutrients and metabolic biproducts.
• The chemical environment of the cell is altered.
• Different biochemical pathways are activated as a result.

Goldermann and Hanke [69] have suggested that the first cellular components to respond to the altered gravity conditions, in gram-negative bacteria, could be the ion channels. Their experiments with native *E.coli* ion channels reconstituted into planar lipid bilayers showed a reduction in the open state potentiality of the ion channels.

In response to the stress of limited nutrient availability in microgravity, both planktonic and biofilm bacteria appear to function even more successfully that in terrestrial gravity[70]. This has also been noted in modelled microgravity, using clinostats to mimic low shear environments, and rotating wall vessels to homogenise the direction of gravity for the sample. Lynch *et al.*, found that under low-shear modelled microgravity (LSMMG), *E.coli* grew thicker biofilms[71]. Lynch identified this as being partly due to the up-regulation of a transcription initiation factor (or sigma factor) RpoE. Wilson *et al.* also identifies the RNA-binding regulatory protein Hfq, important for mRNA translation, and the environmental stress response RpoS as being important contributors to the observed changes[72]. Kim *et al.*[32] found spaceflight increased the number of viable cells and the biofilm biomass, and allowed the formation of a new 'canopy' biofilm structures not seen before in terrestrial biofilms (see Fig. 6).

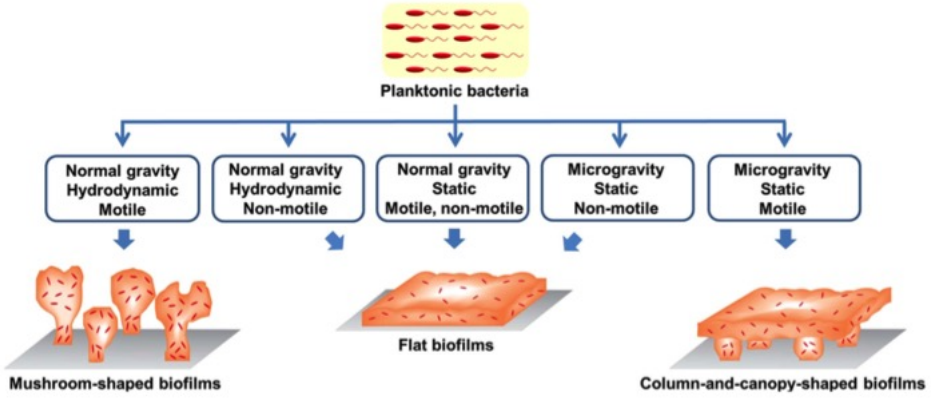

Figure 6: Image taken from Kim *et al.* (2003) showing the microgravity specific structure (right) and the two most typical terrestrial gravity biofilm structures (centre and left).

2.4.2 Increased Resistance

An increase in growth rate and population numbers is also accompanied by greater resistance to stresses. In the same set of Lynch's LSMMG experiments that saw an increase in thickness of *E. coli* biofilms (see 2.4.1), an increased resistance to salt, ethanol, and two antibiotics - paracetemol and chloremphenicol - were reported[71]. As well as increased resistance, greater virulence and pathogenicity have also been observed from LSMMG and microgravity experiments, as shown by the experiments with *Salmonella typhirium*[72] and *Pseudomonas aeruginosa*[73][74].
Onboard inhabited space stations, bacterial populations proliferate to the disadvantage of the human crew and life support systems, and have been resistant to attempts to remove them[75]. While the Russian orbital station Mir was officially decommissioned in 2001 due to lack of funding, there is some evidence that the station would not have been habitable for much longer due to extreme contamination by anthropotechnological microorganisms[76]. Over 230 bacterial and fungal species were identified, some of which were hazardous to the health of the human crew, and other that were degrading the integrity of the materials composing the Mir and its critical systems. The International Space Station is subjected to regular intensive cleaning regimes by all members of the crew[77], and even so the proliferation of microorganisms remains a concern[78][79], especially as human immune systems are comprimised over the course of long-term microgravity exposure[80]. In addition to being a concern for crew health on long-duration flight missions, the resilience and resistance conferred to microorganisms by altered gene expression in reduced gravity increases the risk of forward contamination. Unmanned robotic probes and rovers are constructed in clean rooms, which have extensive harsh decontaminating proceedures, but have still been found to contain extremotolerant species of bacteria. As one stress tolerance is often indicative of others, extensive work is being undertaken to try and further refine protocols so that Mars and other bodies are not contaminated by terrestrial organisms, undermining the search for life from an independent origin [81].

2.5 Bacteria Studies Under Hypergravity

After a review of the available literature, it appears that while experiments have been conducted on bacterial growth at hypergravity, no experiments have been reported on the effects of hypergravity on biofilms. There was one exception, but it was performed on a parabolic flight with 20 second intervals of 2 x g [82], which does not give adequate time for a biofilm to mature, and is a very low gravity regime compared to the other experiments conducted at hypergravity.
With planktonic bacteria in bulk solution, populations grown at acceleration

consistently have lower populations than the 1 x *g* controls. As explained with the section above, bacteria are too small to be directly affected by gravity, but changes in the gravitational environment of the bacteria still produce an effect. Once again the fluid dynamics of the system the bacteria occupy must be understood in order to gain insight into the chain of events that lead to the altered growth patterns. While density driven differences are reduced or removed in lower gravities, they become more apparent in response to acceleration. This leads to the bacteria being condensed into a high concentration of cells against the surface that stands between them and the direction of gravity. Initially, at low accelerations, this can prove beneficial. Nutrients and useful metabolic by-products are concentrated in the same region as the cells, shortening the lag phase. However, as acceleration increases, the effects of buoyancy are exaggerated, leading to the separation of the lighter nutrients and by-products into a layer above the microenvironment of the sedimented bacteria. Additionally, depending on the volume of water, higher accelerations will lead to higher hydrostatic pressure - reaching, for example, levels of 126.5 Mpa at 403,000 x *g*[83]. For planktonic bacteria, this combination of factors would lead to stress, starvation and lower population numbers.
As starvation conditions are - up to a point - beneficial for biofilm formation, it is possible that biofilm biomass could increase in response to low levels of acceleration, but this has not been explored until this thesis.
At 2 x *g*, 3 x *g*, 5 x *g*, and 10 x *g*, hyperacceleration results in a shorter lag phase, but not a significant reduction of final population size[84][85]. Between 10 x *g* and 20 x *g* a reduction in final cell count begins to manifest[86]. Brown (1999) grew *E.coli* in simulated microgravity with a clinostat, and accelerations up to 400 x g for 80 hours to determine growth curves at 0 x *g*, 0.5 x *g*, 1 x *g*, 50 x *g*, 180 x *g*, and 400 x *g*. His results showed that between 1 x *g* and 180 x *g*, the lag phase of planktonic *E. coli* is not only much shorter than the terrestrial controls, but also significantly shorter than the reduced lag phase of *E.coli* grown in microgravity. Between 180 x *g* and 400 x *g*, the lag phase begins to lengthen again, until it matches the terrestrial controls[87]. Final cell count decreased with increasing acceleration, but at a decreasing rate (see Fig. 7).

Montogomery et al. (1963) looked at the growth of *E.coli* at 1,000 and 110,000 x *g*, and found that populations dropped by 78% and 98% respectively[88], but the time-frame of this experiment is not available. Yoshida *et al.* (1999) looked at four different species bacteria, two gram negative and two gram positive organisms at an acceleration of 450,000 x *g* for 6 hours. They found that the two gram-positive species, *Bacillus amyloliquefaciens IF014141* and *Staphylococcus aureus IID975* were more sensitive than the two gram-negative species, *Escherichia coli B* and *Thiobacillus intermedius 13-1*[89].
Deguchi *et al.* looked at five different microorganisms' growth curves at up to 403,627 x *g* for up to 120 hours. The species were *Paracoccus denitrificans*, *E. coli*, *Shewanella amazonensis*, *Lactobacillus delbrueckii*, and *Saccharomyces cerevisiae*

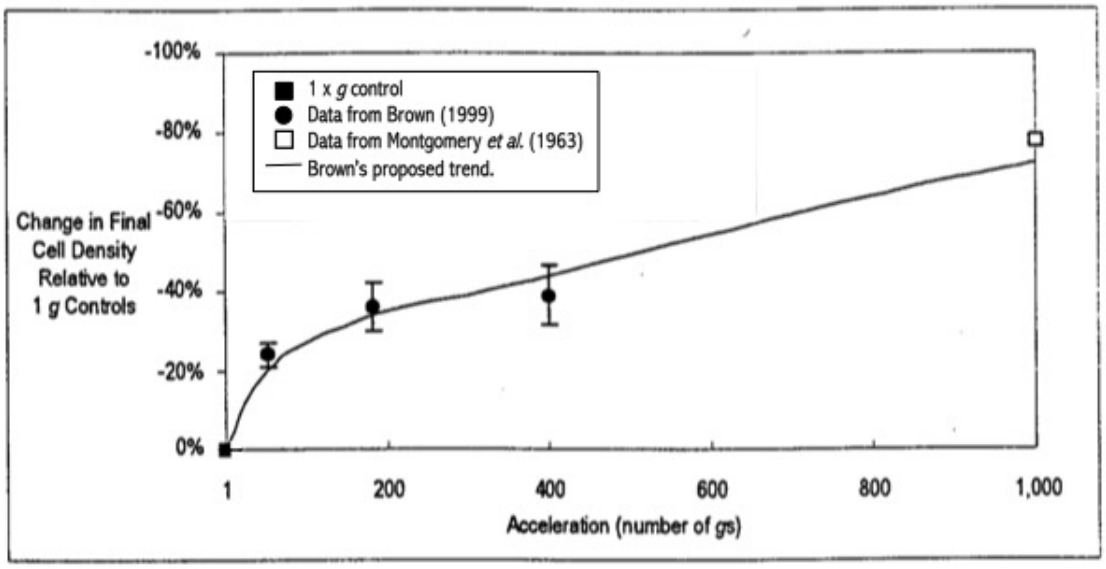

Figure 7: Data from terrestrial gravity to 1000 x g from Brown (1999) and Montgommery (1963) and Brown's suggested linear relationship between acceleration and decreasing population count. Graph modified from Brown [87]

- this last one being a yeast. *P. denitrificans* was the most successful species in the study, proliferating to numbers of 1.5 x 10^7 at 36 hours, after an initial population crash with its nadir at 7 hours[90]. This altered growth pattern was found in two of the four bacterial test organisms, with the other being *S. amazonensis*. This suggests that some populations that are initially more susceptible to conditions arising from hypergravity are able to recover after a crash. This will most likely be due to the death of cells that cannot up-regulate stress response genes, and the survival of cells that do have active adaptive mechanisms and their subsequent successful proliferation (see Fig. 8). Neither Yoshida *et al.* or Deguchi *et al.* found any signs of mechanical deformation to the cells themselves.

2.6 *Sphingomonas desiccabilis*

Isolated from the desert of the Colorado Plateau, *Sphingomonas desiccabilis* is a chemoheterotrophic gram-negative species of the Class *Alphaproteobacteria*[91], with cryptobiotic defences that make it a useful and interesting experimental organism. It has anhydrobiotic resistance against rapid desiccation, and cryobiotic defences against freezing. *S. desiccabilis* are strictly aerobic and non-sporulating. Cells are capable of forming biological soil crusts due to their ability to produce an abundance of Extracellular Polysaccharide (EPS). Planktonic cells are rod shaped and measure 0.25μm x 0.5μm. Colonies are convex, round and smooth, and light

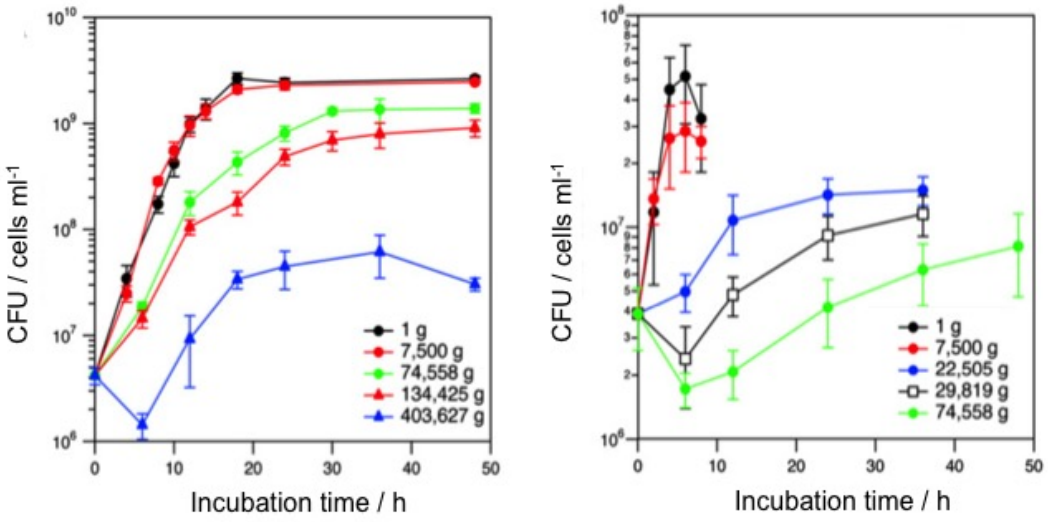

Figure 8: Figure modified from Deguchi *et al* (2011) showing that at high acceleration/hypergravity, growth curves follow a different pattern to the traditional lag-log-stationary pattern. Growth curves are from *Paracoccus denitrificans* (left) and *Shewanella amazonensis* (right).

yellow in colour. *S. desiccabilis* is capable of growth between 8 and 37^{o}C, 25^{o}C being the optimum temperature, and prefers neutral or close-to-neutral pH levels. Most of the bacteria isolated from this region of the Colorado Plateau and the wider Sonoran desert have been cyanobacteria. Of heterotrophic communities, *Actinobacteria*, *Proteobacteria*, and *Bacteriodetes* have so far been shown to be dominant. In its native habitat, *Sphingomonas desiccabilis* would be in mixed species communities, which provides advantages as the weathering actions and products from other organisms can also be used by *Sphingomonas desiccabilis*, as theirs can benefit other organisms too. However, the natural environment would not provide as rich an abundance of nutrients as the nutrient solution provided for the organisms in the laboratory, and so their in vitro growth will be accelerated compared to their natural growth. The species was identified from a streak dilution of a BSC collected from sandy arid soils in the Colorado Plateau, USA (38u 389 5570 N 109u 389 9100 W, and 38u 099 9050 N 109u 449 5090 W). The environment is unique because of the plateau's high altitude, which exposes the organisms in the top layers of the soil to extreme conditions; low humidity, high solar (UV and visible) radiation, extremes of temperature (-3^{o}C-37^{o}C), and low rainfall (175–300 mm)[92][93]. No geological or mineral data of the soil from which the bacteria were isolated is available, but more general data on the Colorado Plateau indicates the Plateau is composed primarily of uplifted horizontal conglomeratic sandstones and mudstones, shale, and some igneous and volcanic

rocks [94].

The *Sphingomonas* genus was first defined by Yabuuchi *et al* in 1990 [95]. Eleven years later, the genera was divided into four subsequent genera: *Sphingomonas*, *Sphingobium*, *Novosphingobium* and *Sphingopyxis* [96], later dubbed the 'Sphingomonads' by Balkwill et al. (2006) [97]. The sphingomonads are mainly distinguished from other α-4 subclass *Proteobacteria* genera by virtue of containing glycosphingolipids (GSLs) as the amphiphilic molecules in their cell envelopes, instead of lipopolysaccharides. The *Sphingomonas* genus is seperated from the other Sphingomonads by having *sym*-homospermidine as the major polyamine component, while the other three genera have biosynthetic pathways for spermidine polyamines instead[96].

Sphingomonads are metabolically versatile, able to to use a wide range of natural compounds as well as man-made contaminants. Due to these biodegradative abilities, and also their biosynthetic capabilities, sphingomonads can and have been used for a number of different biotechnical applications. They produce sphingans, such as gellan, which are used in food, ink, cement, pharmaceutical, and personal care applications[98]. Their exopolysaccharides can be used as viscosifiers, stabilisers, emulsifiers and gelling agents.[99]

In addition, many Sphingomonads produce EPS, and some species have been used in the petrolium industry to prodyce a drilling fluid component, the viscocity of which remains relatively stable under extremes of pH, temperature, and salinity[97].

The biocatalytic transformation faculties of *S. desiccabilis* have been used to create a bioreactor to degrade four low molecular weight polycyclic aromatic hydrocarbons: naphthalene, phenanthrene, acenaphthene and anthracene [100].

Another strain of *Sphingomonas* has been shown to successfully decontaminate fields fouled with γ-hexachlorocyclohexane, an organochlorine insecticide, prohibited in the 1960s, but still in use. It was a small scale test, repeated in three different seasons, and the strain of *Sphingomonas paucimobilis* was able to decompose the contaminant to 95% of its original concentration within two months in two seasons, and within six months in the winter season due to dilution of the bacteria in increased water-soil movement [101].

In the pharmaceutical industry, *Sphingomonas* species have been used to catalyze the hydroxylation of pyrrolidines to (R)- and (S)-N-protected 3-hydroxypyrrolidines. These are useful pharmaceutical intermediates, and examples of their use can be found in treatments for irritable bowel syndrome, the production of anticoagulants, and as intermediates for antibacterial drug and antibiotic synthesis[102].

In addition, the same strain of *Sphingomonas* has been used to catalyse *N*-substituted azetidines, piperidines, and pyrrolidin-2-ones, which have uses in carbapenem antibiotic production, epilepsy treatments, medication for reducing blood pressure in patients with hypertension, and the synthesis of drugs to combat rhinitis, asthma, and blood coagulation in thrombosis patients[103].

Sphingomonads, which have also been noted for their ammenability to genetic manipulation [104][99][97], could be well suited to applications beyond Earth. Many of the applications listed above would also be useful for human exploration and settlement, and in addition, EPS has been shown to be useful in stabilising regolith[105], controlling the movement of dust in life support systems[106], and enriching soil for food production[107]. This thesis will demonstrate that *Sphingomonas* species, in this case *Sphingomonas desiccabilis*, can also be used for the extraction of mineral resources terrestrially, and in situ from the Martian surface, or from asteroids in the absence of a gravitational field.

2.7 Space Exploration Applications

Aside from helping to answer fundamental science questions about how terrestrial and extra-terrestrial extreme environments affect microbial cells and biofilms, investigations into how space conditions affect bacteria can be useful for industry, resource acquisition, life-support systems (LSS), and food production[108].
There is evidence in the records that suggest the Phonetician's used bacteria for manufacturing cement, and that Roman's extracted metal through bio-leaching, understanding the outcome if not the process[109]. In the present day, geomicrobial biofilms extract 15-20% of the world's yearly global copper yield in a process called through biomining, or bioleaching. Geomicrobiology can also be useful for turning barren regolith into fertile soil, filtering particulate matter from air circulation systems, and making microbial fuel cells (see Fig. 9). The research can also elucidate on the behaviour and parameters of non-geomicrobial bacteria, which have applications, in life-support systems and generating food and electricity [107] [110] [111].

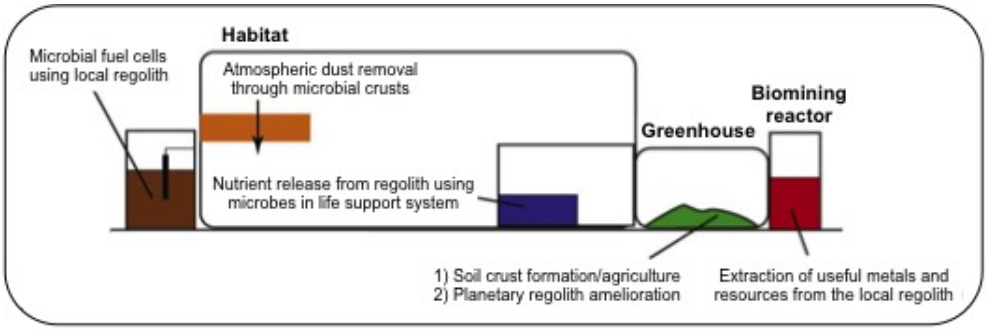

Figure 9: Pictorial representation of the ways in which microbe-mineral interactions could benefit off-world activities. Modified from Cockell *et al.*, (2010).

2.7.1 Life Support Systems

Photosynthesising bacteria can convert carbon dioxide into oxygen, which is useful for human life support systems, but the environment for growth must be maintained at an equilibrium. Geomicrobes can provide fresh nutrients and elements from the local rock or regolith for the benefit of other organisms working in the LSSs to clean air and water, and scrub CO_2. Bacteria can also break down organic waste, producing heat and recycling compounds for agriculture[112][113]. Microbial Fuel Cells (MFCs) can be used to generate electricity at the same time as processing waste in an anaerobic chamber. By introducing *Geobacter* species bacteria to the organic waste and setting up an anode in the anaerobic chamber linked it to a cathode in an aerobic chamber, electricity could also be produced from the bioprocessing[107].

2.7.2 Stabilisation of regolith

The fine regolith on the surface of the moon and Mars can interfere with equipment in two ways. Particles can become electrostatically charged through friction in a process called triboelectric charging, and charges can build up to dangerous levels[114]. Additionally, as the material is very fine, and sharper than most terrestrial dusts, it can enter equipment, causing disruption to moving parts[115], and could enter habitats. Experiments with lunar and martian dust simulants also indicate that the particulate matter would be extremely deleterious to human health, causing inflammation and scarring to the lungs, and subsequent long-term respiratory problems[116]. Sticky EPS polysaccharide produced by geomicrobes forming biofilms in the regolith would help to knit the soil together, as evidenced by Liu *et al.*[106]. The process already transpires in deserts on the Earth, and such biofilms are referred to as biological soil crusts (BSCs). It is possible that a series of filters could be constructed in air flow regions of habitats to trap stray regolith entering through air-locks[107]. By increasing the biodiversity of the microbial inoculum, the process could also be used to fix nitrogen and other useful elements into the regolith[117], creating soil fit for agricultural purposes[113].

2.7.3 Extraction of useful elements

One of the major restrictions for space missions is the mass of the object(s) being propelled out of the Earth's gravity well. The greater the mass, the greater the reserves of fuel that must be expended to lift the vehicle out of the atmosphere. To build a sustainable habitat on another planet or moon will require resources, both for the initial set up, and later for expansion and repairs. Useful minerals and metals also exist on the other rocky bodies, so a portion of those resources

could be acquired in-situ. These could be mined using traditional methods requiring large machinery, high temperatures, and hazardous chemicals that would be dangerous to transport. Another method would be to employ geomicrobial bacteria to extract the desired elements, requiring only a pressurised environment and growth medium[118][119] This latter method would be more cost effective for launching into space, should reduced gravity be found to not impair bioleaching rates.

2.8 Summary and Justifaction

We know the XDLVO forces (electrostatic repulsion, polar charge, Lifshitz-van der Waals forces) are of significance in the instigation of biofilm formation, but we do not know if they are solely responsible for a successful genesis. Biofilms, once begun, are persistent and difficult to dislodge, so they are most vulnerable in the beginning of the biofilm process. Understanding the processes that govern the activity at this scale allows for investigation into preventing harmful biofilms from gaining a beach-head on important pieces of equipment, e.g.- catheters and medical implants, life support systems and water pipes, oil conduits. It can also lead to new techniques for improving the conditions for biofilm formation when they are being employed for the benefit of human endeavours, such as bioleaching, soil enrichment and stabilisation, and air or water purification (see Chapter 4).
Knowing how gravity affects biofilm formation and maturation allows a greater understanding of the effect of macro-scale forces on micro-scale interactions and forces. This also allows for the adaptation and refinement of terrestrial geomicrobiological process for off-world applications. Currently there is a body of literature giving evidence for improved biofilm success in microgravity, but how the biofilm and altered water dynamics affects geomicrobial processes has not been investigated (see Chapter 5).
Hypergravity environments are less prevalent in the environments humans would be likely to search for life or expose themselves to. However, it is considerably more simple to create artificially than microgravity, using acceleration through centrifugation. This allows for easier investigation of the changes to the liquid environment, the bacteria, and the mineral release rates. As a consequence of being easier to simulate for scientific investigation, it would also be easier to employ in industrial applications should a positive relationship be identified. Current studies on planktonic bacteria have shown a benefit for shorter lag times at low accelerations, and a change in the log-lag pattern at higher accelerations, where a population crash is experienced before the exponential phase. There is a knowledge gap in the area of hypergravity biofilms, as there have been no investigations that have been reported or widely considered in this type of altered gravity microbiology until now (see Chapter 6). Additionally, investigating how an increase in gravitational force affects microorganisms will provide a more comprehensive un-

derstanding of gravity's effects on cellular processes and evolution when combined with reduced gravity research.

3 Methodology

Certain techniques were used multiple times throughout the PhD process, an explanation of them here reduces the need of lengthy repetition. The methods will still be covered in the results chapters, but in less detail.

3.1 Culturing

Sphingomonas desiccabilis was cultured in R2A nutrient solution (for recipe see Appendix A), balanced to a pH of 7.2. In order to reduce genetic variation in the bacteria samples used, prior to freezing the bacteria in glycerol, a streaking dilution and colony selection was performed to ensure a collection of isogenic bacteria.

Streak Dilution

Under sterile conditions, either under a bunsen flame or in a laminar flow hood, an existing culture of *Sphingomonas desiccabilis* is diluted across the surface of an agar plate. By streaking the colony out across the surface, it is possible to dilute the culture so that after time for growth - which changes depending on the organism and the media - it is possible to isolate individual colonies.
Using a sterile metal inoculation loop, *Sphingomonas desiccabilis* cells were collected from the R2A culture medium, and streaked across one side of the agar plate. The inoculation loop was then resterilised over a bunsen burner, and the plate rotated 45^o. The resterilised loop was then placed gently on the surface of the agar plate, where the primary culture was deposited, and this primary culture was streaked away from the original streaks in a new direction, over fresh agar. The loop was then resterilised, the plate rotated again, and the resterilised loop repeated the step of streaking the secondary streaks into tertiary streaks. This process was again repeated, further diluting the tertiary streaks into quaternary streaks, and then the agar plate's lid was replaced, and the plate sealed against contamination with parafilm. The quaternary streaks were dilute enough after two days of growth that it was possible to isolate individual colony forming units (CFUs).

Storage in Glycerol

An individual colony was selected from the streak dilution and placed into a glass erlenmeyer flask containing 40ml of R2A, then sealed with a sterile foam bung, which was in turn wrapped in tin foil. This was placed in a shaking incubator overnight, at 100rpm and 25^oC. A solution of 40% glycerol was made up by adding

40ml of glycerol to 60ml of millipore water, 500μl of which was serially allequoted into eppendorff tubes. The overnight *Sphingomonas desiccabilis* culture was then vortexed to create a homogenous solution, and 500μl of this was pipetted into the eppendorff tubes with the glycerol solution. These were labelled, and placed into a box, which was placed in the -80°C freezer, so that at the start of each experiment, fresh bacteria could be used which had not yet had the chance to become genetically divergent from the bacteria used in previous experiments.

3.2 Optical Density

The amount of light transmitted through a material diminishes exponentially as it travels through the material, according to the Beer–Lambert law A=ε(l). Since the absorbance of a sample is measured as a logarithm, it is directly proportional to the opacity of the sample and to the concentration of the absorbing material in the sample. Consequently, using a spectrophotometer, it is possible to quantify the number of bacteria in a set amount of solution by measuring the amount of light lost to scattering.
Samples were prepared for O.D. spectroscopy by vortexing the liquid solution/ suspension until the distribution of opaque material was homogeneous. Using a sterile 1ml pipette tip and a micropipette, 1ml of the homogeneous solution was transferred into a cuvette, which have two opposite opaque sides, and two opposite transparent sides. A blank cuvette was also filled with an abiotic sample so that the spectrometer could be calibrated.
The cuvettes were placed in the spectrophotometer with the two transparent sides forming a path for the light to pass through the cuvette and the solution it contains before reaching the detector. The wavelength of light was set to 600nm, and all samples were running in triplicate.

3.3 Crystal violet

The crystal violet (CV) assay allows for the chemical quantification of biomass attached to solid substrates. The liquid media was removed from the wells containing the samples using pipettes, leaving only the solid sample. Five ml of CV solution was made up in millipore water to 0.04%. The CV must bind to the nucleic acids, and to give it time to do so,the samples were left for 30 minutes. After 30 minutes, the crystal violet was removed from the sample wells, again with a pipette. To wash away surplus CV and biomass that is not adhered to the solid - and therefore not part of a biofilm - the samples were gently washed with phosphate buffered saline (PBS). This involved adding 5ml of PBS and gently sluicing the PBS around the sample with a pipette, and then removing it and repeating the exercise. Once the second washing phase was completed, and all of

the PBS removed from the sample, 5ml of a 33% acetic acid in millipore water solution was introduced and left it for 20 minutes. This freed the CV bonded to the biomass, colouring the 33% acetic acid solution. After 20 minutes, the acetic acid around the samples was homogenised by sluicing with the pipette, and from each sample 1ml of the mixed acetic acid, now with a pinkish-purple tint to it from the released CV, was transfered into a cuvettes for optical density spectrometry. For CV, rather than general *S.desiccabilis* optical density, the samples are read at 550nm, and calibrated with some untreated 33% acetic acid. Abiotic controls of the solid sample treated with crystal violet were also measured, to account for CV that has adhered to non-biological matter. The readings for the abiotic controls were then subtracted from the biotic readings to give final values.

3.4 Microscopy

3.4.1 Confocal Laser Scanning Microscopy

Confocal Laser Scanning Microscopy (CLSM) is a microscopy technique that allows for the construction of 3-Dimensional digital images of solid samples. In this thesis, the samples are exclusively biofilms, and the substrate on which the biofilms are grown are usually - but not exclusively basalt rock slides. Two other substrates were also examined in Chapter 6, quartz sintered discs and 0.22 μm isopore membranes. Samples were prepared initially by removing the liquid culture the bacteria had incubated in, and were then treated with a non-ionic surfactant, 1% Triton X in PBS solution, to permeabilise the biofilm cell membranes. Added in with the surfactant at a 5:1 ratio was the stain 'Sypro Ruby' which stains biofilm matrices and some types of protein, namely glycoproteins, phosphoproteins, lipoproteins, calcium binding proteins, fibrillar proteins (https://www.thermofisher.com/order/catalog/product/F10318).
The samples were left in this mixture for 30 minutes, wrapped in tinfoil to keep the light sensitive Sypro Ruby from photobleaching. After thirty minutes had elapsed, the permeabeliser and dye were removed, and the sample gently washed three times with PBS to remove excess dye that would interfere with the confocal imaging of the biological material.

3.4.2 Scanning Electron Microscopy

Scanning Electron Microscopy uses electrons instead of lasers to build a digital image of a sample. In this thesis it has only been used on abiotic geological samples, to gain a qualitative picture of the porosity of the basalt and of the different minerals that form the majority of the basalt.

Samples were sprayed with gold to aid with electro-conductivity and mounted

on small holder platforms that fit into the SEM stage. The chamber holding the stage and the sample was then closed and sealed, and vented so that the chamber was in vacuum. A focused beam of electrons was scattered across the surface of the sample, and the reflection or passage of the electrons allowed the software to build a detailed topographic image with could resolve to as low as 10nm.

3.5 Inductively Coupled Plasma Mass Spectrometry

ICP−MS can detect and quantify the elements present in liquid samples, and is typically used to measure trace amounts within the range of parts per billion (ppb) to parts per trillion (ppt)(see Fig 10). ICP-MS uses a high-temperature Inductively Coupled Plasma(ICP) source with a Mass Spectrometer(MS) to isolate out pre-selected elements and measure their abundance in a sample. The sample is turned into an aerosol, and injected into argon plasma, where the heat atomises and ionises the sample. Once the ions enter the vacuum chamber, the elements that are being searched for are separated out of the plasma by their mass-to-charge ratio, and fired at the surface of the detector. The detector measures the number of ions striking the detector [120]. For the experiments in this thesis, the mass filter was calibrated using Certipur reference materials. The techniques described above are prohibitive for some of the elements (see Fig. 10) as only elements that can readily be positively ionised make it through the plasma sampling interface into the mass spectrometer[121].

ICP-MS was used in this thesis to quantify the amounts of different elements that were leached from basaltic rock in a liquid environment, with and without the presence of bacteria, in order to contrast biotic and abiotic leaching rates. Samples of the blank nutrient solution, and of the nutrient solution with the bacteria but without the basalt slides, were also exposed to the same conditions and processed in the same way as the biotic and abiotic basalt samples, so that their influence on the elemental composition of the liquid samples could be accounted for.

The liquid samples that go into the ICP-Mass Spectrometer must be a clear solution, not a suspension of particulate matter; but the filtration of a biological materials results in the loss of any leached elements bound to the cellular components of the bacteria. To combat this, the samples were ashed at high temperatures to burn off organics and leave the heavier elements behind. In order to ash the samples, samples were placed in glass vials, with the metal lids only loosely screwed on and placed in the furnace at 100^{o}C for two hours, to allow the water to boil off, then the furnace was turned up to 450^{o}C for five hours, to burn off the remaining organics, and left overnight to cool.

Two drops of 50% nitric acid were then added to each vial, swirled, and left for one hour to help dissolve the remaining powder. The solution was then trans-

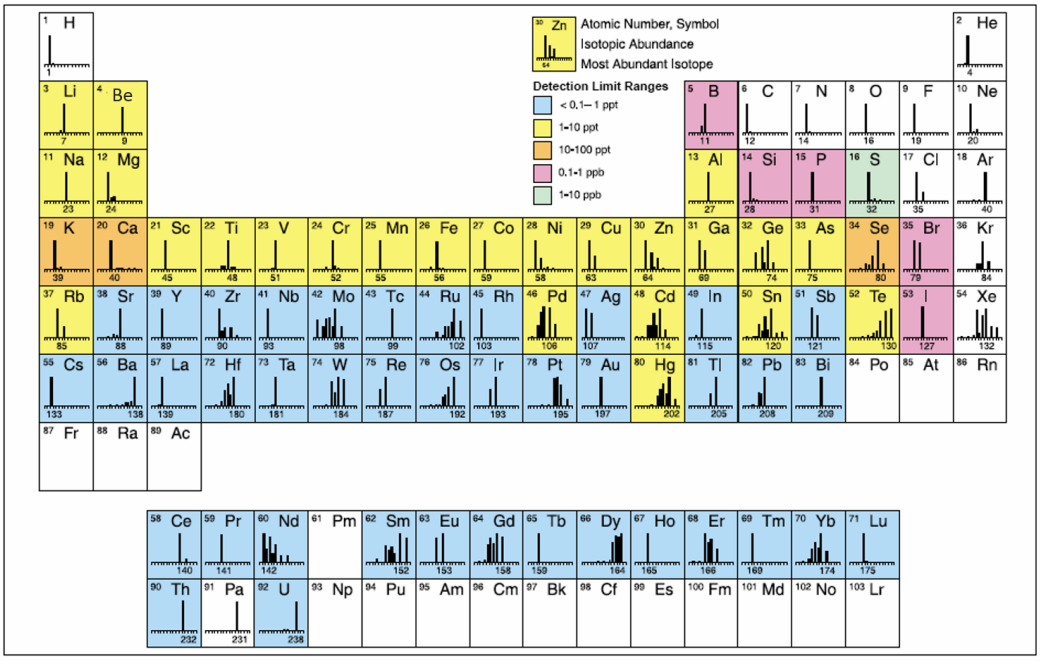

Figure 10: The different ICP-MS spectra and limits of detections for the elements. Elements in the white boxes cannot be measured in this way.

ferred into sterile 15ml falcon tubes, and a further 5ml of 2% nitric acid was added, leaving a clear solution for the ICPMS.

3.6 X-Ray Fluorescence

X-Ray Fluorescence works by firing X-rays at the atoms from a rhodium tube, which at 0.6134 angstroms, or 20.213 keV, has a greater energy than the ionising energy within the atom. As a result, one of the inner k or l shell electrons is expelled, and an outer shell electron falls in to fill the electron hole. In doing so, another x-ray is emitted, this time with a specific frequency/wavelength that identifies the atom as a particular element.

Basalt slides were crushed and ground with a ceramic pestle and mortar, then sieved to achieve the optimum grain size of 50 microns. Two grams of the basalt powder were placed into a glass vial and heated at 110°C for 2 hours. The glass vial was removed from the furnace using long handled platinum tipped tongs, and placed in a desiccator to cool.
The crucible (95% platinum, 5% gold) was weighed, and its weight recorded. Once the vial of powder had cooled, the vessel was tapped on the bench to loosen

the material, and 1g of the contents was transferred into the crucible on the scale. The crucible was covered with a platinum lid and placed on a silica tray, which was transferred to the furnace now heated to 1000°C using the long handled tongs.
After 20 minutes, the sample was removed and allowed to cool before being weighed again to measure any loss on ignition (LOI). Lithium tetraborate flux was added to the basalt powder in a 5:1 ratio and mixed in, to aid in the melting and fusing of the powder into a glass bead. The crucible was returned to the silica tray, the platinum lid was replaced, and the tray was placed back in the furnace at 1000°C with the long handled tongs.
After a further 20 minutes, the tongs were employed to remove the silica tray and to grip the crucible so it could be moved in a horizontal circular motion to gently mix the contents. The crucible, covered again with the platinum lid, was left on the steel block to cool for 10 minutes, then weighed again to see how much more material had been LOI. This was recorded, and more flux was added to bring it up to its target weight of 6g. By this point the fused material had cooled to a solid, and had to be reheated to allow the newly added flux to melt in; a Meker bunsen burner (935° to 1180°C) brought the sample back to the required heat. After 2 minutes, the lid was removed, and the basalt-flux mixture was rotated horizontally for 30 seconds, three times. A clean graphite disc with a steel guide ring placed over it was made ready, and the mixed contents of the crucible was poured in.
An aluminium plunger was immediately inserted into the steel guide ring and depressed slowly and firmly to create the disc. The plunger was left in place for 30 seconds, and then removed, along with the guide ring. A petri dish was placed over the disc to slow the cooling rate and prevent cracking, then the disc was picked up with tongs and quenched in a beaker of water before being moved to a cooler hot-plate. After 20 minutes to allow the disc to properly anneal, the disc was labelled and transferred to the XRF machine.
Dr Nicholas Odling, the senior technical officer of x-ray analysis, operated both the XRD and XRF machines.

3.7 X-Ray Diffraction

Due to the repeating stereochemical structure of mineral crystals, a focused beam of X-Rays will be diffracted in a unique way by each different type of mineral, allowing for identification of mineral content and abundance within a suitably prepared sample.

The basalt was treated with a 3% solution of ethanoic acid to remove the bulk of the carbonate fraction. The residue was then ground under acetone in an

agate grinder. The powder was then placed in the Tema Orbital Grinder, a tungsten carbide mechanical grinder for 3 minutes to further refine the grain size. The resulting powder was sieved to less than 50μm. It was then compressed into a pellet using 8 tons of weight across 40mm for 2 minutes, using the SPEX 3630 X-PRESS. The compressed basalt powder sample was then placed into the Bruker D8-Advance X-ray Diffractomoter, in the School of GeoSciences, Edinburgh University. The X-rays are generated by a Cu-anode x-ray tube, and the diffracted x-rays are detected using an NaI scintillation detector. The resulting diffractograms are then compared to the 2016 International Centre for Diffraction Data database library, and imported to the TOPAS analysis software for Rietveld analysis, performed by Nic Odling, the Senior Technical Officer at the school of GeoSciences.

3.8 Zetasizer

When a surface is placed into a liquid, the partial charges on its surface attract ions to adsorb there, creating a charged layer. An additional diffuse layer of counter ions will congregate around the first layer, held in place by the coulomb force, although this second layer will not be fixed, but will move based on thermal motion and electric attraction; these two layers are collectively known as the electrical double layer. The Malvern Zetasizer uses Electrophoretic Light Scattering (ELS) to measure electrophoretic mobility and calculate the samples' zeta potentials. Having determined the chemical composition of the basalt through XRF, minerals that matched these compositions which are commonly found in basalt were selected and purchased from Richard Tayler Minerals (see section 4.2.1 for more details on mineral identification and selection).
Approximately 10g of each mineral was crushed to powder in a tungsten carbide vibratory disc mill. The zetasizer capillary cells contain a 'u-bend' capillary tube positioned between the positive and negative electrodes, and if the particles are too large sedimentation can occur. As a result, it is preferable to have grain sizes in the region of 10μm or lower. One gram of each mineral powder was weighed out and filtered through Whatman filter papers, with a particle retention size of 11μm inserted into 50ml falcon tubes. Millipore water was added slowly, to a final volume of 30ml. After seeing an accumulation of enough visible powder at the base of the falcon tube, the whatman filter paper was removed, and the falcon tubes were centrifuged for 20 minutes at 2000rpm. The supernatant water was then extracted with pipettes, and the tubes placed in a heater for four hours at 50°C to help remove excess water. Once the powder was dried, it was weighed out so that buffers of different ionic strengths of $NaNO_3$ could be made up to concentrations of 1mM, 10mM, and 100mM.
TO accomplish this, a starting dilution of the mineral powders in the different

buffers was created for each mineral powder, of 0.025g per 1ml. These were then serially diluted to 0.00125g in 1ml, 0.00025g/ml, and 0.0000625g/ml. One ml of each respective sample solution was then injected into the capillary cell and inserted into the zetasizer for ELS and electrophoretic mobility measurements. Powder:buffer concentrations of 0.00025g/ml (10mM) proved to give the most reliable and stable results for all of the different mineral samples.

3.9 Tensiometer

The tensiometer combines optics and computer 'Drop Shape Analyser' software to calculate the contact angle of a droplet of water on a surface, which provides information about the hydrophobicity of a surface.
To ascertain the hydrophobicities of the different samples, samples were placed on the sample stage; once placed on the stage the sample does not need to be manipulated, as the stage can be adjusted across three axis. An aqueous syringe with millipore water in its chamber was then attached to the tower that stands over the sample stage (see Fig. 11). The syringe in the tower is connected to hardware controlled by the user at the software terminal to depress the plunger a given controlled amount, for precision droplets. When measuring sessile drops of water on a solid substrate, 5μl drops are preferable, as drops any larger deform under their own weight, altering the contact angle. However, the smaller the droplet size, the faster the effects of evaporation become apparent, altering the contact angle. Consequently, it is important to capture the image of the droplet on the software as soon as the base diameter of the droplet at the liquid-solid interface stabilises.
The first priority when loading the syringe into the tower is to make sure there are no bubbles in the syringe, which would alter the volume of water expelled by the plunger from the desired value. After holding the syringe upside down and tapping to get the bubbles to the top, the syringe plunger was depressed to evacuate them from the chamber. The syringe was then securely installed into the tower, and the tower was lowered to a level where its tip was visible from the camera. The back-light was turned on, and the value of the desired volume (5μl) was entered into the 'dosing' terminal on the Drop Shape Analyser software. The hardware depressed the syringe by the desired amount, and sample stage was raised to intercept the drop, as the drop should not fall to the sample; the impact deforms the drop and alters its contact angle. Once the droplet was on the sample, the camera was digitally manipulated until the droplet was in focus, and then the contact angle, 'theta', was recorded. The higher the value for 'theta', the greater the hydrophobicity.

In Figure 12, two droplets, one on hydrophobic augite and one on more hydrophilic anorthite, show how the contact angles change depending on the hy-

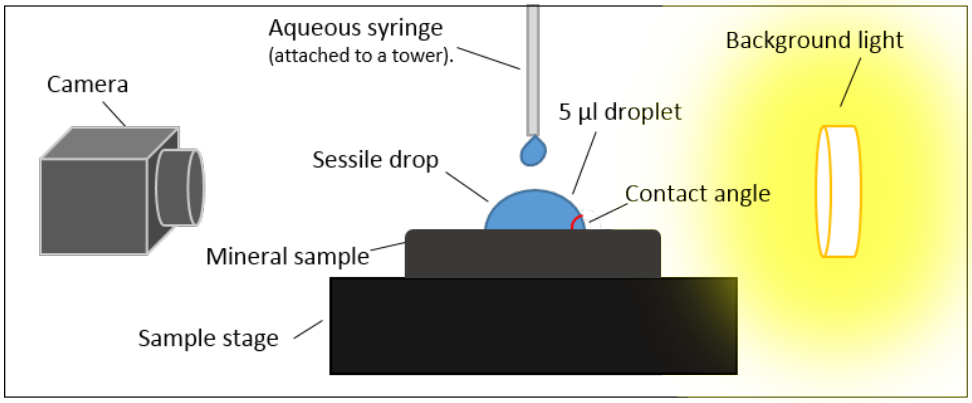

Figure 11: Diagram of a tensiometer, showing its integral components.

drophilic properties of the minerals; the hydrophobic mineral has a more acute angle, while the hydrophilic properties allows a shallower contact angle with more of the droplet coming into contact with the surface.

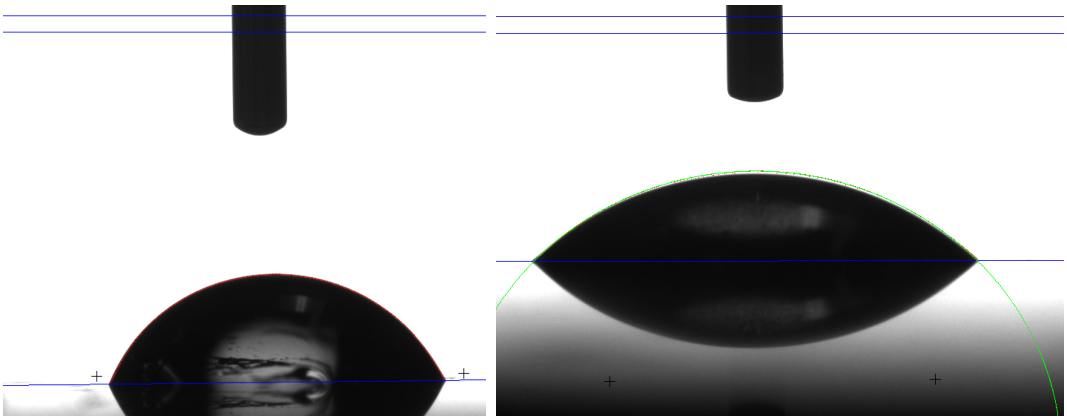

Figure 12: 5μl droplet on the more hydrophobic surface of augite (left) and more hydrophilic anorthite (right).

3.10 Bioinformatics

In order to learn more about the genetic make-up of our model organism, *Sphingomonas desiccabilis*, its DNA was extracted and concentrated for a whole gene sequence (WGS). The (WGS) was performed by Edinburgh Genomics, who used Illumina Next Generation Sequencing. They used a MiSeq sequencer for paired-end sequencing, which allows the DNA fragment to be read in both directions, and which gave read lengths of up to 150 base pairs, specified by the reagent kit.

In order to extract enough DNA for the WGS, two 1.5ml eppendorff tubes were filled with the model organism from a monoculture in exponential growth phase. These were spun for 10 minutes at 4,000 x *g*. The supernatant was then removed by placing the pipette-tip close to the pellet and slowly drawing out the solution. A TE/lysozyme mix was prepared: 10μg of lysozyme to 1ml of TE buffer. Before adding the TE/lysozyme mix, 190μl of the unadulterated TE buffer was added to the pellet from the centrifuge, followed by 10μl of the TE/lysozyme mix. The Eppendorff tubes were then placed in a shaking incubator at 30^{o}C for 20 minutes, before being centrifuged at 4,000 x *g* for 5 minutes. The supernatant was carefully removed again, and a lysing reagent made up to add to the pellet, consisting of: 800μl of DNA lysis buffer, 40μl of Proteinase K, and 30μl of RNaseA (20mg/ml). The lysing mix was split between the two eppendorff tubes, which were then both vortexed for 10 seconds and placed in a water bath at 70^{o}C for 30 minutes, with interruptions for further vortexing at 10 minute intervals.
After the water bath, two Perfect Bind DNA columns were placed into two 2.0ml collection tubes. The contents of each respective ependroff tube and 100μl of DNA Binding Buffer were transferred into each Bind DNA column. The columns were then centrifuged at 10,000 x *g* for 1 minute, and then the collection tube and its contents were discarded, and the DNA column was transferred into a fresh collection tube. Six-hundred and fifty μl of DNA wash buffer was then added, and the samples were spun again at 10,000 x *g* for 1 minute. The DNA column was again transferred to a fresh collection tube, 650μl of DNA wash buffer was added to each sample, and they were spun again at 10,000 x *g*. This time without discarding the collection tubes, the waste from the collection tubes was discarded, and the columns were placed back in their collection tubes for a further 2 minutes of centrifugation at 10,000 x *g*. At this point, all that should be left in the columns is concentrated DNA.
The DNA columns were placed into sterile 1.5ml eppendorff tubes with 30μl of elution buffer and left for 3 minutes before centrifugation at 6,000 x *g* for 1 minute. Using a NanoDrop Microvolume Spectrophotometer, with the dsDNA option selected, 2μl of elution buffer was placed onto the metal stud to blank the spectrophotometer. The eppendorff tubes with the DNA were then vortexed to homogenise the distribution of the contents, and 2μl from each tube was placed on the stud for reading. The stud was wiped clean between the samples.

The DNA, having reached the desired concentrations, was then handed over to Edinburgh Genomics for Whole Gene Sequencing, who performed a quality check on the DNA before queueing it for sequencing.

4 The Properties of Basaltic Minerals and their Effects on Microbial Adhesion

4.1 Introduction

Bacterial adhesion to a solid substrate, both reversible and irreversible, are the primary stages of biofilm formation. Attachment most commonly refers to the initial reversible stage of physical contact of a bacterium to a solid substratum, while the term adhesion refers to the complete process of a cell becoming irreversibly attached - including the initial reversible stage of attachment.
As bacteria are predominately found in biofilms in any nutrient-sufficient aquatic system[3], and biofilms begin with the attachment and adhesion of a single bacterial cell, there has been significant body of research conducted on the process of microbial adhesion. As bacteria have adapted to take advantage of every type of surface available, these adhesion studies have been conducted in many different fields, such as biomedicine, soil and plant ecology, the food industry and any industry that relies on piping liquids, such as the oil and waste industries. Classically, microbial attachment and aspects of the subsequent irreversible attachment, has been described using the DLVO (named after Derjaguin, Landau, Verwey, and Overbeek), or more commonly in recent times, the extended DLVO theory (XDLVO)[11][12] [13] (see section 2.1.1 for more details). DLVO theory, which was initially developed for colloidal physics, asserts that the forces dominating during attachment are the hydrophobic and coulomb interactions[122]. Hydrophobic interactions can further be broken down into long range Lifshitz-van der Waals interactions and short range hydrogen bond interactions[123].
Recent studies in medical microbiology have shown that, for pathogenic microbial attachment to host cells, the DLVO theories fails to adequately predict or describe microbial attachment. Unlike the homogenous surface of a colloid, a cell surface is heterogeneous, and it is impossible to describe the surface of a cell - bacterial or otherwise - with a single value, however this is a necessary approach in the DLVO theories, where a single value is given for e.g.- the electrophoretic mobility of a surface. In addition, over the time scales of evolution, bacteria have developed appendages that are narrow enough to penetrate the energy barriers and over-come the repulsive forces present at the surfaces of solids. These nanofiber appendages, known as fimbriae or pili, are constructed of repeating protein subunits, tipped with specific adhesins that can bind to sites on host cells and abiotic substrates. They are generally recorded as growing up to 2μm, but one paper claimed they could grow between 0.2 and 20mm in length[124], which was most likely a typing error. The length of the pili allows for a microbial cell to make initial contact with a surface from a distance that is potentially beyond the effects of some of the DLVO and XDLVO forces.

Pathogenic bacteria are not the only bacteria with pili; many bacteria, both gram negative and gram positive, have been identified as having fimbriae of some kind[125]. It is known from the Whole Gene Sequence performed on the model organism *Sphingomonas desiccabils* (see section 5.3.3 for more details) that the species contains fimbriae known as Tad pili (from **T**ight **Ad**herence), or Flp (**f**imbrial-**l**ow-molecular weight **p**rotein) (see Appendix C), which are associated with initial adhesion, cellular aggregation and biofilm formation[126][127].
This chapter is attempting to determine whether the DLVO theory can still be applied to microbe-mineral interactions, as mineral surfaces are less complicated than biological surfaces, and the characterisation of the mineral surfaces may still allow for some useful predictions. However, while a mineral surface is more simple than a host cell surface, in a liquid environment it will develop a layer of adsorbed molecules, known as the conditioning layer. The research conducted attempted to categorise the physical properties of the mineral surfaces, and see whether the DLVO theories can still be applied to the adhesion of bacterial cells to mineral surfaces.

Certain mineral surfaces within a rock will have physical characteristics that will make them easier for the bacteria to approach, according to the DLVA and extended DLVA theories. In this chapter, the hydrophobicity, surface charge, and porosity of the different minerals are being measured and discussed, along with the elemental composition and subsequent mineralogical structure of the minerals, in order to attempt to rank these properties in order of greatest contribution to microbial attachment, and to see whether any pattern in preferential attachment and DLVO theory can be found. All measurements are being conducted in neutral pH conditions (6 - 8), as acids and alkalis influence mineral disaggregation, increasing nutrient availability and altering the surface texture of the minerals.

4.2 Physical Characteristics of the Basalt

Basalt is made up of a number of different minerals, each of which will have different physical properties, resulting in a heterogeneous surface at the basalt interface.
While different physical and chemical factors could also influence attachment, four were selected for investigation; the chemical make-up of the minerals, the specific surface area, the hydrophobicity, and the surface charge. Hydrophobicity and surface charge were chosen as the principle factors in the colloidal physics XDLVO approach, and specific surface area and the available nutritional elements (stereochemistry) were chosen as likely geomicrobial influencers based on reviews of the appropriate literature.
For these investigations, the following methods were employed; X-Ray Diffraction

(XRD) and X-Ray Fluorescence (XRF) to determine the mineral and elemental content of the basalt, Scanning Electron Microscopy (SEM) to give an indication of specific surface area, tensiometry (also known as goniometry) to measure the hydrophobicity of the mineral surfaces; and a zetasizer was employed measure the electrophoretic mobility/surface charge of the individual minerals.

4.2.1 Basaltic Composition

Basalt is the most abundant rock type in the Earth's crust, and is also a ubiquitous component of the rocky bodies in our solar system [128]. It is formed when basaltic magma comes to the surface and cools, solidifying into a fine grained rock, of dark colour. Despite being fine grained, it can have high porosity and permeability due to air bubbles caught in the cooling magma, and the contraction of certain igneous grains. The basalt used in the research here and in the subsequent chapters is of Icelandic origin, and is vesicular. Its chemical and mineralogical compositions are listed below, determined using XRF and XRD (see 5.6 and 5.7 for detailed methodology):

XRF

To prepare the basalt for XRF, 3 grams were ground into a fine powder and sieved to remove particles larger than 50μm. Two grams of the powder was then heated at 110^{o}C for two hours, and then 1000^{o}C for 20 minutes. It was then mixed with lithium tetraborate flux to facilitate the formation of a glass bead, before the sample was returned to the 1000^{o}C furnace for an additional twenty minutes. Once all of the flux and basalt had melted into the liquid and mixed, it was poured into a mould and compressed into a disc.
XRF is a fully quantitative method of analysis, checked against referenced standards. For basalts these were the following rocks: Govindaraju for the international standard, BHVO-1 as a well characterised rock used by the University of Edinburgh, and BIR1, as an Icelandic basalt, similar to the one being tested here. Based on the analysis, the compounds in Table 1 were determined as being the major and trace components of the basalt matrix, and are represented in a pie chart in Figure 13.

Table 1: X-Ray Fluorescence Results; Chemical Analysis of the Basaltic Minerals

Chemical Composition	Percentage of Basalt
SiO_2	47.48
Al_2O_3	15.35
Fe_2O_3	12.12
MgO	10
CaO	11.69
Na_2O	1.92
K_2O	0.162
TiO_2	1.344
MnO	0.186
P_2O_5	0.128
Loss on Ignition	-0.57
Total	99.82

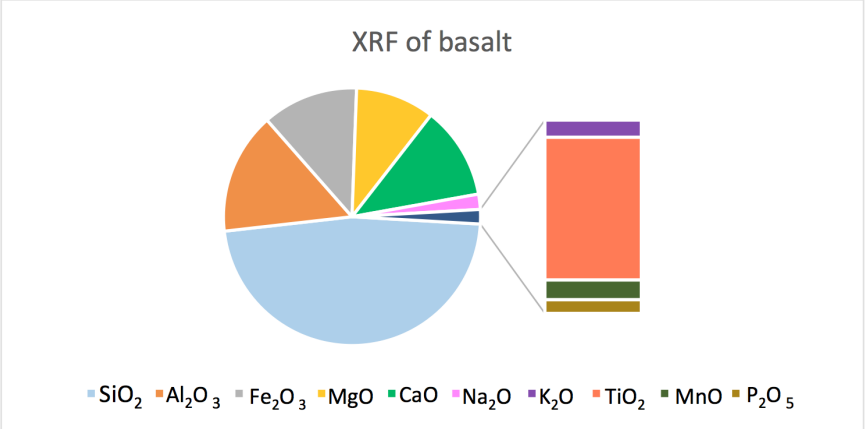

Figure 13: Pie chart showing the percentages of the major compounds making up the basalt rock. Data from X-Ray Fluorescence.

Table 2: X-Ray Fluorescence Results; Trace Elements Within the Basalt

Element	Quantity in PPM
Cr	402.1
V	268.8
Ni	183.7
Sr	176.6
Cu	108.7
Zn	87.7
Zr	65.5
Ba	42.8
Sc	35.9
Y	20.5
Ce	14.8
Nd	9.5
Nb	7.5
Rb	3
Pb	0.9
U	0.6

XRD:

Five grams of basalt were crushed by hand in a mortar and pestle, and then poured into a tungsten carbide grinding mill (a Tema Orbital Grinder) for 3 minutes to mechanically complete the process of grinding it into a fine powder. This was then sieved to ensure particles greater than 50μm were removed, for better signal-to-noise ratio. The powder was then compressed in a SPEX 3630 X-PRESS hydraulic laboratory powder press, and placed in the X-ray Diffractor for analysis.

Figure 14 shows the output of the spectral analysis and Table 3 shows the mineral composition of the basalt along with percentage values. This table has been simplified from the original, with certain sub-groupings of minerals condensed into their category mineral type. The more extensive broken down XRD table is available in Appendix B. It is worth noting that XRD is a semi-quantitative analysis, with +/- 10% relative error.

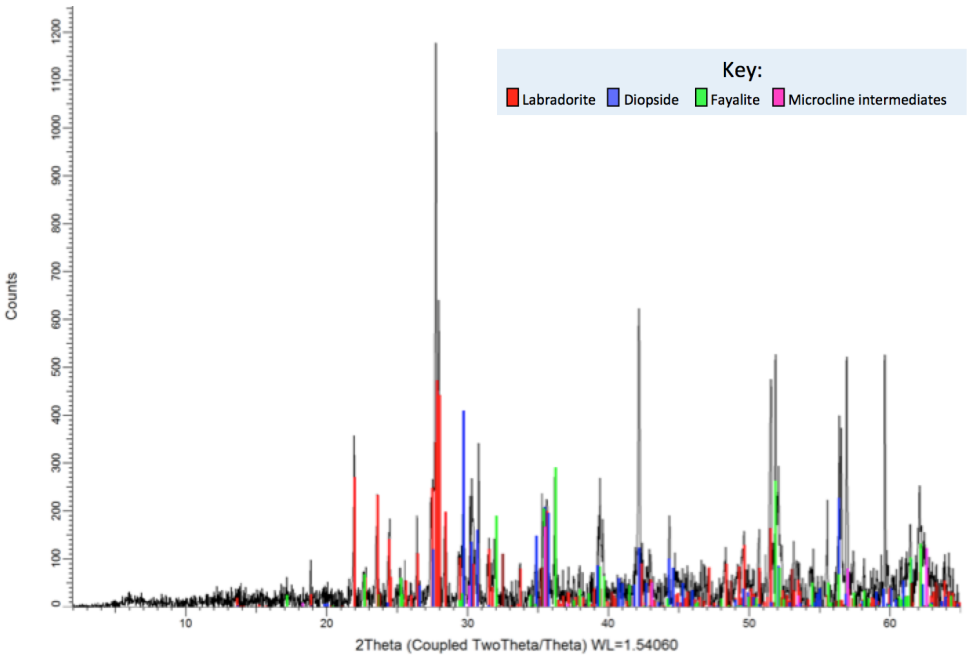

Figure 14: The output from the XRD spectral analysis. The largest peaks are labradorite, a plagioclase; diopside, a calcic clinopyreoxene; fayalite, an olivine; and microcline, an alkili feldspar.

Table 3: X-Ray Diffraction Results; Basaltic Minerals and their Percentages

Mineral	Percentage of Basalt
Plagioclase (labradorite)	62.4%
Calcic Clinopyroxene	16.5%
Olivine	9.6%
Microcline	8.4%
Muscovite	2.3%
Orthoclase	0.7%

Mineral selection and justification

Using the XRF and XRD results, the following candidate mineral crystals were selected for the investigation into the properties of basaltic minerals that dominate attachment:
Quartz: SiO_2; to act as a negative control. While quartz crystals were not found in high abundance in the basalt sample, SiO_2 was the most abundant compound

in the basalt. Of the bonds present in silicates, Si:O bonds are generally the hardest to break [129], [130], [131], consequently it is expected that quartz will be weathered and attached to the least of all the minerals.
Anorthite: $CaAl_2Si_2O_8$. Anorthite and albite were selected as the two end members of plagioclase, with anorthite as the Ca extreme and albite being the Na extreme ($NaAlSi_3O_8$). However, when experiments with albite were attempted, it was discovered that the mineral was too flaky to treat in the same manner as the other minerals, and anorthite became the only plagioclase.
Augite: (Ca, Na)(Mg,Fe^{+2},Fe^{+3},Al,Ti)(Si,Al)$_2O_6$. Augite was chosen to represent the calcic clinopyroxenes.
Olivine: (Mg^{+2}, Fe^{+2})$_2SiO_4$. Olivine represented 9.6% of the composition of the basalt rock. It can be composed of pure Fe_2SO_4 - fayalite, or pure Mg_2SO_4 - forsterite, but is most commonly a mixture of the two. The basalt used for these experiments is a mixture, but XRF was not performed, so the ratio of Mg:F is not known.
Microcline: $KAlSi_3O_8$. Microcline constituted 8.4% of the basalt rock. It is a potassium-rich feldspar, with triclinic axes - which means one of its axes are canted compared to monoclinic and orthorombic crystals. It is more stable at lower temperatures than orthoclase, suggesting it may be more resistant to microbial weathering.
Orthoclase: $KAlSi_3O_8$ Orthoclase was chosen to represent the felsic monoclinic minerals instead of muscovite, despite being present in a lower concentration. This is because it has the same chemical composition as microcline, allowing for a clearer comparison of the influences of its other properties.
Basalt was also used as a positive control in all of the experiments, but not all of the data is included here.
For clarification, any of the bracketed elements may hold the position within the mineral structure, and are typically listed in order of likely abundance.

Results on the controls for an ICP-MS experiment conducted on *Sphingomonas desiccabilis* in Chapter 5 (results not shown) indicated a 7% increase in magnesium compared to the ICP-MS of the nutrient solution, and a 14% increase in potassium compared to the ICP-MS of the nutrient solution alone. The other nutrients did not show any meaningful increase, although it was not possible to measure the sodium or silicon content of the cells with the broad range semi-quantitative ICP-MS run. This would suggest that *S. desiccabilis* cells contain high levels of K and Mg, and require it for their cellular processes.

Table 4 serves as a guide to the biological function of the elements that compose the minerals listed above, with information taken from:[132] [133], [134], [135], [136], [137], [138] and [139].

Table 4: Bio-Applicability of Mineral Elements

Elements of the compounds in order of their bio-applicability to the model organism	
Element	Biological Function
Fe	Component of cytochromes and certain nonheme iron-proteins. A cofactor for some enzymatic reactions. Important for respiration, the tricarboxylic acid cycle, oxygen transport, gene regulation, and DNA biosynthesis.
K	Main cellular inorganic cation and cofactor for certain enzymes. Essential for protein and polysaccharide synthesis, as well as for transport and antiport across membranes. Four main roles: (i) an osmotic solute, (ii) an activator of intracellular enzymes, (iii) a regulator of internal pH, and (iv) a second messenger.
Mg	Inorganic cellular cation, cofactor for certain enzymes. Binds with ATP to make it biologically active, and stabilizes ribosomes and cell membranes.
Na	Cellular cation, a gradient of which can provide energy for transport of nutrients and ATP synthesis in certain bacteria. Found in enzymes and transporters/antiporters.
Ca	Inorganic cellular cation, used for structural components of cells, and as a cofactor for certain enzymes.
Si	Specialised uses in some life, mostly inert.
Al	Aluminium does not provide any biological functions and in many cases is considered toxic, as it can compete with magnesium and iron, and bind to active sites on DNA and membranes.
Ti	Can be bactericidal, especially in its Ti^{+4} cation.

Based on the current understanding of which elements are important for prokaryotic cellular functioning, it is possible to loosely rank the minerals in order of their nutritional relevance to the model organism, as follows:

1) Olivine $(Mg^{+2}, Fe^{+2})_2SiO_4$: Olivine contains Fe and Mg, which are both biologically useful for cellular activities, and does not hold any of the elements that could have a negative impact on cellular activities.
2) Microcline/orthoclase $KAlSi_3O_8$: The potassium content of the mineral will be valuable for a number of cellular functions, but the benefits may be slightly off-set by the presence of aluminium.
3) Augite $(Ca, Na)(Mg,Fe^{+2},Fe^{+3},Al,Ti)(Si,Al)_2O_6$: Augite is an elementally variable mineral. Ca and Na are both somewhat advantageous, although required in lower volumes by prokaryotes compared to Mg and Fe. Mg and Fe are both possible place-holders on the second site, but so is Al and Ti, neither of

which are useful, and which may be detrimental.
4) Anorthite $CaAl_2Si_2O_8$: Ca can be a useful element for cellular processes, as a cofactor or a structural component, however Aluminium could be deleterious by competing with Mg and Fe for binding sites.
5) Quartz SiO_2: Quartz is chemically stable, and therefore relatively inert. It will contribute little, if anything, of benefit or detriment to the cells.

A note on Orthoclase and Microcline Microcline and orthoclase have the same chemical composition, but their atoms are latticed in different crystalline structures. Microcline is triclinic, meaning the atoms are arranged in a system of three axes of unequal lengths, at nonperpendicular angles to each other, whereas orthoclase is monoclinic, with three axes of unequal lengths, two of which are perpendicular to each other.
The main difference this leads to is in the type of twinning (symmetrical growth) that can occur in the crystalline structure. Microcline, as a triclinic feldspar, can form polysynthetic twins, where reflected symmetrical crystal growth segments are joined across a composition plane, creating a crystallographic repeating pattern of closely stacked smooth planes (see Fig. 15) a). Orthoclase, as a monoclinic feldspar cannot form these polysnthetic twins, but forms carlsbad twins, which are formed by a 180^o rotation on the c-axis, leading to a more irregular crystallographic structure(see 15 b). In other words, at the scale that bacteria occupy, microcline can present a smoother surface than orthoclase, although it is also capable of forming other twinning types.

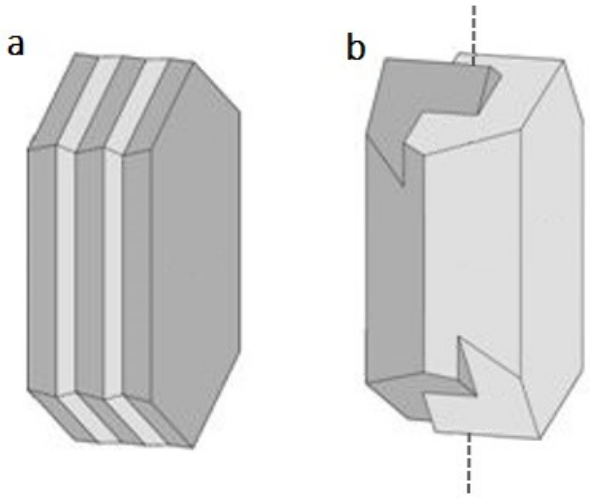

Figure 15: Figure showing the different twinnings that separate microcline and orthoclase. a) Polysynthetic twinning, symmetrical and closely stacked repetitions along the composition plane; b) Carlsbad twinning, symmetrical but irregular repeating pattern, rotated around the c-axis.

4.2.2 Porosity

Establishing the porosity of the different minerals that made up basalt served two purposes. As discussed in the background chapter, surface area has a large part to play in the rate of weathering; the greater the surface area, the more available space for the bacteria to attach and alter the chemistry of the surface. Surface area is determined by 'roughness', pore size, and pore distribution[140]. Roughness, or rugosity, also provides an advantage of more Gibb's free energy at the edges and defects in a crystal's lattice structure. Atoms at these sites will have a lower coordination number, meaning they are more reactive as there are more free sites for molecules to link with. Defects come in the form of point, line, and planar defects, and also include kink sites, where a change in the lattice occurs in more than one direction, exposing yet more low coordination atoms [141].
The second reason to measure porosity was to aid in the determination of the hydrophobicity of the different minerals required establishing the porosity (see 6.2.3, Hydrophobicity subsection).

To paraphrase Lawrence and Jiang (2017) in their chapter exploring the different techniques for analysing pore spaces, porosity is a difficult parameter to quantify because pore spaces can range from single digit nanometres to the millimetre scale, and no one methodology that can cover that range.

SEM was chosen over other methods because of the equipment available at the

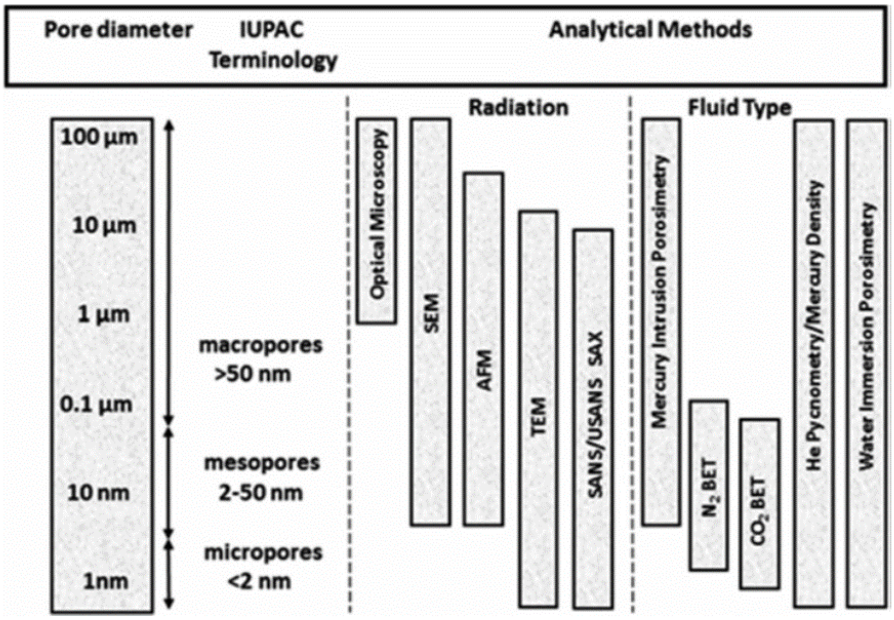

Figure 16: The different methods for analysing porosity and pore size distribution of solids at different scales. From Anovitz and Cole, 2015; and Lawrence and Jiang, 2017).

James Clerk Maxwell Building, and because of financial and resource limitations (see section 4.5.1 for more details), and because it has been shown to be a successful indicator of porosity[142].

In order to establish porosity, samples of each material were cut and sanded to a 'smooth' surface, then given to the technician to spray with gold, so that the electrons from the Scanning Electron Microscopy (SEM) could move freely across the surface of the samples without a build up of dangerous charge. The samples were then examined and photographed at high resolution, with photos taken in the μm range.

To determine average pore sizes, six photos per mineral were opened in FIJI, the software analysis tool-kit. The images were transformed to grey-scale, and the brightness was enhanced to its maximum setting. Using the 'threshold' command, so that the surface of the mineral was entirely white, with no shadows or contouring, apart from where a pore space was too deep for the 'light' to penetrate, which showed as black. This black and white image was then subjected to the 'Analyse Particles' analysis, which gave a numerical value for the amount of the image that was black vs white, corresponding to the amount of mineral surface that was pore vs solid substrate (see Fig. 17).

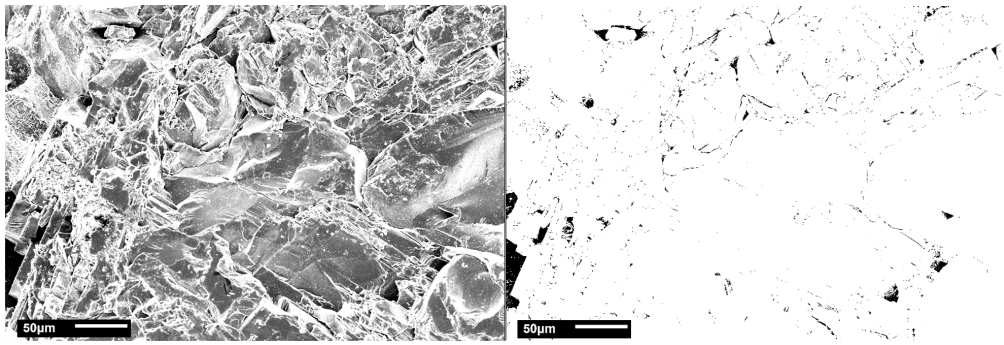

Figure 17: Example of the FIJI technique for determining porosity. Both images are of the same area of basalt area captured through the SEM. The left image shows the surface pre-alteration on FIJI, and the right image shows the image post-alteration on FIJI. The percentage of the area covered by pore spaces here is 11.34%.

These values were then averaged, and standard error calculated (see Fig.18). Anorthite was the most porous, followed by augite, orthoclase, microcline, olivine, and quartz, with the last three being in the range of 0.009 - 0.02%, and the more porous minerals being above 0.2%.

4.2.3 Hydrophobicity

Hydrophobicity is widely accepted as an important factor in the DVLO and XDVLO models of bacterial adhesion.
Gram negative bacteria are generally hydrophilic due to the phospholipids bilayer structure of their outer membrane. *Sphingomonas* species, while still hydrophilic, have been shown to be more hydrophobic than other gram negative bacteria, due to their distinguishing feature of having glycosphingolipids in their outer membrane instead of lipopolysaccharides, which have a shorter carbohydrate moieties[97]. Brown and Jaffé (2006) measured the contact angle of a *Sphingomonas* sp. as having a contact angle of 37^o[143], compared to *E.coli*, which had an average contact angle of 25.3^o [144]. Hydrophilic bacteria attach more readily to hydrophilic surfaces, and hydrophobic bacteria to hydrophobic surfaces [122][124].
Hydrophobicity and hydrophilicity are relative terms, but generally an angle lower than 45^o is considered hydrophilic, and an angle greater than 45^o is considered hydrophobic [145]. The hydrogen bonding between water molecules near a hydrophobic surface is more disordered, and more structured around a hydrophilic surface[124].

In order to quantify the hydrophobicity of each mineral, the minerals in question had to be cut and sanded, then embedded in epoxy resin and sanded down again

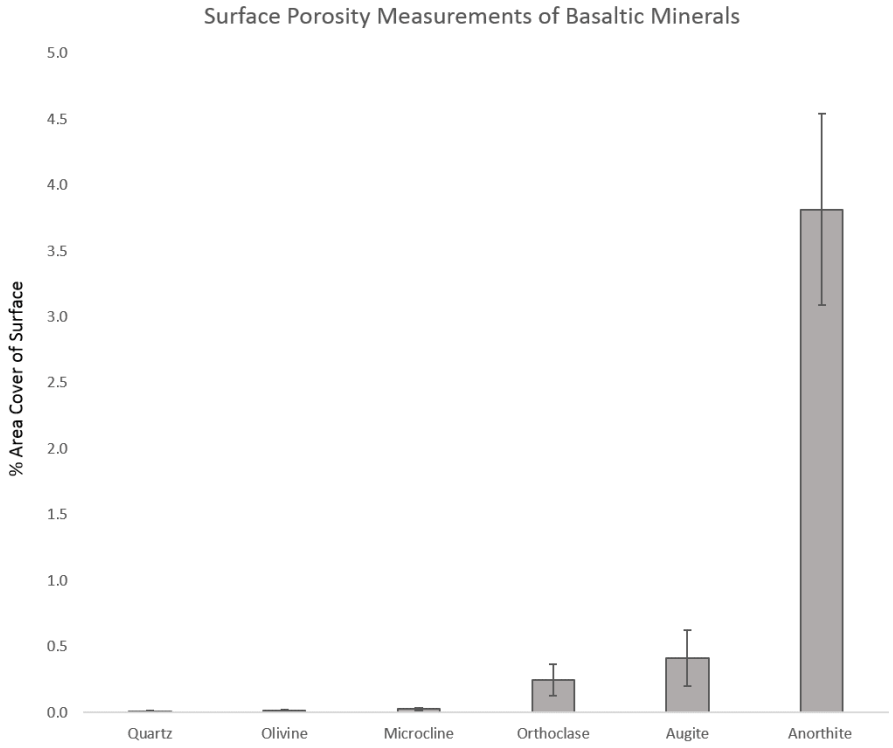

Figure 18: Two-dimensional measurements of the porosity of the different major minerals that comprise the basaltic rock. Measurements reflect the percentage of the surface that was occupied by pore spaces. Basalt porosity (30.8%) not included.

to give a completely smooth non-porous surface. If pore spaces remained, the water would move downwards through them, altering the shape and contact angle of the droplet. The porosity of the samples was established so that the absolute hydrophobicity could be calculated without the epoxy affecting the measurement, using equation 2, below.

By taking a photo of a 5μm droplet on a surface, the tensiometer, with the use of the software 'Drop Shape Analyser', measures the contact angle where the water meets the surface and becomes deformed by its own weight (see Fig. 19). The shallower the angle, the less hydrophobic the surface. The contact angle measurement needs to be taken as soon as the droplet has been placed on the mineral sample and its base diameter has stabilised, as evaporation will begin quickly, reducing the size of the droplet and changing the apparent contact angle. Ten repeats per mineral were taken to minimise error.

Scanning Electron Microscopy (SEM) was performed on the different minerals

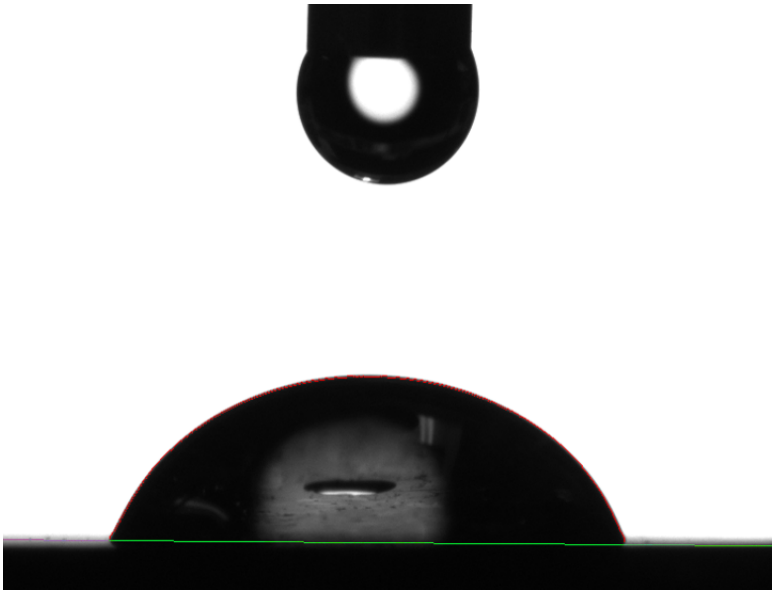

Figure 19: 5μl droplet on the surface of basalt

to get an average size of their pore spaces (see above, section 4.2.2), so that the effect of the epoxy resin on the mineral hydrophobicity could be subtracted, using the following equation:

$$\cos\theta = \frac{(\cos\theta^* - f_2 \cos\theta_2)}{f_1} \tag{2}$$

In equation (2), cos theta is the contact angle of the substrate we are trying to determine, cos theta * is the apparent angle, the angle measured of the mineral with the epoxy, and cos theta 2 is the contact angle of droplets on epoxy resin, which was also measured as a control. The SEM gave values for f1 and f2, which are the surface areas occupied by the mineral (f1) and the epoxy resin (f2)[146].

Once the effect of the epoxy had been removed, the contact angles for the different minerals are shown in Table 5.

Table 5: Mineral Contact Angles

Contact Angles of Basaltic Minerals	
Mineral	Contact Angle
Anorthite	48.9
Quartz	49.2
Orthoclase	56.6
Microcline	57.5
Basalt	68.9
Augite	70.1
Olivine	77.9

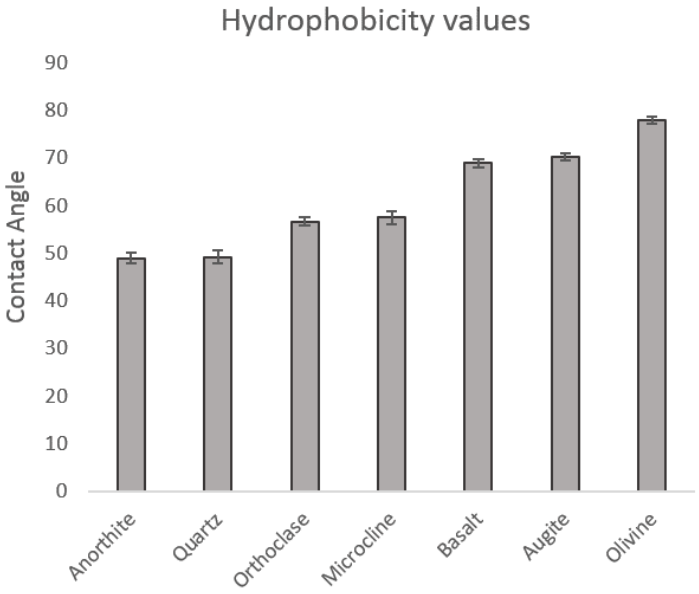

Figure 20: Basalt and its composite minerals, seen from left to right in order of least to most hydrophobic.

As hydrophilic bacteria are more inclined to attach to hydrophilic materials, Figure 20 could be read from left to right as the most to least favourable minerals for initial attachment of *Sphingomonas desiccabilis*, based on hydrophobicity alone.

4.2.4 Surface Charge

As surface charge is considered one of the most important short-range forces in the DVLO theories, the electrophoretic mobility of the bacteria and the minerals in question needed to be ascertained. For the minerals this involved grinding them into a fine powder and ensuring the particles were no bigger than 11μm.

The different minerals were ground up into powders using a tungsten carbide grinding mill, the Tema Orbital Grinder, for 3 minutes on its only setting.
Three different concentration of sodium nitrate buffers were made up, at 1mM, 10mM and 100mM, as it was not certain which buffer would provide the best conductivity for the samples. The best conductivity would lead to the most stable reproducible results, so the minerals were tested in each buffer to find the results that didn't climb or fall over the course of the multiple runs.
One gram of each mineral was weighed out, and washed through grade 1 Whatman Filter papers, folded into quarters and inserted into a 50ml falcon tube in a tight cone. The paper allows particles smaller than 11μm to pass into the falcon tube, and 30ml of nanopore water was washed through the powder in the tubes. The tubes were then centrifuged at 2000rpm for 20 minutes to ensure sedimentation of the particular matter. The water was then extracted with a pipette, leaving the powder in the bottom of the tube. Some water was still present, and so the tubes were placed in a heater for four hours to ensure the powder was dry. The mineral powders were then weighed, and 0.005g was placed in 2ml of each respective $NaNO_3$ solution, shaken, and 1 ml of the resulting suspension was prepared for insertion into the Zetasizer.

Electrophoretic mobility was performed using a Malvern Zetasizer Nano. Having checked the capillary cells were uncontaminated and the contacts were springy and clean, 1ml of the culture was injected slowly into the cell to avoid bubbles forming. The holes were stoppered, and the cells placed into the Zetasizer. The computer was then turned on, and the Malvern software was activated.
When measuring the electrophoretic mobility of the minerals, the material was selected as 'silica', the dispersant 'water'; temperature '24^{o}C'; model 'Smoluchowski'. Capillary cell type 'DTS1060'. The $NaNO_3$ solution with the best ion concentration for stable results was the 10mM solution, all mineral electrophoretic mobility results given in this chapter are from the measurements of the 10mM solution.

For the measurement of *Sphingomonas desiccabilis* electrophoretic mobility, attempted cell dilutions were the 4 day culture at 10^3, 10^1, and 10^0, and the overnight culture at 10^0 dilution. The culture dilution that gave the most stable readouts was the overnight culture, at no dilution. When measuring the electrophoretic mobility of the bacteria, the material was selected as 'bacteria'; the

dispersant 'water'; temperature '23^{o}C'; model 'Smoluchowski'; sample viscosity 'dispersant'. Measurements were taken at 20V and 50V, to ensure readouts were in the same range at both voltages.

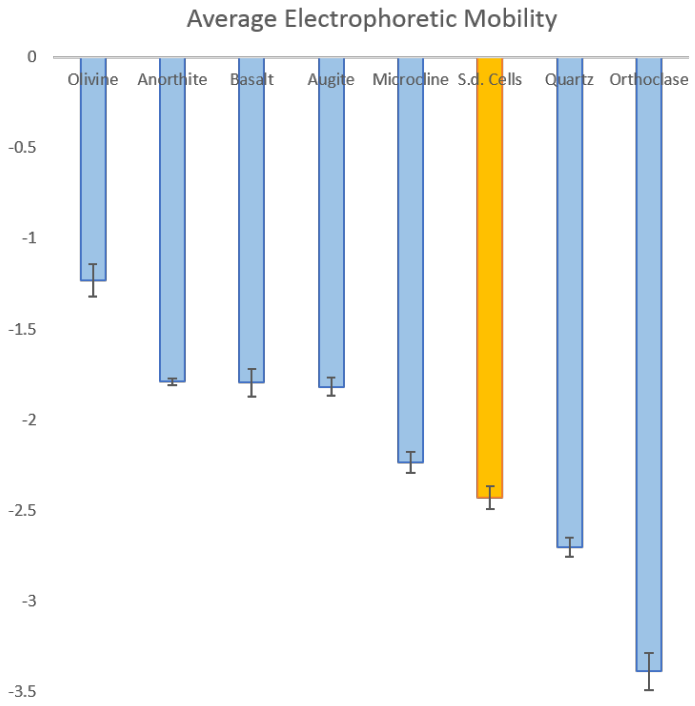

Figure 21: The blue bars show the electrophoretic mobility (μ_e) of basalt and its constituent minerals arranged according to charge. The yellow bar 'S.d. cells' shows the μ_e) of *Sphingomonas desiccabilis*.

Sphingomonas desiccabilis and all of the mineral powders exhibited a negative electrophoretic mobility. The results can be seen in Figure 21.

As all of the materials measured here are negative, there will be a slight repulsive force acting on the bacteria as it approaches any of the mineral surfaces. The efficacy of this repulsive force will vary depending on the ions and other solutes in the solution, some of which may act to neutralise the negative charge carried by the materials. The bacteria themselves will not have a uniform surface charge across the whole membrane, different surfaces and appendages will have their own electrical potential, rather the electrophoretic mobility recorded represents an average once the cations and anions across the whole surface have balanced out [147].

4.2.5 Summary

Quartz:
In terms of stereochemistry, quartz, as a representation of SiO_2 - which makes up 47% of the basalt's chemical composition - provides the least amount of nutritional value. As discussed in section 2.3, its stability would make it difficult for the bacteria to access the elements present there, and, as shown in Table 4, silicon itself is not known to have any cellular applications. Quartz also provides the least amount of surface area for bacterial attachment, being the least porous compared to the other minerals tested here, with a porosity of only 0.009%. It has an electrophoretic mobility of only $0.3\mu_e$ more negative than *Sphingomonas desiccabilis*, and is the second most hydrophilic of the minerals, after anorthite, with an average contact angle of 49.2^o.

Anorthite:
The chemical formula of anorthite is $CaAl_2Si_2O_8$. The most useful elemental contribution it can make to the metabolism of *S.desiccabilis* is calcium, the benefits of which may be tempered by the presence of aluminium. SEM analysis showed anorthite to be an order of magnitude more porous than augite and orthoclase, and two orders of magnitude more porous than quartz, olivine, and microcline. Anorthite had an average contact angle of 48.9^o, making it the most hydrophilic. Its electrophoretic mobility was -$1.8\mu_e$, making it the second least negative after olivine, theoretically making it the second least repulsive mineral surface of those measured.

Augite:
The chemical formula for augite is more variable than for the other minerals, being: $(Ca,Na)(Mg,Fe,Al,Ti)(Si,Al)_2O_6$. Ca and Na both provide useful cations, so the augite will be able to contribute some useful nutrients, whichever of those two elements constitutes the first part of the mineral equation in each specific case. The second part of the equation is yet more diverse, with four possible elements filling in the space. Mg and Fe could be of use to *Sphingomonas desiccabilis*, but Al and Ti are both potentially toxic. The third part of the equation, has Si or Al, which would mean an either neutral or negative ion for contact with the cell. Augite was the second most porous of the minerals, with a surface porosity of 0.04% area coverage. It was the second most hydrophobic of the minerals after olivine, with a contact angle of 70.1^o, and it had an electrophoretic mobility of -$1.8\mu_e$, making its charge less negative than the *Sphingomonas desiccabilis*.

Olivine:
Olivine has one of the most advantageous chemical make-ups for *Sohingomonas desiccabilis*: $(Mg^{+2}, Fe^{+2})_2SiO_4$. It has a comparable porosity to quartz, at just

0.01% of its surface area containing deep enough 'shadows' to register as a pore. It is the most hydrophobic, and has the least negative charge of all the minerals, at -1.2μ_e.

Microcline:
The chemical formula of microcline is $KAlSi_3O_8$). Potassium is a useful element for *S. desiccabilis*, but this is balanced out by the presence of potentially toxic aluminium. Microcline had a low surface porosity, with a percentage area coverage of 0.024%. It fell into the middle of the results for hydrophobicity, with a contact angle of 57.5^o, not dissimilar to its chemical counterpart orthoclase. Its surface charge was slightly higher than that of *S. desiccabilis*, at -2.2μ_e.

Orthocalse:
The chemical formula for orthoclase is the same as microcline: $KAlSi_3O_8$), which - as discussed above - contains a beneficial and potentially negative element in equal quantities, essentially neutralising the nutritional advantage of this mineral. Its porosity was an order of magnitude higher than microcline, at 0.24% surface area. The hydrophobicity value was a fraction lower than microcline, with a contact angle of 56.6^o, and it had the lowest of all the mineral electrophoretic mobilities, with -3.4μ_e.

4.3 *Sphingomonas desiccabilis* Mineral Attachment

4.3.1 Growth across minerals

Introduction

Once the chosen physical characteristics of the different minerals had been established, a test was performed to see how *Sphingomonas desiccabilis* growth and attachment would be affected by the recorded combinations of mineral properties. Planktonic growth was measured using optical density of the media to see how the mineral chemistry would affect growth, as elements would leach out of mineral over the course of three weeks, both from biotic and abiotic action. A crystal violet assay was used to assess three-week biofilm biomass on the minerals, to see how the different mineral characteristics affected attachment.

Methodology In order to determine how the different minerals would affect *Sphingomonas desiccabilis* planktonic growth and biofilm formation, a minimal media of M9 was made up (see Appendix A), and mineral crystals were cut to the same weight (0.7g +/- 0.1g) and autoclaved. Minerals were then placed in 6 well plates with 5ml of M9, with biotic and abiotic triplicates. Biotic triplicates were

inoculated with 50μl of an overnight culture of *Sphingomonas desiccabilis*, which had an O.D. of 0.248A before being added to the 5ml of M9. The 6-well plates were covered in a breathable multiwell membrane to avoid contamination and evaporation, along with a lid which was parafilmed into place. The samples were left to grow for three weeks, and then the liquid media was extracted, 1ml from each sample going into cuvettes for O.D. measurements at 600nm to determine planktonic counts. The minerals were relocated to fresh wells for the crystal violet biomass assay, so that biofilms that had grown on the well walls were not counted as mineral biomass. Crystal violet assay was performed at 550nm, as per Section 3.3, including the controls of crystal violet exposed to abiotic minerals. One way ANOVAs were performed between data sets to assess the significance of the results.

Results

The planktonic growth tests were designed to establish the nutritional advantage that each mineral would offer *Sphingomonas desiccabilis*, independent of the attachment process; although it is worth noting that faster attachment would also lead to a greater leaching of potentially useful nutrients to the planktonic bacteria.

As predicted in 4.3.1, quartz provided the least advantage in nutritional supplementation, and did little to augment the minimal M9 media. Anorthite was assessed in 4.3.1 as being the second least beneficial, as it is comprised of $CaAl_2Si_2O_8$; the calcium of which may be useful for cellular structures, but little else, and the aluminium of which could be limiting, by binding with proteins at sites that should be occupied by iron and/or magnesium. However, the results from the planktonic growth experiment show that *S.desiccabilis* grew to its highest average numbers in the presence of anorthite. While this is the case, it is also possible to see - from looking at Figure 22 - that growth in the presence of olivine, orthoclase, and augite was at a similar level, and there is no significant difference between them ($P = 0.69$). The only 'significant' change in growth was between the following two groups: quartz and microcline; and augite, orthoclase, olivine, and anorthite, $P = 0.036$. As a result it was not possible to draw any robust conclusions about the validity of the proposed table of elemental nutritional advantages in 4.2.1. For purposes of interpreting the heirachy of forces in this chapter, the Table 4 in section 4.2.1 will continue to serve as guide to stereochemical nutritional influences.

For biofilm biomass, quartz had the least amount of attachment, with an average O.D. of 0.075A. Olivine had the second least attachment, with an average O.D. of 0.106A but also the most variation with a standard error of 0.04A. Microcline biomass was at 0.15A, followed by anorthite with 0.17A, augite at 0.23A. Orthoclase had the highest biomass, with an O.D. of 0.29A (see Fig. 23).

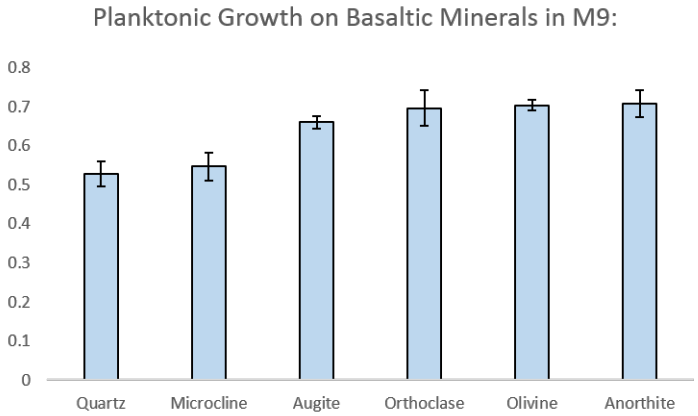

Figure 22: Optical density of planktonic growth (600nm) in the minimal media surrounding the different minerals, with growth influenced by the different leached products of biotic and abiotic mineral weathering in solution.

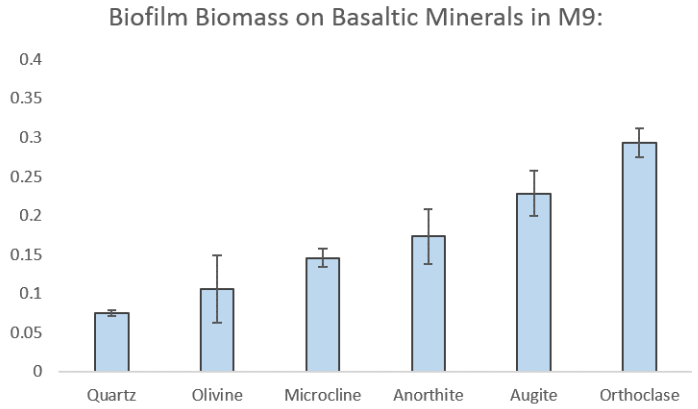

Figure 23: Optical density of crystal violet (550nm) released from the biomass of the biofilms colonising the different minerals which make up the majority of the experimental basaltic rock.

Plotting the crystal violet biomass data against the individual properties of the minerals showed no discernible pattern, it is only when looking at the data from all four of the physical variables together that a pattern begins to emerge. To compare the crystal violet microbial attachment results to the physical properties of the basalt, the table in Figure 24 combines the data with colour coding as a visual aid. Each colour is specific to one mineral, with the initial allocation of colour representing the order of respective biomass attachment, with red as lowest and purple as highest.

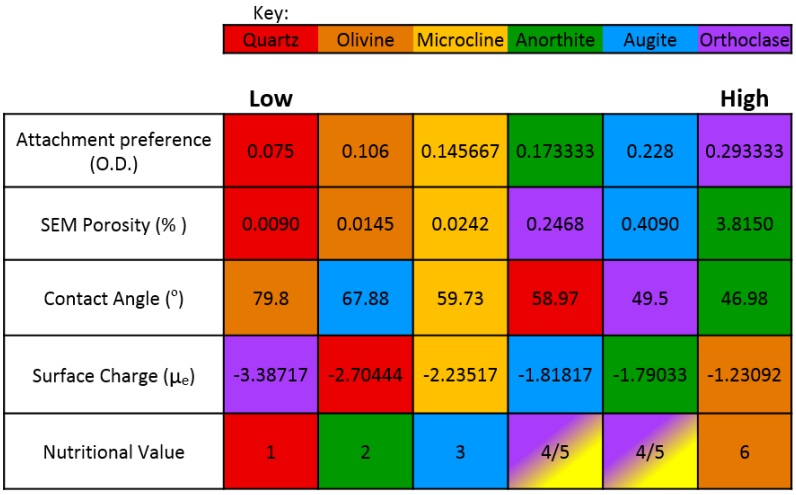

Figure 24: Comparison of the attachment preference of *Sphingomonas desiccabilis* to different properties of the minerals, ranked from low to high (left to right). Colours are specific to the different minerals, and colour-coded according to the order of preferential attachment, with red as the lowest biomass and purple as the highest biomass. Nutritional value ordering comes from Table 4 not the results of Fig 23.

4.4 Discussion

Based on the findings in this suite of experiments, the property that most drastically reduced the ability of bacteria to form attachments to the mineral surface was porosity, or specific surface area. The three minerals with the lowest porosities had the lowest biomass, indicating this property is the limiting factor that dominates up to a certain threshold. As discussed in the 4.2.2, a smooth crystal plane where all reaction sites are bound in a cohesive lattice offers little-to-no purchase for the initial attachment, whereas a crystal plane with steps and faults will have exposed atoms with lower coordination and therefore greater availability. With quartz, olivine, and microcline, which had surface area porosities in the range of 0.009 - 0.02%, biological weathering is slowed primarily by the lack of free energy on the surface. The co-limiting factors, such as nutrient content and hydrophobicity, are not observed as having an effect, suggesting the absence of free energy limits growth before these other parameters can display a positive or negative effect. Olivine, for example, had the most advantageous set of characteristics for hydrophobicity, surface charge, and nutritional value, and was still very poorly colonised. It is suggested that there is a threshold somewhere between 0.02% and 0.2% surface porosity, where the texture/porosity of the surface is no longer the main limiting factor.
If the quartz, olivine, and microcline can be discounted from the other factors

due to their low porosity, only anorthite, augite, and orthoclase can be looked to for interpretation of the hierarchy of the other factors. Of the remaining categories, the biomass growth patterns on the three remaining minerals follows the predictions based on the elemental nutritional benefits of the minerals, with the highest growth on orthoclase, followed by augite, and finally anorthite. This suggests that the nutritional qualities of the minerals was the second most influential factor affecting attachment, after porosity. One possible explenation for this, is that the pili or other bacterial appendages have evolved over time to bond to beneficial vs deleterious elements.

Augite was colonised less than orthoclase, which contradicts DLVO expectations based on both hydrophobicity and surface charge properties of the minerals. The contact angles of anorthite and orthoclase were only separated by 2.52^o, which is unlikely to be a sizeable enough difference to cause the observed separation of 0.12Abs in the O.D. of the biofilm biomass values. Orthoclase was a poorer fit for surface charge than augite or anorthite, indicating that the benefits it provides for microbial attachment may instead be down to the stereochemistry of the minerals, as explored in 4.2.1.
Surface charge could be the easiest variable for biofilm forming bacteria to overcome; it appeared to have the least effect on attachment, based on the results of this study. One possible explanation is that the presence of ion channels in the bacterial cell membranes allows the bacteria some ability to influence the charge of their immediate environment.

From previous research, and the studies performed in this chapter, it is possible to rank the properties in the following order, from most to least influential:
1) Surface texture
2) Stereochemistry /nutritional value
3) Hydrophobicity
4) Surface Charge

While these studies may not prove conclusively that the forces dominating attachment are ranked in this order, it does seem to contradict expectations based on the DLVO and XDLVO theories.

4.4.1 Limitations

The factors that influence microbial attachment are more numerous than those that are described here, and - as has already been mentioned - the interplay between them is not yet fully understood. The research in this chapter tests a number of these factors against each other in an attempt to rank which forces dominate over the others, but does not assume to have encompassed all of the factors that can have an impact.
The techniques used in this chapter were chosen for practical purposes, based on

the instrumentation available at the University of Edinburgh's School of Physics and Astronomy. Performing the experiments with a greater number of repeats would have been beneficial, however acquiring adequate mineral crystals for the experiments was difficult, as it is rare to find large crystals of pure minerals, and when they are found they are prohibitively expensive.

A preferred method for quantification of porosity would have been mercury intrusion porosimetry, or gas adsorption porosimetery. However the minimum amount of material required for gas adsorption porosimetry was prohibitive; the specific amount varies between instruments, but is at least two orders of magnitude larger than pure crystals of the minerals generally form. Another possible route to assessing relative surface area of the different minerals could have been to create surface profiles produced with a stylus instrument (e.g. - a Dektak). While 2D imaging methods and software analysis may be less precise than the other methods, they still serve as a guide to the relative hierarchy of surface areas provided by the different minerals.

If the experiments were to be repeated, it is suggested that researchers look for abundancy of etch pits in addition to using CV, providing there is access to a great enough quantity of mineral crystals. CV may be quantitative while SEM is qualitative, but the CV results show highest biomass growth with the higher porosities; CV would also be caught in pore spaces, even after washing in PBS, so having visual confirmation or contradiction would assuage any doubts.

For the surface charge measurements, the minerals were measured in $NaNO_3$ buffer solutions, which would have behaved differently to the minimal M9 media the bacteria grew in, if the experiment were to be repeated, it would provide a more accurate comparison of the minerals to the bacteria.

4.5 Conclusions

The DLVO theories works well as a model describing the interactions of homogenous colloid surfaces in simple systems. However, bacteria are not homogenous, nor is the interface of a solid substrate in a liquid environment. Bacteria have complex proteinous surfaces, appendages, and can produce EPS. Solid substrate in a liquid environment contains adsorbed molecules known as the conditioning layer. Predictions were made on which basaltic minerals would be preferentially colonised based on the DLVO theories, but the results showed that hydrophobicity and surface charge, important components for adhesion in the DLVO theory, appeared to have the least significant for *Sphingomonas desiccabilis* biofilm formation, when compared to porosity and stereochemical make-up. Whether this is

due to some other influence at the mineral surface, or whether the primary DLVO forces can simply be overcome by fimbriae, would benefit from further study.

5 Model Organism and Hardware Characterisation in Preparation for Reduced Gravity ISS Experiments

5.1 Introduction

It has been shown in multiple experiments that reduced gravity, and the simulation of it, results in altered growth kinetics. Specifically that populations of bacteria, both planktonic and sessile, have shorter exponential phases that result in larger populations than their terrestrial counterparts[60][61][68]. Investigations so far have not included research on populations of rock-weathering bacteria, or onto the effect any changes would have on the microbe-mineral interactions.

In order to investigate the effect of reduced gravity on geomicrobial biofilms and geomicrobial weathering, a new experiment will be flying to the International Space Station (ISS) in 2019: BioRock. New hardware has been developed in collaboration with Kayser Italia, and preparations have been under way to characterise the model organisms and ensure hardware compatibility. The experiment is in coordination with European Space Agency (ESA) and has science teams in the University of Edinburgh, SCK-CEN in Belgium, and at DLR in Germany. The PI of the experiment is Charles Cockell, and the majority of the preliminary work and preparations have been conducted here at the University of Edinburgh. The BioRock experiment aims to address two fundamental science questions:

Question 1: Do Martian gravity and microgravity induce alterations in geomicrobial biofilms formed by microbes associated with rocks? *Hypothesis*: Reduced gravity will change the structure and morphology of microbial biofilms formed on solid rocks substrates.

Question 2: Do Martian gravity and microgravity affect microbially induced rock alteration? *Hypothesis*: Martian gravity and microgravity will impact mixing regimes, and the extraction of minerals by the model organisms will be altered significantly.

Three different experimental organisms will be used to try and identify universal geomicrobial responses to the altered gravity conditions. Two of the model organisms, *Bacillus subtilis* and *Cupriavidus metallidurans*, which will be studied by the teams in Germany and Belgium respectively, are well characterised organisms with stress tolerance mechanisms and DNA repair mechanisms[148], [149]. They have also been the subject of space-flight experiments prior to BioRock [150], [60], [151], [152]. The model organism that is being studied by the University of Edinburgh is the relatively new and uncharacterised *Sphingomonas desiccabilis*. Subsequently, auxiliary experiments were undertaken to ensure that the organism was suitable for the rigorous steps in transportation to and from the ISS, and

stowage on-board. The preliminary experiments studying the model organism *S. desiccabilis* explored the anhydrobiotic tolerance of the bacteria, the best nutrient conditions to promote biofilm growth, and pertinent genes that may contribute to biofilm formation and stress resistance.
In addition to expanding the episteme of *S.desiccabilis*, validation experiments required for the ESA experiment development and integration process were performed. Experiments were performed to assess how best to design the experimental equipment around the needs of the bacteria; specifically the materials and the dimensions of the bioreactor that the experiment will be taking place in. Experiments were also conducted to find a fixative that would work for both the bacteria and the regulations in place on board the ISS. A test of the first stage of the experiment was performed in microgravity, on board a series of three parabolic flights, to learn how starting conditions may differ for the different gravity regimes.
The two main tools that will be used for post-flight analysis on the returned samples will be inductively coupled plasma mass spectrometry (ICP-MS) and confocal laser scanning microscopy (CLSM). Experiments were undertaken to refine the ICP-MS protocol, in order to reliably quantify elemental release rates. CLSM was used for assessing the successful colonisation of basalt slides to answer questions about nutrient density, giving researchers an opportunity to familiarise themselves with the technique and check its efficacy for the examination of *S.desiccabilis* biofilms.

5.2 BioRock

The BioRock experiment has been designed to answer questions about the growth and behaviour of geomicrobial biofilms in reduced gravity environments; specifically: will there be alterations to the biofilm growth and structure compared to 1 x g controls, and will this impact the rate of geomicrobial weathering? The experiment will use three different heterotrophic bacteria with rock weathering capabilities; *Sphingomonas desiccabilis*, *Bacillus subtilis*, and *Cupriavidus metallidurans*. The research teams in Edinburgh, Belgium, and Germany are all responsible for testing the responses of different organisms, with Edinburgh focusing on *Sphingomonas desiccabilis*. The original *Sphingomonas desiccabilis* culture was isolated from the Colorado plateau in the USA, and Edinburgh researchers acquired it from DSMZ(16792). The rock used in the experiments in this thesis, and that will be used in the BioRock experiment is Basalt, is cut from the same large piece of Icelandic basalt, currently stored at Aahrus in Denmark (see Section 4.2.1 and 4.2.2 for chemical and elemental composition). Slides of the basalt, cut to uniform dimensions, will be inoculated with a monoculture of the one of the model organisms, or left abiotic as a control, and allowed to dry to desiccate the bacteria. Once dried, they will placed in a BioMining Reactor (BMR) (see Fig.

25), new hardware designed for the experiment by Kayser Italia. Once installed in the Experimental Units (EUs), the payload will be flown up to the ISS, and installed inside the two Kubik Centrifuges in the Columbus Laboratory module. Some of the EUs will be attached in stationary positions around the interior of the centrifuge for 0 x g, while others will be installed to spin at 1 x g or 0.38 x g to simulate Earth and Martian gravity respectively (see Fig. 26).

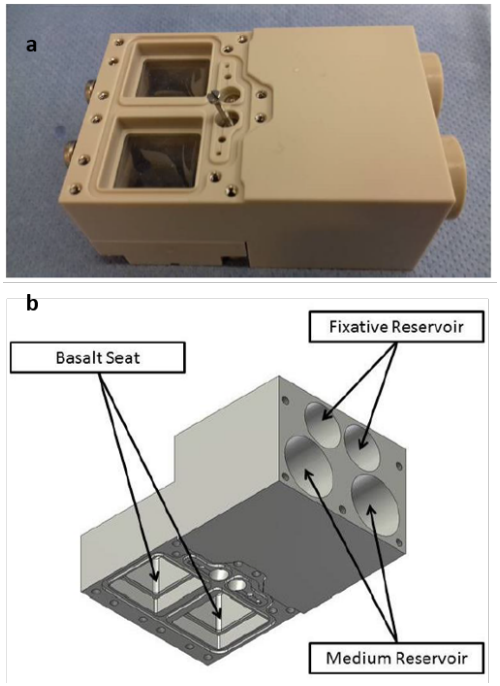

Figure 25: a) A photo of the BioMining Reactor as it is assembled, b) Annotated drawing of the locations of the basalt, R2A and fixative in the BMR Experimental Unit

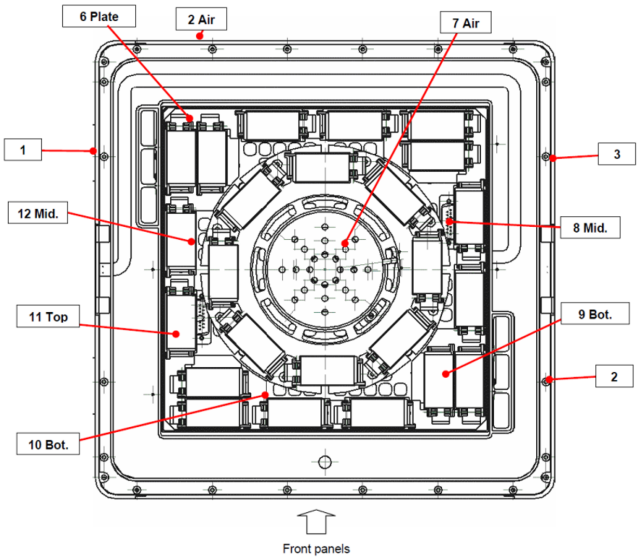

Figure 26: The lay out of the Experimental Containers within the Kubik Centrifuge in the Columbus Laboratory module on board the International Space Station.

Once the EUs are installed and have been spun up to the required speeds to meet the desired gravity conditions, the nutrient solution will be injected into the culture chambers containing the basalt and the dried down bacteria. This will revive the desiccated microorganisms, which will resume their usual behaviour of harvesting nutrients and elements from the solution, forming biofilms, and weathering the basalt slides. After three weeks, growth will be arrested by the introduction of a fixative, to prevent further alteration of the rock as a result of bacterial endeavours when the EUs experience the excess gs of atmospheric re-entry and insertion from free-fall orbit into the terrestrial gravity well.
The EUs will be returned to Earth for post flight analysis, where the elemental release rates from the different organisms and gravity conditions will be characterised by ICP-MS, and the structure and morphology of the biofilms will be examined using CLSM. See Figure 27 for the experimental flow diagram, modified from the ESA Experimental Requirements document.

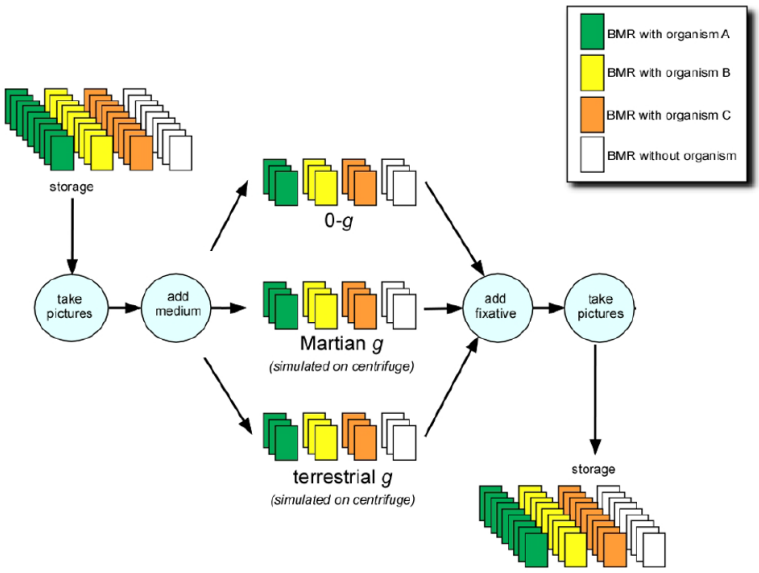

Figure 27: A pictorial representation of the BioRock experimental plan.

5.3 Characterisation of Model Organism *Sphingomonas desiccabilis*

5.3.1 Desiccation Tolerance

Introduction

Sphingomonas desiccabilis was chosen as the model organism for the experiment because - as the name suggests - it is notable for its resistance to desiccation; an important quality for the first stage transfer to the ISS. Launch windows can be moved or cancelled right up until the last moment, and so there is some unavoidable uncertainty as to the duration of this transfer phase. In order to guard against the loss of viability from a delayed launch, the model organisms were tested for the longevity of their desiccation resistance.
In order to ascertain the viability of *Sphingomonas desiccabilis*, two experiments were performed; one at a range of temperatures to determine whether the inclusion of the preserving sugar trehalose would be necessary to ensure the viability of the bacteria, and one at room temperature to observe the trend of population death as a result of desiccation.
The aim of the first experiment was not to compare viable cell counts before and

after desiccation, but to establish whether there would be enough viable cells remaining after two months of desiccation to confidently contribute to biofilm formation on board the ISS, should there be delays to the launch.
The aim of the second experiment was to gain a better understanding of the process of loss of viability over time.

Methodology

For the first experiment, glass microscopy slides were autoclaved and brought to the laminar flow hood, along with a monoculture of *Sphingomonas desiccabilis* in R2A, with an optical density of 0.652Abs and an average CFU count of $17x10^8$. For the samples without trehalose, 25μl spots of the culture were pipetted onto the surface of the glass slides. The *S. desiccabilis* and trehalose spots were 50μl, a 1:1 mixture of 25μl of bacterial culture at 0.652Abs, and 25μl of trehalose. The slides were kept horizontal in the laminar flow hood during desiccation to allow the liquid to evaporate quickly in a sterile environment.
Once dried, the inoculated slides were placed in petri dishes with sterile tweezers, and the petri dishes were wrapped in parafilm. One third of the slides were placed in the cold room at 4^oC, another third were kept on the lab bench at room temperature, 21^oC, and the remaining third were stored in the warm room at 30^oC.
After 2 months of storage, the petri dishes containing the glass slides were brought back to the laminar flow hood. each dried down culture was revived with 100μl of R2A. Initially 50μl of R2A was slowly pipetted on the site of desiccation, and agitated by re-pulling the solution back into the pipette and re-depositing it onto the slide six times. The solution was then transferred to a labelled eppendorff tube, and another 50μl of R2A was agitated at the site of the desiccated *S.desiccabilis* to capture any remaining bacteria, and this was added into the same eppendorff tube as the first 50μl, for serial dilution and plating onto R2A agar plates. Two days after plating, the agar plates were examined for CFU counts.
The experiment was then repeated without the trehalose and without the temperature variable. Here, as the pattern of viability loss was the focus, samples were rehydrated after 10 minutes, 2 hours, 24 hours, 1 week, 2 weeks, and 1 month, instead of at a single end point. The starting population of the culture for this second experiment was higher, at 0.857Abs, otherwise the procedure was the same.

Results and Discussion

Results from the colony forming unit counts after two months of desiccation showed that the desiccated spots still held large enough populations of *Sphin-*

gomonas desiccabilis to form biofilms.
Counter-intuitively, given that reactions take place slower in colder temperatures, the populations of viable cells revived without trehalose had their highest revival numbers in the samples stored at 30^oC, with CFU counts ranging from 68 - 88 x 10^3 per 25μl. The next highest population counts were those stored in the 4^oC cold room, with population counts of 55 - 57 x 10^3, and the room temperature samples only had 30 - 38 x 10^3 per 25μl. A one-way ANOVA test gave a p-value of 0.0005 to the likelihood that the observed differences were due to the temperature conditions the desiccated samples were stored in. It is possible that this higher survival rate at higher temperatures is a reflection of the conditions present where the *Sphingomonas desiccabilis* population were originally isolated; the Colarado desert in the US. It could be possible that their tolerance to desiccation at higher temperatures is bolstered by a currently unknown mechanism or combination of genes.
The cultures stored with trehalose had higher populations and less significant variation between conditions, according to the statistics, combined with greater variation within conditions. All the CFUs in the 25μl spots plated onto the agar were in the 10 - 55 x 10^4 range (see Fig. 28). Those revived from the cold room produced the highest populations, and those revived at room temperature produced the lowest viable populations. A one-way ANOVA showed the differences in populations at different conditions could no longer be confidently attributed to temperature, with a p-value of 0.22.

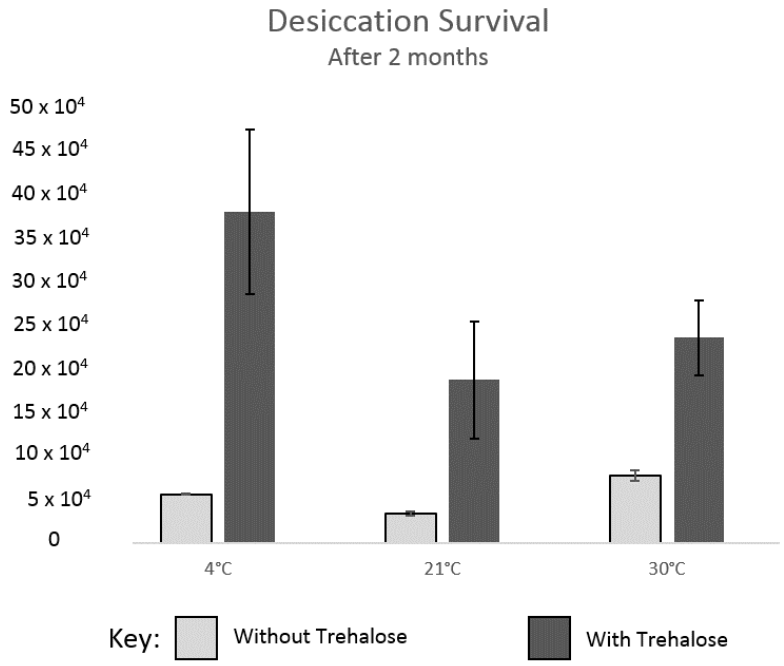

Figure 28: Colony forming units per 25μl for *Sphingomonas desiccabilis* desiccated with and without trehalose, after 2 months of storage at 4^{o}C, 21^{o}C, and 30^{o}C .

T-tests between the bacteria stored with and without trehalose showed that while there was a definite trend, the differences were not significant: P = 0.079 at 4^{o}C, P = 0.15 at 21^{o}C, and P = 0.067 at 30^{o}C. As the samples stored without trehalose still had populations which were considered within tolerable limits for biofilm formation, it was decided not to include trehalose in the BioRock experiment, as it could have had other affects on the biology or geology that would have been difficult to separate.

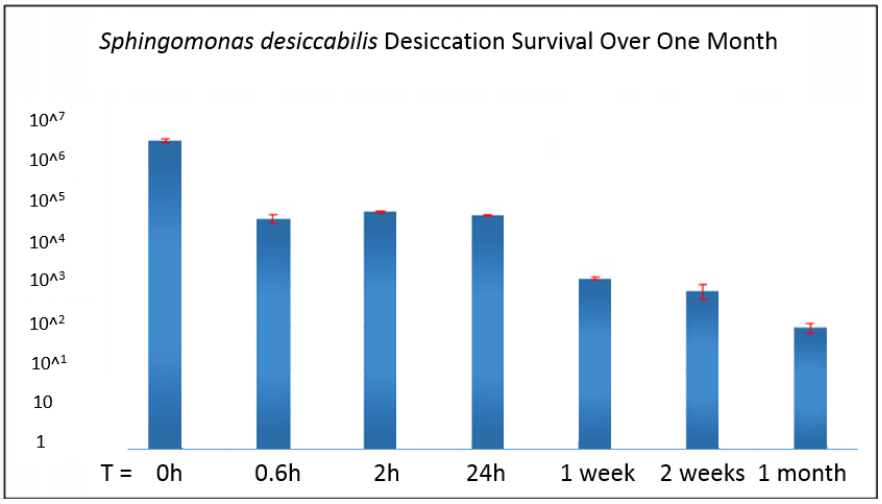

Figure 29: Colony forming units per 25μl for *Sphingomonas desiccabilis* desiccated without trehalose, after 1 months of storage at 21^{o}C.

The second desiccation tests, which used multiple time points to characterise the rate of loss of viability, showed the same pattern that had been seen in other desiccation experiments (work not shown here). Namely, that there was a significant drop in cell viability in the first ten minutes/0.6 hours (P = 4.7 x 10^9), followed by a much slower decline over the following month (see Fig. 29). To give a better understanding of the pattern over the full month, without the compression that the time points give when plotted next to each other, another graph has been made up to show the same data with space included for the days when data was not collected (see Fig30) in order to get a more accurate picture of loss over time.

Figure 30: Colony forming units per 25μl for *Sphingomonas desiccabilis* desiccated without trehalose, after 1 months of storage at 21^{o}C.

This data is positive for the BioRock experiment, as it suggests that after the initial loss of bacteria upon the first instance of desiccation, the decline in viability is subsequently a great deal slower. The initial loss is predominantly due to cells that either do not possess or have not up-regulated their stress-tolerance mechanisms. The slower decline over the subsequent month is likely due to accumulation of oxidative damage. Any delays in the launch window should not affect the biofilm forming population of *Sphingomonas desiccabilis* too detrimentally, providing all of the samples are exposed to the same stresses.

5.3.2 Relationship of Biofilm Growth to Nutrient Concentration

Introduction

In order to capitalise on the three weeks of biofilm growth and microgravity exposure, experiments were performed to determine whether biofilm growth could be accelerated by reducing the availability of nutrients. While complete nutrient deprivation will lead to the death or dormancy of a biofilm, previous studies have shown that - within limits - nutrient restriction leads to increased biofilm formation, as it is the most favourable survival strategy for most bacteria [5]. The cooperative nature of biofilms confers an advantage for the cells that constitute it, the EPS acting as an increased catchment area for nutrients, and forming water channels that allow for increased efficiency in the delivery of available nutrients[3]. Additionally, it has been shown that the presence of glucose can inhibit the expression of biofilm relevant genes located throughout the genome. Experiments with different bacteria showed variable rates of biofilm suppression from 30% to 95%, but biofilm formation was inhibited in all cases[153]. To explore this, diluted R2A nutrient solutions, along with M9 enriched with different quantities of glucose, were made up to investigate the severity of this effect on *Sphingomonas desiccabilis*. Due to restrictions on altering ESA's experimental protocol after the acceptance of the Scientific Requirements, it was not possible to consider other solutions apart from R2A. The hypothesis was that that lowering the overall nutrient solution would have a positive impact on biofilm growth, and the M9 solutions were intended to provide clarification on whether glucose was the main biofilm inhibitor, or whether a reduction in all nutrients would result in the same pattern.

Methodology

R2A was made up as per the recipe in the appendix A, and then 20ml was diluted down to 50% with millipore water, and a further 20ml was diluted down to 20% with millipore water.

Eighteen basalt slides were cut from the mother-rock and filed down to 1.5 x 1.5 x 0.4cm, and autoclaved. They were placed into the individual wells of six well plates and inoculated with a fresh monoculture of *Sphingomonas desiccabilis* at an optical density of 0.682Abs. Using just the 100% R2A media and the 20% R2A media, 5ml of each different R2A media dilutions were added to nine basalt slides, and the six well plates were covered with sterile lids and parafilm. Three of each condition were then placed in the warm room during growth, at 30°C, three were kept at room temperature, at 21°C, and three were kept in the cold room at 4°C.
After three weeks, the plates were gathered in the laminar flow hood, and basalt slides were extracted from the wells, and placed in fresh wells. They were permeabilised with using 1% Triton X 100 in PBS, with Sypro Ruby stain at a 5:1 ratio. The wells were covered with tin foil to avoid photo bleaching, and left for half an hour, then rinsed twice with PBS and covered again with foil. Biofilms were examined at 200x magnification.

The experiment was repeated later with the all of the diluted R2A solutions, and also with M9 minimal media that was made up, as per the recipe in the appendix, but with glucose levels adjusted (see Appendix A). Traditonal M9 minimal media is made up to 20% glucose, (with 10ml of 20g in 100ml into 1L of M9), so one batch of M9 was made to this level, and two other litres of M9 were made up with 10 ml of 5g in 100ml, and 10 ml of 50g in 100ml, giving 5% and 50% glucose solutions.

Twenty-four basalt slides were cut and filed to 1.5 x 1.5 x 0.4cm, and autoclaved. These were placed into six well plates and inoculated with 20μl of *S. desiccabilis*, which had been grown overnight and had reached an optical density of 0.677Abs. To allow three replicates for each of the nutrient solutions, 5ml of each media was pipetted into three wells per plate. The six-well plates were then covered, parafilmed, and left at room temperature (21°C) for three weeks. An additional three inoculated slides per R2A diluted solutions were also made up, so that population growth could be quantified at both 1 week and at 3 weeks. Quantification was performed using crystal violet, at a concentration of 0.04%, after introducing the crystal violet, the samples were left for 30 minutes and then washed twice with PBS. Abiotic basalt controls for the crystal violet were made up, so that the amount of crystal violet that had been caught by the rock could be subtracted. The PBS was removed, and then 5ml of 33% acetic acid in millipore water solution was pipetted into the wells in the fume hood. After 20 minutes, 1ml of each sample was transferred into cuvettes, for optical density readings at 550nm, calibrated with the acetic acid in millipore water mix.

Results

Using the CLSM, it was possible to see that after three weeks, and under lower concentrations of nutrient solution, *S. desiccabilis* cells had attached to the basalt surface in greater numbers, and had developed larger and thicker biofilms.

30°C The inoculated basalt slides in the 20% nutrient solution, kept at 30°C, yielded the largest biofilms. In Figure 31, the difference between two of the representative biofilms can be observed. The temporal hyperstack of the 20% R2A biofilm is comprised of 86 layers, and shows multiple smaller biofilms that have joined together. In the middle of the 'horseshoe' shape are more of the smaller biofilms, that are in the process of merging. The side orthogonal views, which only show a cross section through one line of the temporal hyperstack, gives an additional visual representation of the depth of the biofilm, supplementing the colour-coding of the hyperstack. The picture selected to showcase the biofilms that formed in 100% R2A media at 30°C is comprised of 93 layers, but the biofilms occupy less surface area of the layers over-all. The biofilms seen here are less of a coloured mix than the 20% R2A growth condition, suggesting they occupy a more specific range within the 93 layers. It is possible to see from the orthogonal views that they do not occupy the layers with as much consistency. Again there are the smaller coloured dots which represent microcolonies that are juvenile biofilms.

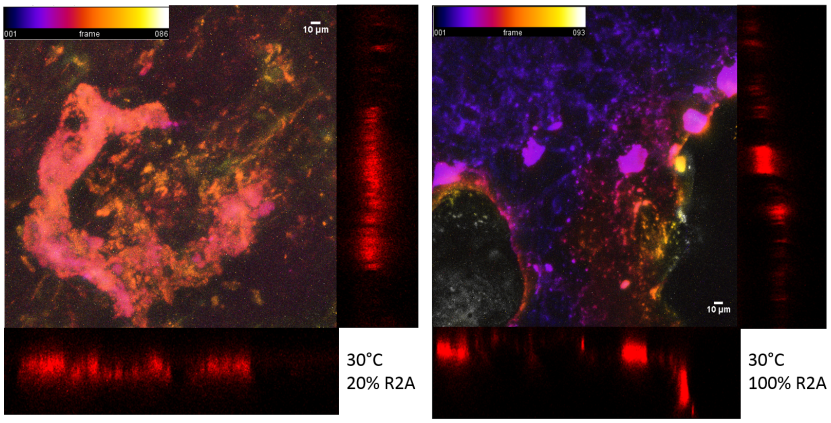

Figure 31: Biofilms at 30°C in 20% and 100% R2A. Central Z-stacks are composed of multiple layers of confocal images, which allow for a 3-D model of the biofilm. Sections to the right and lower edges of the images are the orthogonal view, showing a cross section of fluorescence through the stack. Stack on the left is comprised of 86 layers, stack on the right is comprised of 93 layers, but the biofilms occupy less of the layers over-all. Multiple images of multiple biofilms were taken, these two images were selected as representative.

21°C

The biofilms grown at 21°C display the same increase in growth when cultured in 20% media versus 100% media (see Fig. 32. The image representing biofilms grown at 21°C shows a cluster of biofilms and microcolonies on what appears to be the rim of an incline of rock. The picture representing biofilms cultured in 100% media has fewer biofilms and microcolonies, despite being a photo of one of the most extensive biofilms within that condition. The hyperstack of the 20% media biofilm is made of 83 layers, and while the orthogonal view shows a thinner band of red than the 100% R2A picture, the portion of red shown there is within a stack of only 32 layers; comparatively the biofilms are probably of a similar depth.

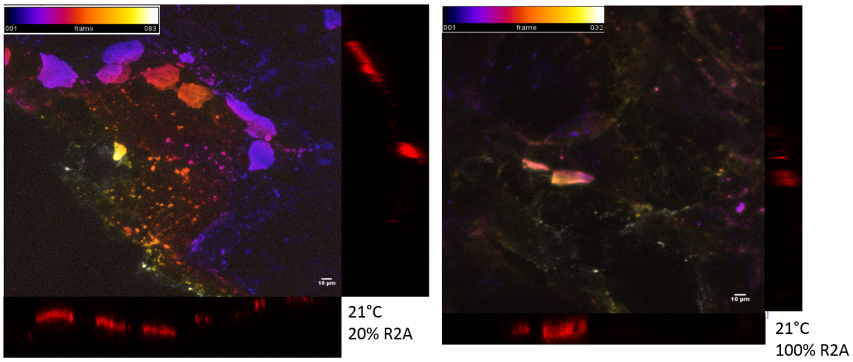

Figure 32: Biofilms at 21°C in 20% and 100% R2A. Central Z-stacks are composed of multiple layers of confocal images, which allow for a 3-D model of the biofilm. Sections to the right and lower edges of the images are the orthogonal view, showing a cross section of fluorescence through the stack. Stack on the left is comprised of 83 layers, stack on the right is comprised of 32 layers. Multiple images of multiple biofilms were taken, these two images were selected as representative.

4°C The biofilms grown at 4°C share the same pattern of increased growth when cultured in 20% R2A versus 100% R2A. The 20% R2A biofilms at 4°C also have increased growth when compared to the 100% R2A grown at 21°C. The biofilms have less depth at this lowest temperature, with the hyperstacks shown being at 39 layers for 20% and at 43 layers for 100% (see Fig. 33).

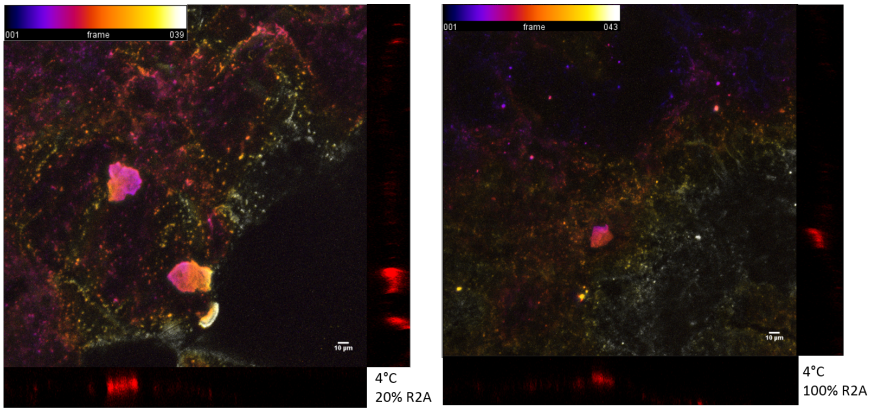

Figure 33: Biofilms at 4°C in 20% and 100% R2A. Central Z-stacks are composed of multiple layers of confocal images, which allow for a 3-D model of the biofilm. Sections to the right and lower edges of the images are the orthogonal view, showing a cross section of fluorescence through the stack. Stack on the left is comprised of 39 layers, stack on the right is comprised of 43 layers, but the biofilms occupy less of the layers over-all. Multiple images of multiple biofilms were taken, these two images were selected as representative.

Tests comparing the cell counts of planktonic and biofilm bacteria in different R2A nutrient solutions were conducted to quantify the change reduced nutrients would have on cell populations. Similar experiments were performed with different M9 solutions in order to discover whether glucose was the main biofilm inhibitor, or whether reducing the overall nutrient content of the R2A would result in the same pattern. The results were in keeping with the CLSM images, showing an increase in biofilm biomass with nutrient restriction. Inversely, the planktonic cell counts were highest in the higher nutrient concentrations (see Fig.34).

The O.D. readings for the biofilm biomass, taken at 550nm, as per the crystal violet protocol, were as follows:
Week 1 100%: 0.00087Abs, 50%: 0.0121Abs, and 20%: 0.0163Abs.
Week 3 100%: 0.00467Abs, 50%: 0.016Abs, 20%: 0.04633Abs.

Planktonic growth followed the inverse pattern, with highest populations at the highest nutrient conditions and lowest populations in the media with the lowest available nutrients. Optical density readings were taken at 600nm.
Week 1 100%: 0.632Abs, 50%: 0.413Abs, 20%: 0.216Abs
Week 3 100%: 0.832Abs, 50%:0.444Abs, 20%: 0.305Abs.

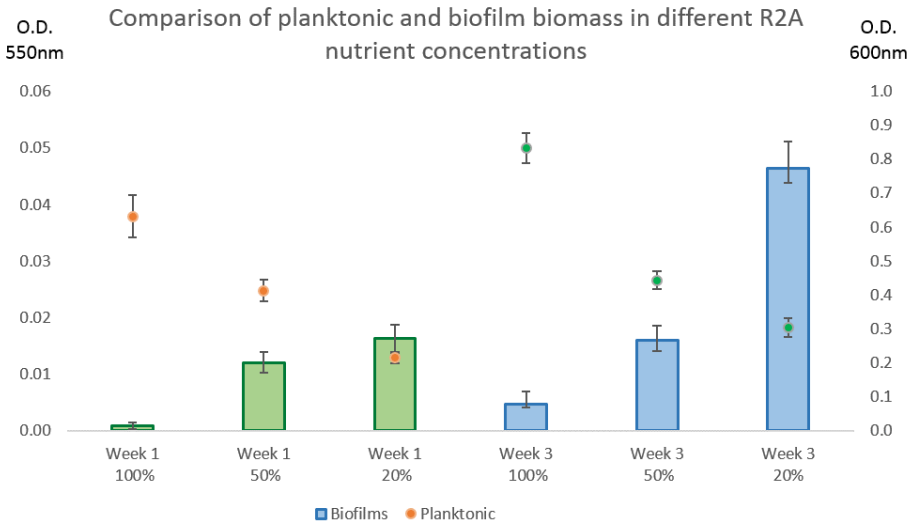

Figure 34: Bar chart showing planktonic and biofilm biomass values of *Sphingomonas desiccabilis* in different R2A nutrient concentrations at 21°C. Bars represent crystal Violet (C.V.) results for biomass, and have had their control values subtracted. Markers represent optical density (O.D.) for planktonic cell measurements. Results on the right were analysed after 1 week of growth, results on the left were analysed after three weeks of growth. Left axis is the O.D. for the C.V. biofilm biomass readings (550nm), right axis is the O.D. for the planktonic counts (600nm). Error bars represent standard error. Results show nutrient starvation has a negative relationship to planktonic growth and a positive relationship to biofilm formation.

Statics comparing the groupings of data showed that there were no significant difference in the growth of *S. desiccabilis* after 1 week of growth in the different nutrient conditions. T-Tests run on the results from biofilms grown over 3 weeks showed higher confidence in the observed differences being attributable to nutrient concentration (see Table 6).

Table 6: t-Test p-Values of Growth Changes in the Different R2A Concentrations

t-Tests on 3 Week Biomass Results	
Comparison	P-Values
100% vs 50%	0.0325
50% vs 20%	0.0117
100% vs 20%	0.0015

The literature suggested that high levels of glucose could be inhibiting biofilm formation by triggering carbon catabolite repression [153]. To test whether or not the reduction in glucose was the main factor behind the observed increase in biofilm formation, the crystal violet experiment was repeated with a minimal media (M9) with a standard glucose content, 20%, and two extremes 5% and 50%. The experiment showed that biofilm growth was inhibited at both of the extremes of glucose concentrations biofilm after 3 weeks (see Fig.35). This was supported by P-values from comparing the 50% and 20% glucose conditions, and the 20% and 5% conditions. The 50% and 5% glucose solutions had comparable growth responses, and the P-value between them was 0.9, indicating no significant difference (see Table 7). After subtracting the control values, the results from performing optical density at 550nm were:
Week 3 50%: 0.053Abs, 20%: 0.219Abs, and 5%: 0.054Abs.
As with the reduced R2A media, planktonic populations, measured at 600nm, were largest with the highest levels of glucose, and smallest with the lowest levels of glucose.
Week 3 50%: 0.855Abs, 20%:0.574Abs, 5%: 0.164Abs; all read at 600nm.

Table 7: t-Test p-Values of Growth Changes in the Different M9 Glucose Concentrations

t-Tests on 3 Week Biomass Results	
Comparison	P-Values
50% vs 20%	0.0457
20% vs 5%	0.209
50% vs 5%	0.906

Discussion

The highest biofilm biomass values from the R2A dilutions were in the 20% solution, and the second highest values in the 50% solution, supporting the hypothesis that biofilm growth could be accelerated by reducing the nutrient content of the media.
The confocal stack images show that there is an increase in the surface area and depth of biofilms grown at lower nutrient solutions. The higher temperature condition, 30°C, and lowest concentration of nutrient solution, 20%, led to the most advanced biofilm growth, with a mature 'horseshoe' shaped biofilm, and what appears to be several smaller biofilms merging together inside the 'corral'. Given another week of growth, the 'horseshoe' shape may have filled in. Measured from tip to tip around its circumference, the biofilm is 360μm in length. In the images

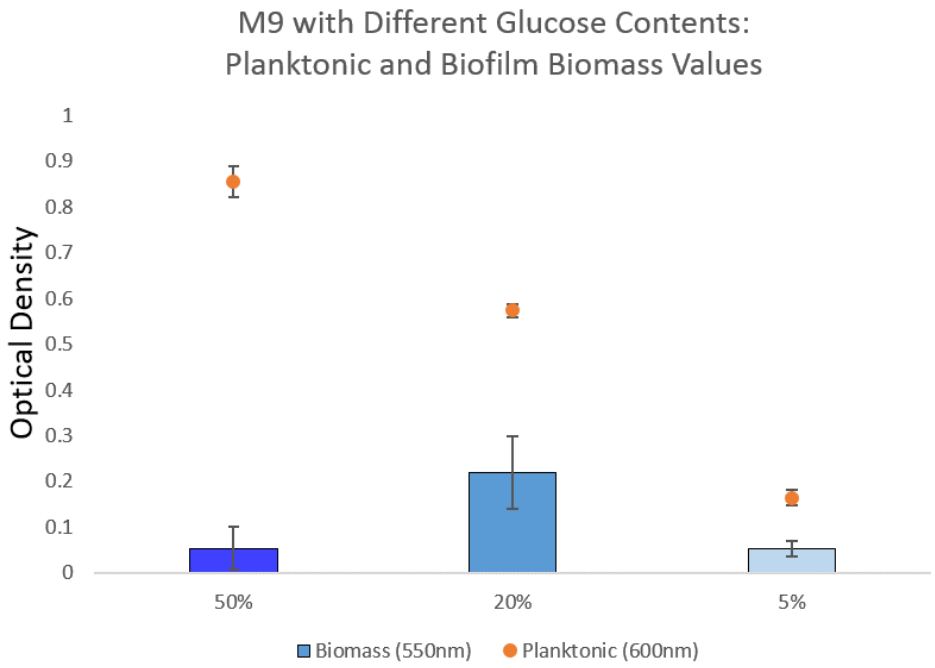

Figure 35: Bar chart showing planktonic and biofilm biomass values of *Sphingomonas desiccabilis* in different M9 glucose concentrations at 21°C. Bars represent crystal Violet (C.V.) results for biomass. Markers represent optical density (O.D.) for planktonic cell measurements. The wavelength for the O.D. on the C.V. biofilm biomass readings was 550nm, and6 600nm for the planktonic counts. Error bars represent standard error. The results show that both high and low glucose concentrations will inhibit biofilm formation.

taken at 30°C in 100% R2A, it is possible to see biofilms that average 25μm, along with some microcolonies that appear as small brightly coloured dots on the temporal hyperstack. It is possible that once the majority of the nutrients in the R2A are used up, more cells gather on the surface of the rock, and biofilm formation begins to accelerate. The least favourable biofilm conditions were at 4°C, in 100% nutrient solution.

The same pattern, of increased growth in lower concentration media is seen in the other confocal images, and biofilm production decreases with temperature. This was backed up with the crystal violet experiments performed on the biofilms at 21°C after three weeks' growth. Nutrient limitation as the trigger of a stress response has been proposed as one of the causes that leads to enhanced biofilm growth in microgravity[70]. These results support this by showing that nutrient restriction does lead to more extensive biofilms.

The experiment with the altered-glucose M9 solutions provided little in the way of new science, but confirmed what others have found, and allowed an increased understanding of the metabolic conditions constraining biofilm formation in the model organism *S.desiccabilis*. In a solution with depleted glucose, biofilm growth is inhibited due to starvation. In a solution replete with glucose, which will inhibit biofilm formation, due to carbon catabolite repression [5][153].
Between the R2A and M9 solutions, growth was much higher in the M9 minimal media, with the highest biofilm growth at 3 weeks in 20% R2A being comparable to the most repressed growth in the M9 glucose solutions. The M9 minimal media would have had fewer nutrients than the 20% R2A, indicating that the trend of decreasing nutrients increasing biofilm growth extends beyond the 20% value. Based on these results, it was decided that the nutrient solution should be lowered to 50%, but not as far as 20%, as microgravity already exerts a stress on the cells by reducing nutrient availability.

5.3.3 Genetic Components Influencing Biofilm Formation in *Sphingomonas desiccabilis*

Introduction

Genomic analysis has been used to isolate genes and identify the role they play. This is most effectively achieved by creating mutant strains that lack the gene under investigation, so that its response to one or more variables can be explored[154]. Using knowledge of existing genes that have been identified in this way, and genomic data obtained from sequencing, it is possible to learn the relevant genes in your organism for a given parameter. To get a deeper understanding of the biofilm capabilities of the organism used for the BioRock experiment, a whole gene sequence (WGS) was undertaken. *Sphingomonas desiccabilis* is a sparsely studied organism, isolated from the Colorado desert by Reddy and Garcia-Pichel in 2007 [91]. The researchers used 16S rRNA to confirm its status as a new species, but a whole gene sequence had not yet been carried out, and was deemed a worthwhile step to aid in future analysis, as well as useful for locating the genes behind its biofilm and desiccation capabilities.

Methodology

To extract the DNA for genomic analysis, *Sphingomonas desiccabilis* was taken from the glycerol stock in the -80^{o}C freezer, and grown up overnight in R2A in a shaking incubator at 25^{o}C, 100rpm. Two 1.5ml eppendorff tubes were filled with the overnight culture, and then prepared as per section 3.9 in the methodology chapter, by systematically heating, vibrating, and using chemicals to strip away

the outer parts of the cell, and using centrifugation and weight differentiation to seperate and collect the DNA.
The first eppendorff tube had a DNA concentration of 18.9ng/μl, and the second had a concentration of 18.9ng/μl, giving a total of 50μl with a total concentration of 27ng/μl. These were given to Edinburgh Genomics for a Whole Gene Sequence. The annotated gene was then delivered back, and searches were performed on the National Center for Biotechnology Information (NCBI) and GenoScope's Microbial Genome Annotation and Analysis Platform (MaGe) to find genes that can be confidently linked to biofilm formation.
In order to gather some intelligence on the stress resistance abilities of *S.desiccabilis*, searches on MaGe were conducted to identify genes that contribute to desiccation and temperature stress, DNA repair, and xenobiotic metal stress, which is likely to be encountered during mineral leaching processes.

Results

Using GenoScope's 'MaGe' platform to search for genes which are known to contribute to EPS, 9 genes were found that could confidently be identified as relating to EPS production. The following summaries are based on the output from the search results, and on research into organisms with similar conserved regions on their chromosones. For clarification, a 'syntone' is a homolog of the selected gene found in other organisms.
After gleaning as much information from the MaGe platform as possible, which is a useful tool but limited to comparisons against only 3582 other microorganisms, the FASTA sequences of the biofilm-relevant genes were BLASTed against the NCBI's database for more Sphingomonad comparisons. These confirmed that additional Sphinomonads also carry these genes, which were also associated with biofilm formation. The slanted cladograms are the results of these BLAST searches, showing Sphingomonads which have the best confidence of aligned sequence (>=200), arranged using the 'neighbour-joining method'[155] to indicate evolutionary distance. When no Sphingomonads with close cladistic ties to *Sphingomonas desiccabilis* could be found, circular cladistic trees have been constructed to allow a wider taxonomic context within *Sphingomonadaceae*.

Gene 1: GumE
Label: SDES-v1-30299 **Product**: Xanthan polysaccharide biosynthesis protein (biosynthesis exopolysaccharide polymerase).
Syntones in other Sphingomonads: *Sphingomonas paucimobilis*, *Sphingobium japonicum*, *Sphingobium yanoikuyae*, *Sphingobium* sp. Ndbn-10, *Sphingobium* sp. 22B, *Sphingobium* sp. AM, *Sphingobium* sp. YBL2, *Sphingobium* sp. HDIP04, *Sphingobium chinhatense* IP26.

Notes: No putative conserved domains were detected on NCBI, although GumE genes are found widely in the Sphingomonad pool.

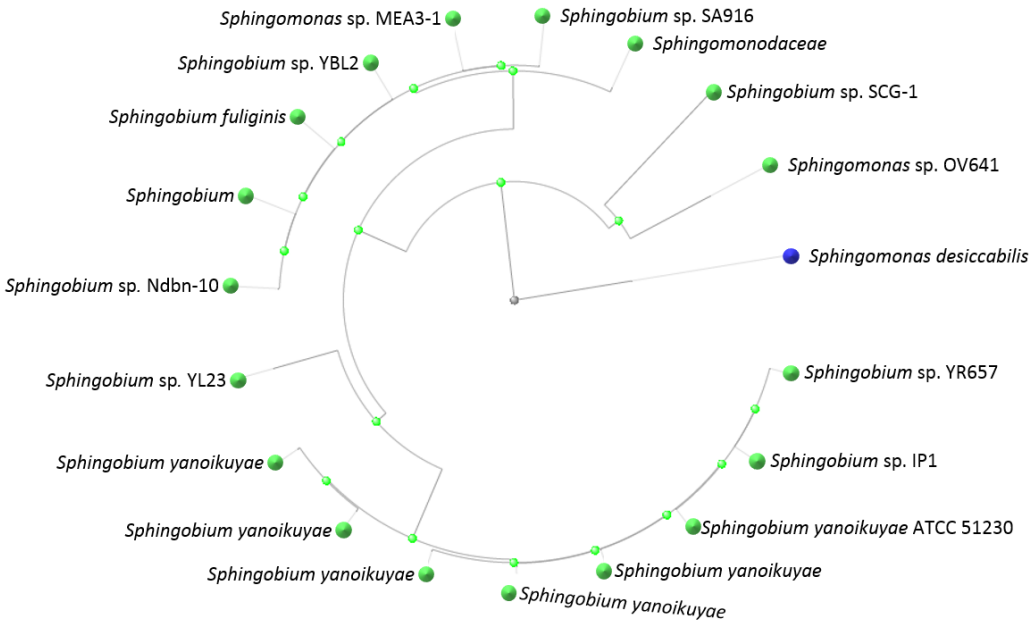

Figure 36: Circular cladistic tree showing neighbour joining of other Sphingomonads in possession of a homolog of the gene labeled SDES-v1-30299. Data from an NCBI protein BLAST.

Gene 2:ExoY **Label**:SDES-v1-20211
Product: Exopolysaccharide biosynthesis polyprenyl glycosylphosphotransferase family protein.
Syntones in other Sphingomonads: *Sphingomonas* sp. S17,*Sphingomonas guangdongensis*, *Sphingobium chlorophenolicum* L-1.
Notes: No Sphingomonads were identified as having a (>=200) confidence on the SDES-v2-20211 region, so a cladistic diagram has not been constructed. However, an NCBI search showed that *Sphingomonas guangdongensis* is also in possession of a gene labelled 'ExoY', along with three *Novosphingobiums*: *mathurense*, sp.CF614, and sp. KN65.2.

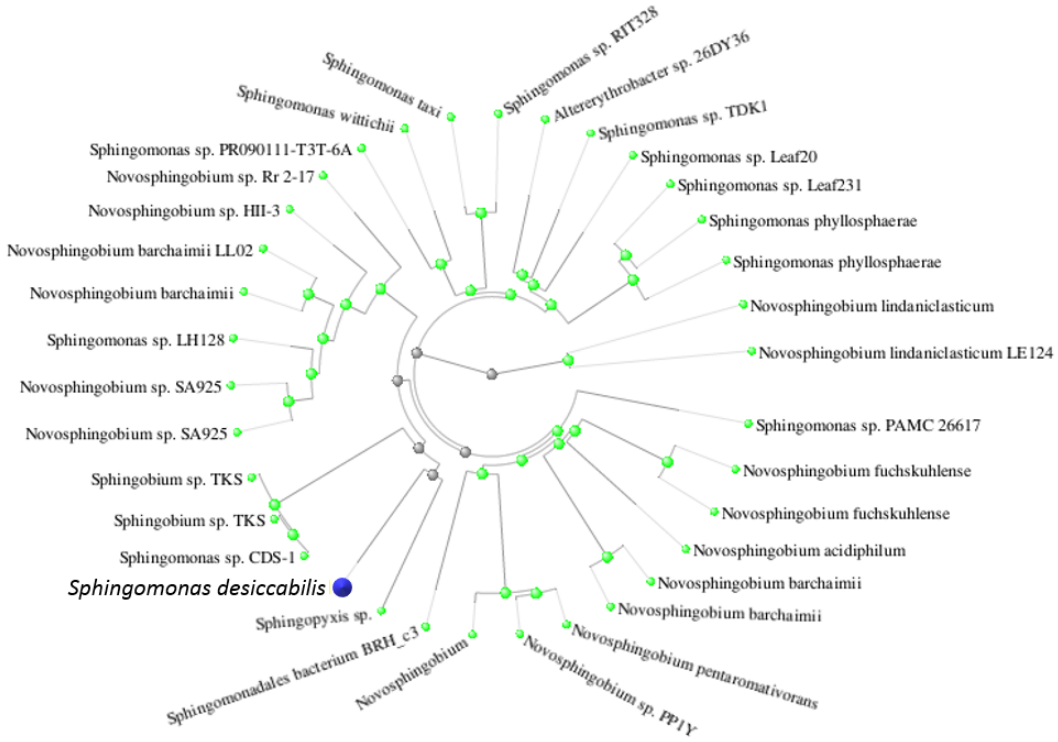

Figure 37: Circular cladistic tree showing neighbour joining of other Sphingomonads in possession of a homolog of the gene labeled SDES-v1-20211. Data from an NCBI protein BLAST.

Gene 3: Unnamed, linked to 'YveL', and 'YwqD'
Label: SDES-v1-10782
Product: Exopolysaccharide/pepcterm locus tyrosine autokinase
Syntones in other Sphingomonads: *Sphingomonas* sp. Leaf11, *Sphingopyxis* sp. MC1, *Sphingopyxis alaskensis* RB2256, *Sphingopyxis baekryungensis* DSM 16222, *Sphingobium* sp. SYK-6, *Sphingobium japonicum* (BiD32 and UT26S), *Sphingomonas wittichii* RW1, *Novosphingobium aromaticivorans* DSM 12444, *Novosphingobium pentaromativorans* US6-1.
Notes: Tyrosine kinases have been shown to be required for the formation of structured *B.subtilis* biofilms [156], although it is worth adding the caveat that the activity of bacterial protein tyrosine kinases is variable, depending on their interaction with modulator proteins.

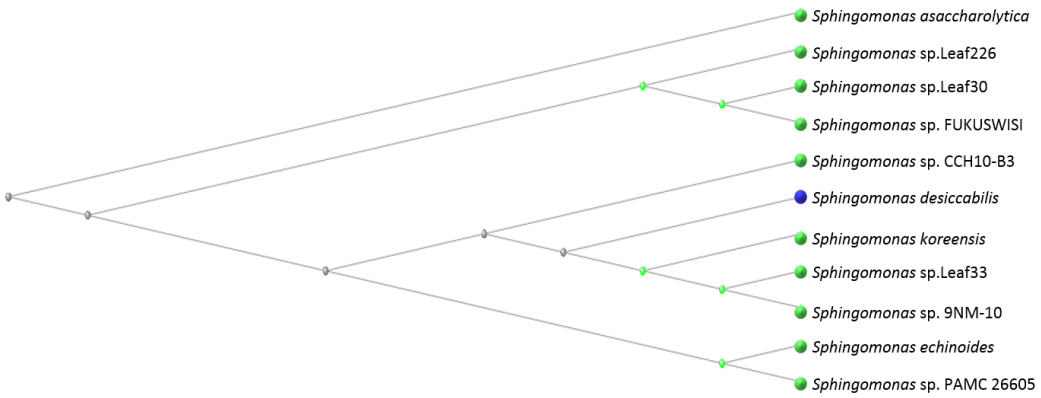

Figure 38: Slanted cladogram showing neighbour joining of other Sphingomonads in possession of a homolog of the gene labeled SDES-v1-10782. Data from an NCBI protein BLAST.

Gene 4: Unnamed, linked to 'GumC', 'Wzc', 'Ptk [H]', 'yveL', and 'pssPch'.
Label: SDES-v1-11033
Product: Capsular exopolysaccharide biosynthesis protein
Syntones in other Sphingomonads: *Sphingomonas wittichii* RW1, *Sphingopyxis baekryungensis* DSM 16222, *Sphingobium* sp. SYK-6, *Sphingomonas* sp. Leaf11, *Sphingopyxis* sp. MC1, *Sphingopyxis alaskensis* RB2256
Notes: A link was identified between this gene and two other *S. desiccabilis* genes, labelled: SDES-v1-11047 and SDES-v1-11048. Both of these genes are conserved membrane proteins of unknown function.

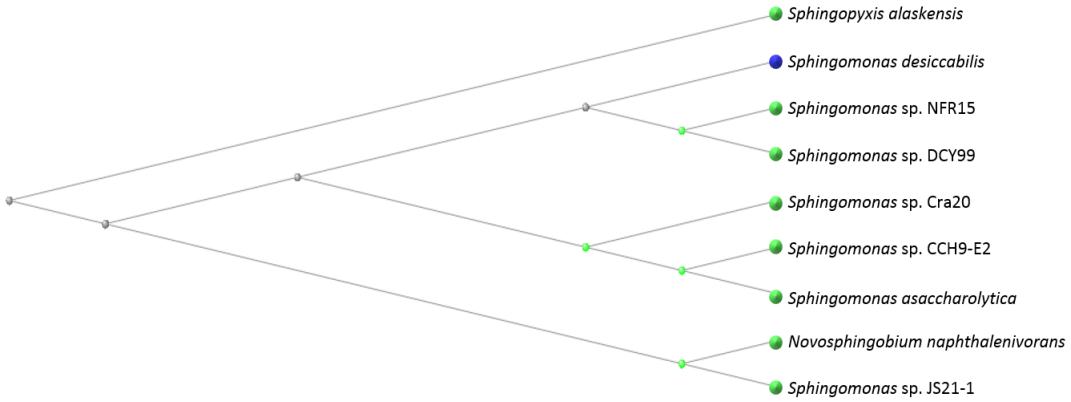

Figure 39: Slanted cladogram showing neighbour joining of other Sphingomonads in possession of a homolog of the gene labeled SDES-v1-11033. Data from an NCBI protein BLAST.

Gene 5: Unnamed, linked to 'pssP'.
Label: SDES-v1-20213
Product: Putative Capsular exopolysaccharide biosynthesis protein
Syntones in other Sphingomonads: *Sphingobium japonicum* BiD32, *Sphingomonas wittichii* RW1

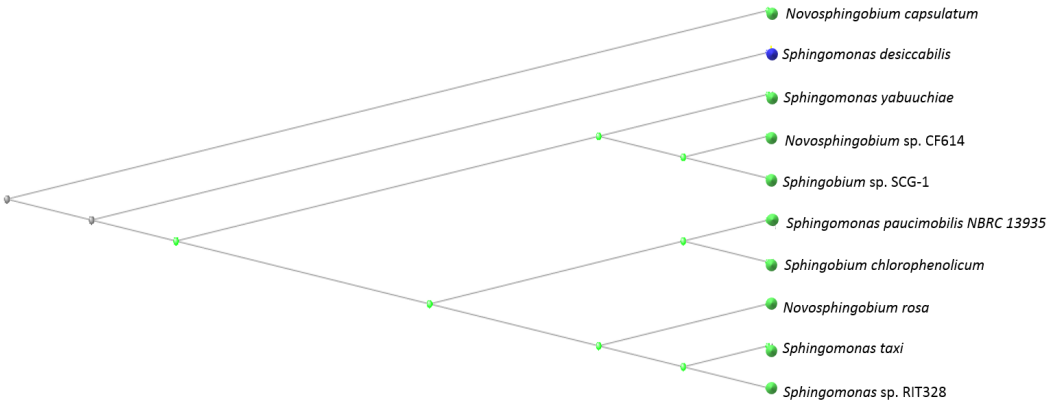

Figure 40: Slanted cladogram showing neighbour joining of other Sphingomonads in possession of a homolog of the gene labeled SDES-v1-20213. Data from an NCBI protein BLAST.

Gene 6: Unnamed.
Label: SDES-v1-20465
Product:Exopolysaccharide biosynthesis protein
Syntones in other Sphingomonads: None found on MaGe database.
Notes: This gene was ellusive on the MaGe database. Conversely, when run through NCBI it brought up too many sphingomonad homologs to concisely describe here, and yet none of them were shown to be closely related to *S.desiccabilis* see Fig.41.

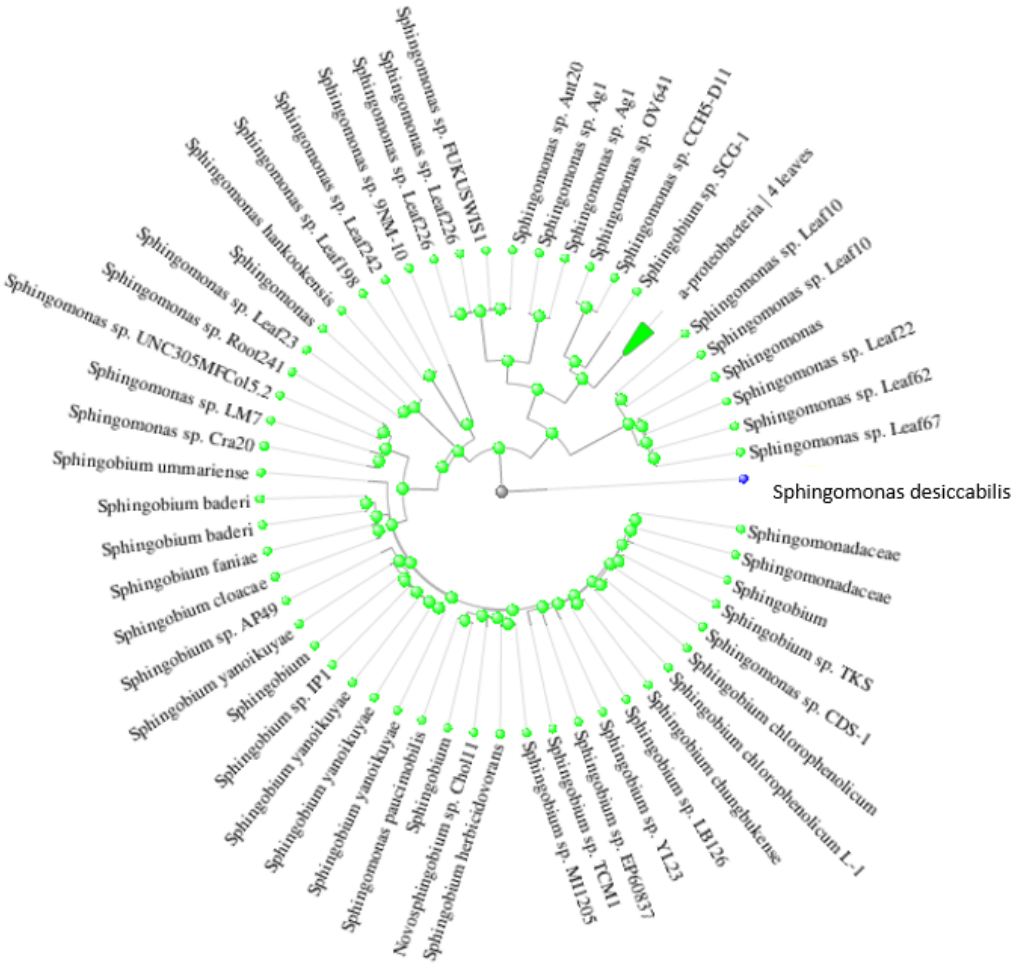

Figure 41: Circular cladistic tree showing neighbour joining of other Sphingomonads in possession of a homolog of the gene labeled SDES-v1-20213. Data from an NCBI protein BLAST.

Gene 7: Unnamed, linked with 'GumC'.
Label:SDES-v1-40251
Product:Exopolysaccharide biosynthesis protein
Syntones in other Sphingomonads: *Sphingomonas* sp. Leaf11, *Sphingomonas wittichii* RW1, *Sphingopyxis baekryungensis* DSM 16222, *Sphingobium japonicum* (BiD32 and UT26S), *Sphingobium indicum* B90A, *Sphingopyxis* sp. MC1, *Sphingobium* sp. SYK-6, *Sphingopyxis alaskensis* RB2256, *Sphingobium chlorophenolicum* L-1, *Novosphingobium aromaticivorans* DSM 12444.

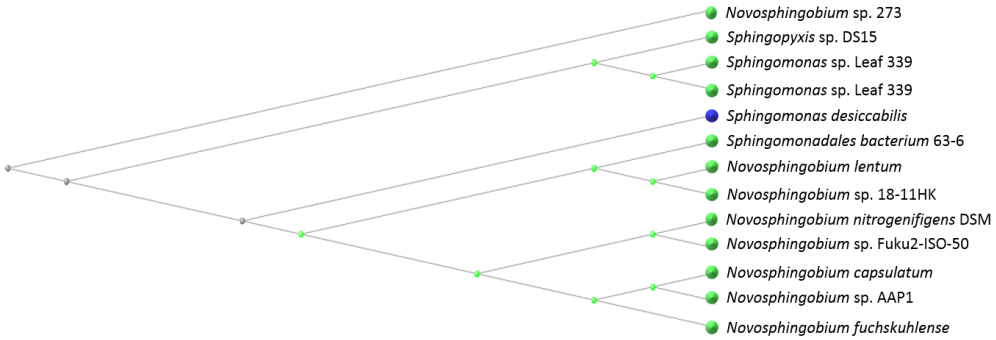

Figure 42: Slanted cladogram showing neighbour joining of other Sphingomonads in possession of a homolog of the gene labeled SDES-v1-40251. Data from an NCBI protein BLAST.

Gene 8: Unnamed, linked with 'PssZ' and 'Pss'.
Label: SDES-v1-90005
Product: Exopolysaccharide biosynthesis polyprenyl glycosylphosphotransferase family protein.
Syntones in other Sphingomonads: None.
Notes: Linked to an inner membrane protein, found in *Magnetotactic ovoidal bacterium* MO-1, dealing with the biosynthesis and degradation of surface polysaccharides and lipopolysaccharides.

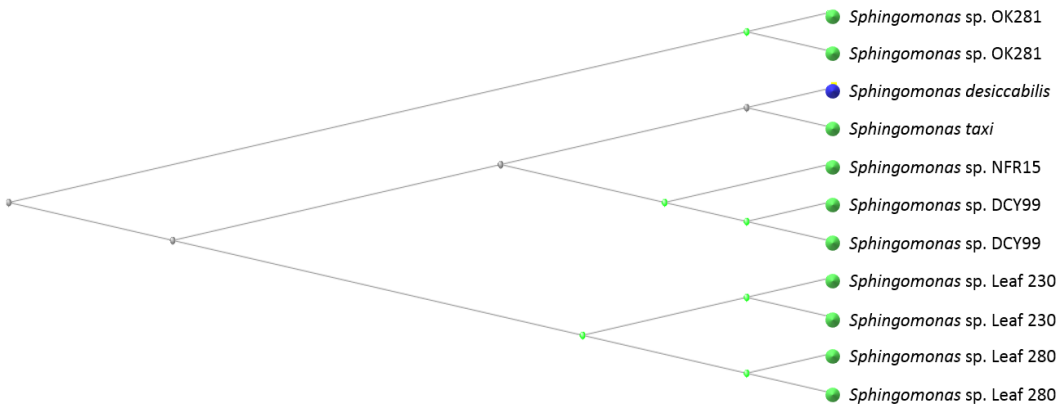

Figure 43: Slanted cladogram showing neighbour joining of other Sphingomonads in possession of a homolog of the gene labeled SDES-v1-90005. Data from an NCBI protein BLAST, duplicate species names show that the homolog has been found in different sequences of the same subspecies.

Gene 9: Unnamed, linked with 'Gum C'.
Label: SDES-v1-90013
Product: Exopolysaccharide biosynthesis protein
Syntones in other Sphingomonads: *Sphingomonas* sp. Leaf11, *Sphingopyxis baekryungensis* DSM 16222, *Sphingobium chlorophenolicum* L-1, *Sphingobium sp.* SYK-6, *Sphingobium indicum* B90A, *Sphingobium japonicum* UT26S, *Novosphingobium aromaticivorans* DSM 12444.

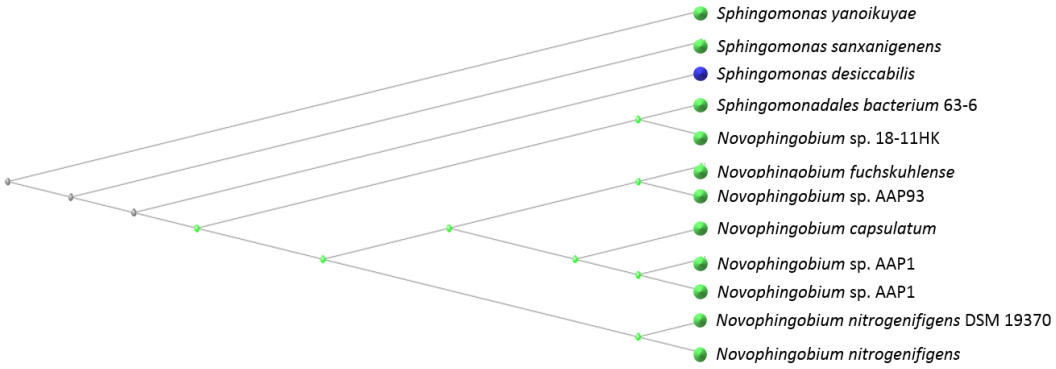

Figure 44: Slanted cladogram showing neighbour joining of other Sphingomonads in possession of a homolog of the gene labeled SDES-v1-90013. Data from an NCBI protein BLAST.

Discussion

According to work done by Reddy and Garcia-Pichel[91], the closest relative to *Sphingomonas desiccabilis* is *Sphingomonas panni*, with a 97.9% 16S rRNA gene sequence similarity. The DNA-DNA relatedness to the type strain of *S. panni* was only 18% however, and the two organisms were isolated from very different environments. While *S.desiccabilis* was isolated from biological soil crusts in the arid Colorado desert, USA, *S.panni* was isolated from a sponge in the Medical Clinic for Small Animals and Ungulates at the University for Veterinary Medicine Vienna, Austria[157], suggesting they may be adapted to substantially different environments. *S. panni* was not available on the MaGe platform for comparisons, and did not register as a high probability match on any of the gene Blasts using the NCBI platform.
In Figure 45, a table from Saitou and Nei[155], which shows the position of *S. panni* and its closest cladistic neighbours has been highlighted to show those that have exhibited one or more of the biofilm-related genes identified in *Sphingomonas desiccabilis*.

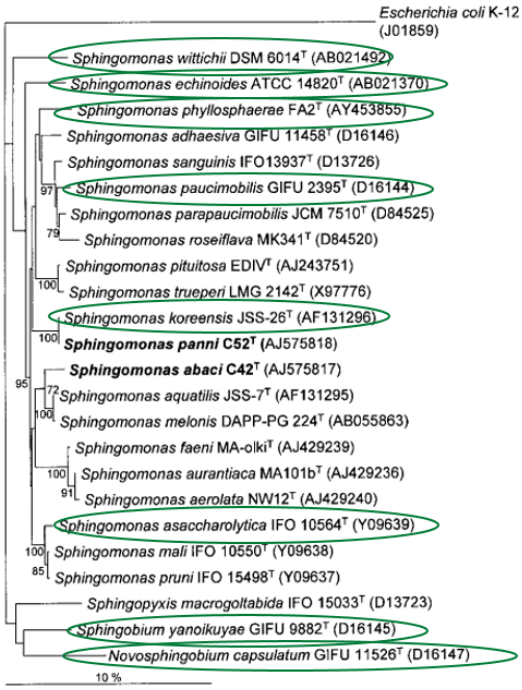

Figure 45: Neighbour-joining tree (Saitou and Nei, 1987) indicating the closest related species to *Sphingomonas panni*, which is reportedly the closest relative to *Sphingomonas desiccabilis*. The organisms that share one or more biofilm relevent gene with *S.desiccabilis* have been highlighted.

Tables 8 and 9 have also been constructed from the MaGe and BLAST results, showing the Sphingomonads that are marked as sharing more than one of the exopolysaccharide genes. The organism which possess the greatest number of homologs to the biofilm related genes idenitified in *S.desiccabilis* was *Sphingobium japonicum*, followed by *Sphingopyxis baekryungensis*, and *Sphingomonas* sp. Leaf11, which does no appear in any publications, but is also be associated with Tatiparthi Reddy.

Table 8: Shared Biofilm Genes from MaGe

Sphingomonad Genera and species:	N° of Shared Biofilm Genes:
Sphingobium japonicum	7
Sphingomonas sp. Leaf 11	4
Sphingopyxis baekryungensis DSM 16222	4
Sphingomonas wittichii	3
Sphingobium chlorophenolicum	3
Sphingopyxis alaskensis RB2256	3
Sphingobium sp. SYK-6	3
Sphingobium indicum B90A	3
Novosphingobium aromaticivorans DSM 12444	3
Sphingopyxis sp. MC1	2

Table 9: Shared Biofilm Genes from BLAST Results

Sphingomonad genus and species	N° of Shared Biofilm Genes
Novosphingobium capsulatum	3
Novophingobium sp. AAP1	3
Sphingomonas taxi	3
Sphingomonadales bacterium 63-6	2
Novophingobium sp. 18-11HK	2
Novophingobium nitrogenifigens DSM 19370	2
Novophingobium fuchskuhlense	2
Sphingomonas yanoikuyae	2
Sphingobium sp. SCG-1	3
Sphingomonas sp. NFR15	2
Sphingomonas sp. DCY99	2
Sphingomonas asaccharolytica	2

An additional 19 genes were found which are involved with temperature and osmotic shock, including genes for the synthesis of trehalose, 14 genes involved DNA repair, and 24 genes involved in efflux pumps that contribute to the resistance of xenobiotic stresses - such as drugs and toxic heavy metals; see Appendix C. At least one of the efflux pumps, AcrD, is shared by *C. metallidurans*, which may help *S.desiccabilis* with its mineral leaching capabilities.

5.3.4 Conclusion

These three different lines of investigation were intended to determine the suitability of *Sphingomonas desiccabilis* for the space-flight experiment, and to learn more about the organism, its stress resistance, and its biofilm forming capabilities.
From the desiccation experiments it appears that *S. desiccabilis* is also a suitable space-flight model organisms along with *Bacillus subtilis* and *Cupriavidus metallidurans*. This is backed up by the genes identified as contributing to temperature and osmotic stress, which would allow anhydrobiotic resistance, as well as the discovery that *S.desiccabilis* has the capability to synthesise and utilise trehalose, an intracellular sugar well known for conferring cryptobiotic advantages. The gene sequencing also allowed identification of biofilm associated genes, which helped to group the species with others within its order that form biofilms in a similar manner.
Looking at the extent to which biofilm growth was accelerated or slowed by different nutrient concentrations allowed for decisions to be made about how best to create an environment to take full advantage of the three week experimental window. It was decided that a 50% solution would provide enough of a nutrient strain to promote biofilm formation at a faster rate than the full solution, but that the 20% solution might provide too limited a solution in microgravity, where the stress that allegedly sparks faster growth is the reduced mixing and reduced availability of nutrients. It also allowed the use of CLSM to qualify biofilm growth, and as microgravity's effect on bacterial growth may be a reflection of the nutrient availability gradient, the information gathered could help with interpretation of the BioRock results.

5.4 Preliminary Biomining Reactor Growth Tests

5.4.1 Introduction

Before the call for applications to tender the design and construction of the Experimental Units (EUs) could go out, it was necessary for the science team to establish acceptable parameters for a BioMining Reactor (BMR).

In order to determine the extent to which different spatial relationships between the components of the hardware affected growth of the model organisms, a number of different preliminary biomining reactors (BMRs) were built and tested. This allowed investigators to answer two important questions:
1)Would the different dimensions of the BMRs have a bearing on the successful culturing of *S.desiccabilis* biofilms,
2) Would the proposed AF-2400 gas permeable membranes allow for sufficient oxygen diffusion into the system without biological contaminants. [119]

The geometrical dimensions that were altered in the different BMR designs allowed the following parameters to be explored:
i) Volume of R2A nutrient solution,
ii) Membrane effective area,
iii) The distance between the basalt slide and the membrane,
iv) The gravity vector - acheived by turning the BMR upside-down.

There was a reference configuration BMR, (see Fig.46) and, the additional BMRs tested both greater and lesser values for the above parameters (see Table 10 in section 5.4.3).

5.4.2 Methodology

Basalt slides were washed and then autoclaved to ensure that they were sterile. BMRs were instead wiped with ethanol, as it was not trusted that they would survive the temperatures and pressures of the autoclave machine.
The inoculation culture of *Sphingomonas desiccabilis* was made up from the monocultures in glycerol, and grown in R2A. The optical density of the starting culture was 0.038Abs. Before being screwed into the base cavities, 100μl of culture solution was introduced onto the basalt slides inside sterile petri-dishes inside the lamina flow hoods and dried down.
In order to simulate the material BMR conditions as much as possible, the three controls were set up in plastic centrifuge tubes, rather than the usual glass conical flasks. The desiccated inoculated basalt slides of the same dimensions as those used in the BMRs (2cm x 2cm x 2mm) were placed in the centrifuge tubes, and 5ml of R2A was added. Lids were left on to reduce the chances of contamination, but were kept loose enough to allow gas exchange. The BMRs were set up as per test guidelines in the ELIPS-SA-DOC-002 and left at room temperature, 21^{o}C.
After three week, controls in the centrifuge tubes were mixed by pumping air-bubbles into the tubes with the micropipettes with sterile tips, until solution was uniform in colour with no clumps of organisms. From each control 1ml of the culture solution was extracted and placed into cuvettes for O.D. spectroscopy, at

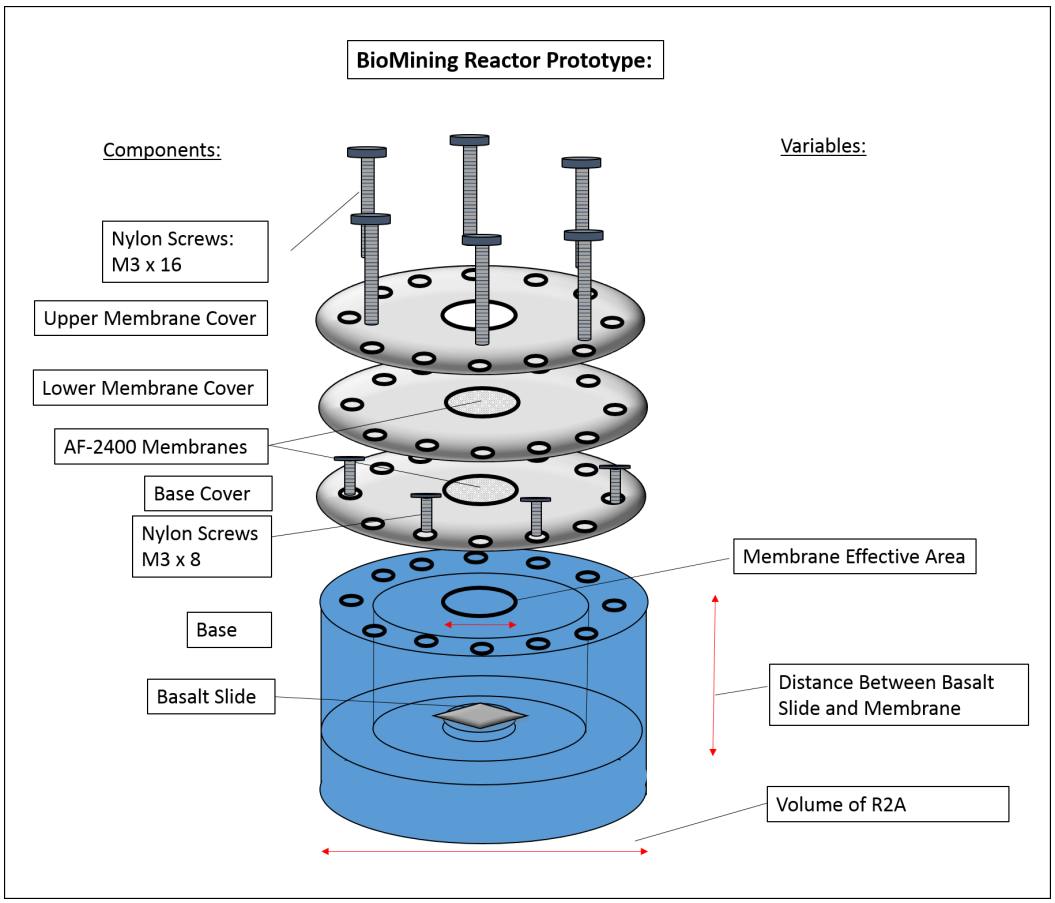

Figure 46: Exploded diagram of the prototype Biomining Reactors. The fourth variable, the change in gravity vector, is not shown here.

600nm.
After readings were taken on the controls, the six M3x16 screws were removed from the first BMR, and the upper and lower membrane covers were lifted free. The lower membrane was transferred with sterilised tweezers into a petri dish for closer examination through a light microscope. The 5ml of culture solution in the BMRs was extracted using micropipettes with sterile tips, and placed inside a centrifuge tube where the solution could be thoroughly mixed with the pipettes, as per the controls, before 1ml was transferred to a cuvette for O.D. spectroscopy. The six M3x8 screws were then removed, and the basalt slide was placed inside a petri dish for later examination through a light microscope. This procedure was then repeated on the remaining BMRs.
After the O.D. spectroscopy, the lower membranes and basalt slides were stained with SYBR green I nucleic acid gel stain, at a dilution of 1: 1000 sterile deionised water. They were then viewed under the blue light filter of an inverse light mi-

croscope in order to establish whether biofilms were forming on the basalt slide, and to see whether there was bacterial growth on the lower membranes.

5.4.3 Results and Discussion

Results from the three week test are in Table 10; from the reference configuration results alone (1i – 1iii) we can see that there is considerable variation in how *Sphingomonas desiccabilis* grows over time, but that every BMR allowed for growth.

Table 10: The Optical Density of Growth in the Different Prototype Biomining Reactors

BMR	Volume of R2A (µl)	Depth (mm)	Diameter (mm)	Membrane effective area (mm^2)	Orientation	Optical density: 0 h	Optical density: 3 weeks
C1	5000	9	36	n/a	Up	0.038	0.683
C2	5000	9	36	n/a	Up	0.038	0.707
C3	5000	9	36	n/a	Up	0.038	0.549
1i	5000	10	26.2	10	Up	0.038	0.308
1ii	5000	10	26.2	10	Up	0.038	0.697
1iii	5000	10	26.2	10	Up	0.038	0.338
2a	10 000	10	36.4	10	Up	0.038	0.444
2b	16 000	10	45.7	10	Up	0.038	0.554
3a	5000	10	26.2	20	Up	0.038	0.639
3b	5000	10	26.2	n/a	Up	0.038	0.581
3c	5000	10	26.2	5	Up	0.038	0.553
4a	5000	27	16	10	Up	0.038	0.804
4b	5000	4	41.5	10	Up	0.038	0.440
4c	5000	17	20.1	10	Up	0.038	0.751
5a	5000	10	26.2	10	Down	0.038	0.421

Visual confirmation of biofilm growth was also established (see Fig. 47).

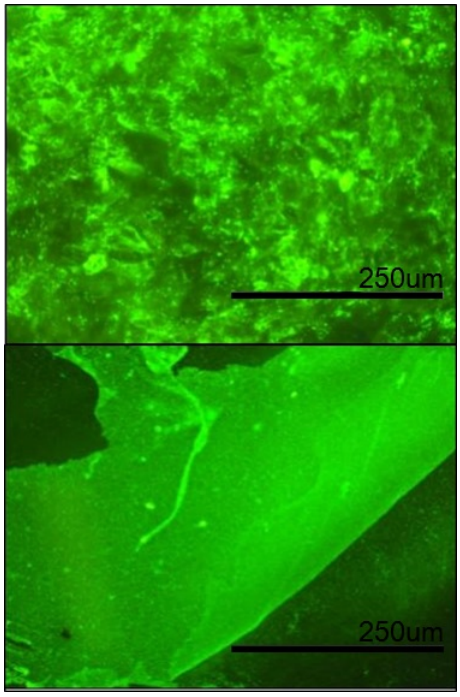

Figure 47: Pictures obtained from light microscopy after 3 weeks of growth in the prototype BioMining Reactors, stained with SYBR Green. Top image shows biofilm growth on the basalt slides, bottom image shows the biofilm growth on the gas permeable membrane.

In order to apply statistics to the test, a number of the BMRs were chosen for repeats. A a one-way ANOVA test was run in order to assess whether the results indicated a difference between the controls and the BMR treatments, and also to assess whether the different BMR treatments had a significant effect on the growth rates of the organisms. The statistics were run on R-3.1.2 for Windows. The analysis was done using the raw data, and no transformations were required. The graph readouts for the Residuals vs Fitted suggested no unusual data points in the data set, and the Q-Q plot indicated that the data was normally distributed. (see Fig. 48).

The final readout on the ANOVA test gave a P-value of 0.2637; and the null hypothesis that the different reactor geometries would have no effect on the growth rates of*Sphingomonas desiccabilis* was accepted.

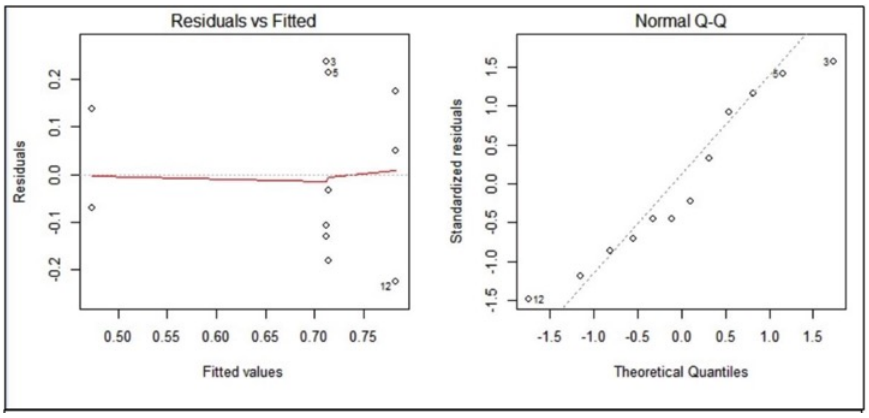

Figure 48: The Residuals vs Fitted plots and the Normal Q-Q plot given by R 3.1.2..

5.4.4 Conclusion

Growth occurred in all versions of the BMR. Conclusions were therefore drawn that the AF-2400 membranes performed as expected, allowing sufficient airflow to pass in order to sustain growth. None of the proposed dimensions appeared to inhibit the growth of the model organisms. It was proposed that the observed variability was that inherent in culturing microorganisms. This was a positive result for BioRock, as the conditions in all of the BMRs was favourable for growth, meaning the experimental design for the ISS mission could remain relatively simple.

5.5 Experimental Unit Growth Tests

New hardware was constructed for the BioRock experiment, based on the experimental design specifications set down by the PI Charles Cockell, research undertaken at the University of Edinburgh (see section 5.4), the dimensions of the Kubik centrifuge on board the ISS, and safety requirements set in place by ESA and other members of the international space community with interests in the International Space Station. The following experiments were conducted once Kayser Italia had completed their initial blueprints, and delivered the first iterations of the Experimental Units (EUs).

5.5.1 Materials Compatibility

All of the different materials which had been proposed for the construction of the Experimental Units, and which would have direct contact with the growing organisms at one time or for the duration of growth, were tested to see if they

would manifest any toxic effects on any of the three test organisms (see Fig. 49). An additional objective was to ensure that the materials would survive the autoclaving procedure at 121^{o}C and pressures of 100kPa.

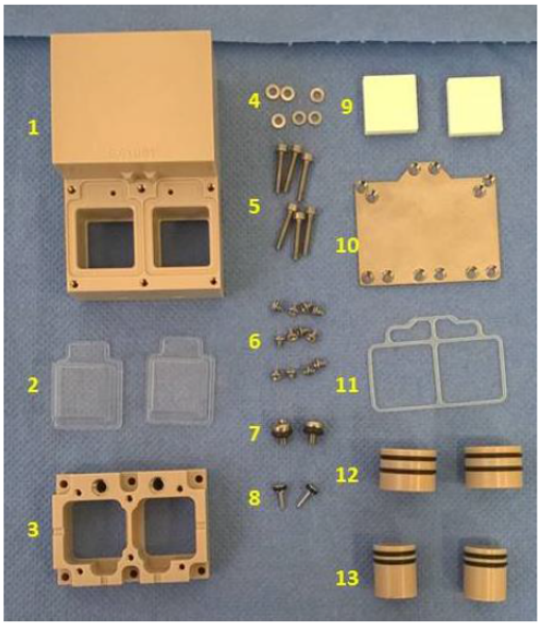

Figure 49: The different components which make up the Experimental Units.

The materials were tested individually, with a later test planned for the assembled pieces to ensure that in combination any negative effects were not compounded to prevent growth.
Sphingomonas desiccabilis, Bacillus subtilis, and *Cupriavidus metallidurans* were cultured, and all materials allowed growth within expected parameters.

Table 11: The Different Mineral Components of the Experimental Units and Whether Growth was Recorded

Material Composition	Growth
Silicone Generic	Yes
Silicone Xiameter RBL-2004-60	Yes
PEEK	Yes
INOX A1 ISO2338 2h8x6	Yes
INOX A4 KI-STR-DRW-036 A151 316	Yes
Silicone SL600W	Yes
PEEK PVX K1-SPH–DRW-013	Yes
Silicone O-ring VMQ 80	Yes
EPDH O-ring	Yes
PTFE - TEFLON	Yes
AISI 420 DIN 6799 23	Yes
VITON O-ring	Yes
INOX A2 DIN 433 M1, 4 AISI 304	Yes
INOX A4 DIN 912 M2x26 AISI 316	Yes
SILICONE SSP – M823	Yes

5.5.2 Experimental Unit Biofilm Growth Tests

Sphingomonas desiccabilis was grown up overnight from stock kept in glycerol in the -80°C freezer. The Experimental Units (EUs) and basalt slides were cleaned and autoclaved.
After sixteen hours of growth, the optical density was measured at 600nm, giving a reading of 0.083 absorbency, indicating that the culture was still at the very start of its growth phase. Using a swab, the pistons were lubricated with silicon oil and inserted into the main body using the Piston Removal Tool, then manoeuvred into the correct alignment using the Piston Positioning Tool.
Fixative steps in the assembly procedure were bypassed for this test, so Fixative Valves were directly inserted into the Fixative Filling Ports without injecting the fixative.
A sterile syringe was filled with 5ml of the *S. desiccabilis* in R2A (at 0.083A), and injected into the Medium Reservoir, with the EU tilted to allow the air to escape as the reservoir filled. This was repeated in a second Experimental Unit.
Sterile basalt slides were placed in the Culture Chamber using sterile tweezers, and the Chamber Inlet Ducts were filled with R2A, with care taken not to pierce the membrane with the needle. The Bottom Gasket was laid in place with ster-

ile tweezers, and the Bottom Cover attached to the Main Body, tightening each screw diametrically across from the one before it, to ensure uniform compression of the Bottom Gasket.
The test screws were checked for tightness, and then the Medium Pistons were slowly depressed with the Piston Removal Tool, until the Culture Chambers were filled with the culture media (see Fig. 50)
One EU was left overnight and the other was left for 1 week. 5 ml of the culture media was also inserted into two falcon tubes to act as controls for the growth in the EUs. Both controls and the EUs were left at room temperature.

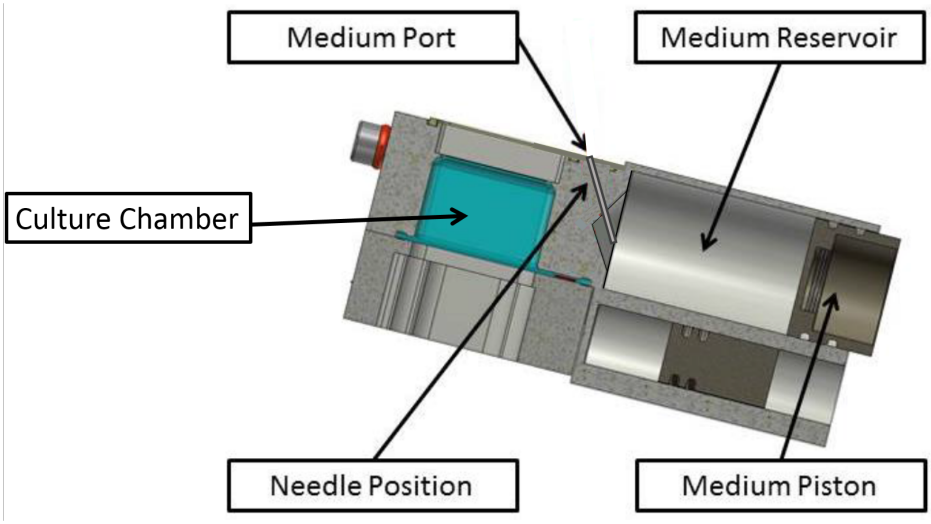

Figure 50: Annotated drawing of the Experimental Unit

After incubation, the Test Screws were removed, and the liquid culture was extracted using a sterile syringe. The Bottom Cover was then removed, and the basalt slide retrieved. The liquid cultures were vortexed to ensure homogenous distribution of the cells within the solution, and then placed in cuvettes for optical density measurements (see below).

Table 12: Optical Density Growth Measurements of *Sphingomonas desiccabilis* in the Experimental Units and Controls After 1 day and 1 Week

	Start culture	Control	Experimental Unit
1 day	0.083	0.295	0.481
1 week	0.083	0.561	0.743

The results indicated that the model organism *Sphingomonas desiccabilis* would be able to successfully grow in the EUs, with the data suggesting that growth was benefited by the conditions of the EU. This is perhaps due to the presence of the gas permeable membrane providing a larger surface area for oxygen diffusion (see Fig.51), which allowed 30mm^2 as opposed to the 47mm circumferance of the top of the falcon tube left a little loose to provide O_2 for the control samples.

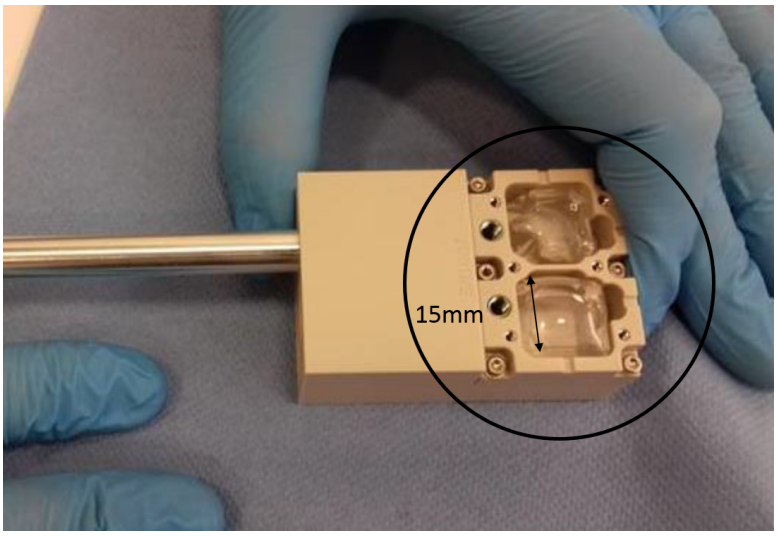

Figure 51: The Experimental Unit, with highlighted membrane effective area.

5.5.3 Conclusion

None of the materials that were selected for the manufacturing of the experimental units (EUs) inhibited growth, and none of the materials were damaged in the autoclaving process. It was noted that the rubber o-rings were slightly less elastic after being autoclaved, but this did not appear to prevent them from fulfilling their function.
The growth tests conducted inside the EUs showed that *S.desiccabilis* grew to higher populations than the control groups in their falcon tubes. This is likely due to the increase in surface area through which oxygen diffusion can take place, and is a beneficial result for the BioRock experiment.
It would have been advantageous to perform the experiment for the three week duration that the BioRock experiment will be conducted, but due to time-constraints for when the Payload Integration Manager required the information, one week of growth was deemed a reasonable compromise.

5.6 Fixative tests

As discussed in section 5.2, the biofilms need to be fixed before returning to Earth. This is to minimise changes to the biofilm structures and limit as far as possible any biologically induced weathering when the experimental units are undergoing the additional *g*s of re-entry, and later, terrestrial gravity.
Due to the toxic nature of fixatives, their use on board the ISS is highly restricted. Experimental protocols which use fixatives must have multiple fail-safes in place to ensure there is no leakage. Even with fail-safes built into the experimental design, the use of the most effective fixatives such as glutaraldehyde and formaldehyde is discouraged. As a result, efforts were made to find a less toxic fixative that would halt growth. The two fixatives that were tested were RNAlater, and NOTOXhisto, as these had already been used on ISS missions[158][74], and have less severe constraints.

5.6.1 RNA later

An initial experiment, with RNAlater at 10%, 20%, and 40% of the sample volume, was performed.
Basalt pieces, 1 x 1 x 0.4cm, were placed in nine wells of a 12-well plate, with 1000μl of 100% R2A and 20μl of *Sphingomonas desiccabilis* culture, grown up from freezer stocks the night before. The samples were left to grow for a week, and then homogenised by pumping action with pipettes. 20μl of each solution was extracted for serial dilution and pre-RNAlater CFU counts. For the remaining sample volumes of 1000μl, RNAlater was added to make up a 20% (2:10) ratio as stated in the Experiment Scientific Requirement document (ESR), and also at 10% (1:10) and 40% (4:10) to give half and double the ESR proportions. The fixative was left in the wells for 24 hours, and then the samples were homogenised and 20μl was extracted for serial diluting and plating for post-RNAlater CFU counts.
The post-RNAlater counts were diluted five times to 10^5, however, counting at 10^5 was not possible, as the bacteria had continued to grow overnight, and all of the plates had joined colony coverage instead of countable spots. As growth was meant to have been arrested, the unchecked growth at 10^5 was unexpected, and while it did not provide quantifiable data, the presence of matt growth indicated that even double the recommended concentrations of RNAlater were not high enough to fix growth. The experiment was repeated using concentrations of 50% (1:1), 83% (5:1), and 91% (10:1).
After exposure to these three different concentrations, the percentage survival was 8.7%, 3.4%, and 2.3% respectively, with CFUs averaging at $10x10^4$, $62x10^3$, and $62x10^3$ respectively (see Fig.52).

Shingomonas desiccabilis showed continued growth 24 hours after exposure to the

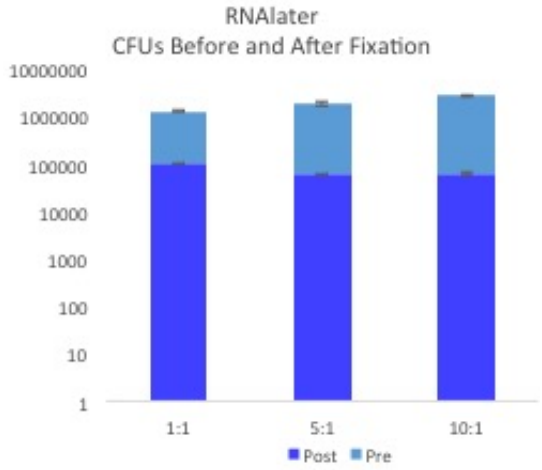

Figure 52: Colony forming units; light blue: aliquots plated from samples before the RNAlaterfixative was added, dark blue: samples plated 24 hours after addition of fixative.

highest levels of RNAlater. Growth was slowed, but the quantities used in the experiment with higher dilutions of fixative would not be possible to work around when making the Experimental Units, and so it was concluded that RNAlater would not sufficiently constrain growth for the time-frames involved in a space-flight experiment.

5.6.2 NOTOXhisto

NOTOXhisto was tested on all three BioRock organisms, and growth was tested after 1 week of exposure to the fixative, and after 4 weeks of exposure, with samples being stored at 4°C and at 8°C. This was to more closely replicate the conditions of the cold stowage facilities on board the ISS, where the samples will be refrigerated in 'MERLIN', a refrigerator/freezer incubation unit, which should keep the samples as cold as 4°C on their return to Earth, but could deviate as high as 8°C.

5.6.3 Methodology

Sphingomonas desiccabilis, *Bacillus subtilis* and *Cupriavidus metallidurans* were each grown up in R2A on 12 basalt slides for a duration of 1 week, then NOTOXhisto was added to all samples. Half of the samples were placed in a 4°C fridge, and the other half were placed in an 8°C fridge. After 1 week of sitting

in fixative at their respective temperatures, thirty-six of the samples – 12 per organism – were removed for analysis. Six of the basalt slides, per organism, were separated for a crystal violet assay, and six remaining slides were returned to their respective fridges for a further 3 weeks.
The liquid cell culture was removed using pipettes. A crystal violet solution of 0.04% was made up with distilled water, introduced to the basalt slides, and left for 15 minutes to allow the crystal violet to bind to the proteins and DNA of the sample biomass. The crystal violet was then removed using 1ml pipettes, and each plate was washed gently in PBS, twice. Once the washing phase was complete, 7.5ml of a 33% acetic acid solution was introduced into the plates and left for 15 minutes, to dislodge the remaining crystal violet from its bound proteins and DNA. To test the optical density of the freed crystal violet, which is proportional to the amount of biomass attached to the basalt, 1ml of each acetic acid/freed crystal violet mixture was put into cuvettes and placed into the spectrometer, zero-ed with R2A and set at 550nm.
This was then repeated for the samples that had been kept at 4^oC and 8^oC for a total of 4 weeks. The two time points and two temperatures were then compared using ANOVAs and two-tailed T-tests.
Six basalt slides were also sterilised and inoculated with *Sphingomonas desiccabilis* and grown for three weeks. Half were treated with NOTOXhisto, and then all were left for a week, then stained for confocal laser scanning microscopy (for detailed methods see 3.4.2).

5.6.4 Results and Discussion

Growth on the basalt slides did continue to increase by a small margin with *Sphingomonas desiccabilis* at 4^oC, but measurements of the 8^oC samples showed a reduction in cell density. The difference in growth at 4^oC between 1 week and 4 weeks of growth was 0.0019 Abs, and at 8^oC, the difference was -0.028Abs (see Fig. 53). According to the t-tests, these differences are significant, with P-values of $P = 0.0063$ and $P = 0.0015$ respectively, indicating that the changes between conditions are greater than the conditions between replicates; however, given the low values of the differences in optical density, the conflicting directions of these differences, and the large error bars of the propagated absolute error, it is reasonable to conclude that the differences are simply a reflection of natural biological variation.

The same can be said for *Cupriavidus metallidurans*, which had large absolute error, and contrasting directions of difference in growth. The t-tests showed that the differences between conditions was not significant, either between time points or between temperature conditions, indicating that Notoxhisto works as desired. *Bacillus subtilis* was the most resistant to the Notoxhisto fixative, with an in-

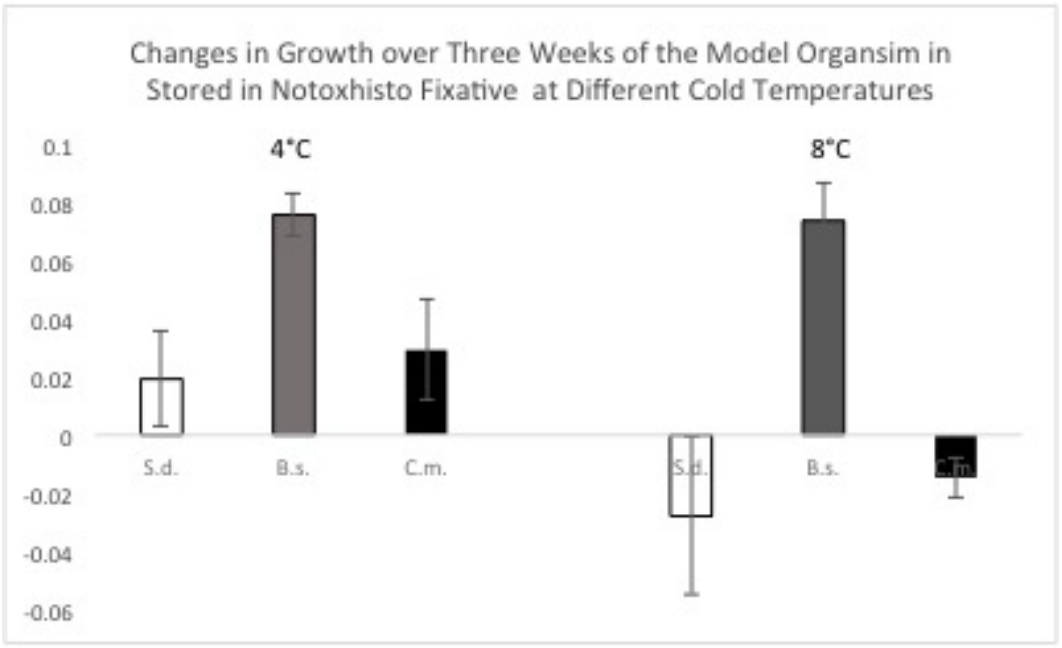

Figure 53: Optical densities of *Sphingomonas desiccabilis* (S.d.), *Bacillus subtilis* (B.s.) and *Cupriavidus metallidurans* (C.m.) after fixing with Notoxhisto and storage at 4^oC (left) and 8^oC (right). Values are the four week growth checks with the 1 week growth checks subtracted.

crease in growth at both 4^oC and 8^oC, of 0.076Abs and 0.074Abs. These values of the continued growth were the highest out of the three organisms, but as with the other organisms, the increase remained low. There was no significant difference between storage at 4^oC and 8^oC.

The images taken of the *Sphingomonas desiccabilis* biofilms with and without exposure to NOTOXhisto alleviated concerns that it may damage the biofilms or disrupt the EPS. An example picture was selected of a biofilm treated with NOTOXhisto is shown in Figure 54.

5.6.5 Conclusion

Neither fixative performed as efficiently as desired, but Notoxhisto slowed the organisms more effectively than RNAlater. We concluded that Notoxhisto fixes growth in *Cupriavidus metallidurans*, and *Sphingomonas desiccabilis*. *Bacillus subtilis* showed a slight increase in growth over four weeks, but growth remained suppressed compared to normal growth rates. Storage at 8^oC showed no adverse effects on the efficacy of Notoxhisto compared to storage at 4^oC, alleviating con-

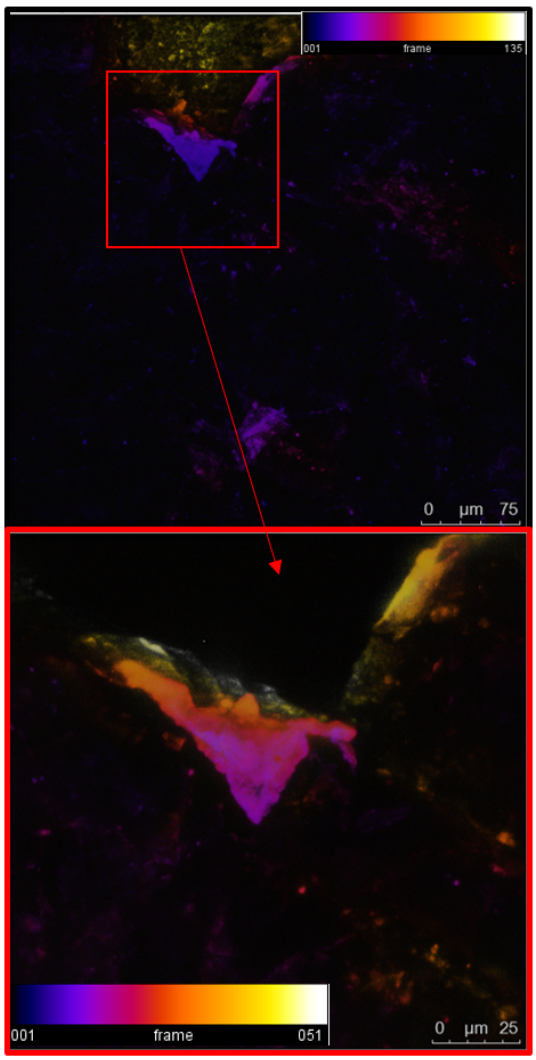

Figure 54: The top image shows a biofilm in a crease of rock at 200 x magnification, and the lower box shows the same biofilm at 400 x magnification. The biofilm shows no anomolies that would suggest it has been altered by the fixative

cerns over possible negative effects of the temperature fluctuation parameters in cold stowage. Therefore the Notoxhisto is to be carried forward as the fixative for the experiment.

5.7 Parabolic Flight

Introduction

In order to investigate whether the injection of nutrient solution into the BMRs in microgravity would wash a different quantity of the desiccated bacteria from the

basalt at 0 x g compared to 1 x g, an experiment was designed to be carried out on parabolic flights. The experimental set-up, dubbed The Two Syringe System (TSS) consist of two syringes attached by a tube, each with a valve that could be closed off as needed (see Fig. 55). Syringe A contained 5ml of PBS, and syringe B contained a thin basalt slide (1cm x 1cm) with dried down *Sphingomonas desiccabilis*. Planktonic bacteria were dried on the surface of the basalt slides as drops from a liquid culture, similar to the desiccation experiments on glass slides, see 5.3.1. Biofilms bacteria were grown on the basalt slides in R2A for 1 week, and then the basalt slides were removed from the nutrient solution and left to dry in the sterile laminar flow hood.
The experiment was conducted with both planktonic and biofilm bacteria, to observe differences between the two states. At the start of each parabola the water in syringe A was injected into syringe B, and after 20 seconds - before the end of the parabola, the water was be pulled back into syringe A. This was repeated with different replicates for ten parabolas per flight, over three flights, giving a total of thirty experiments, fifteen per condition. The same number of experiments was also performed on the ground as control experiments.

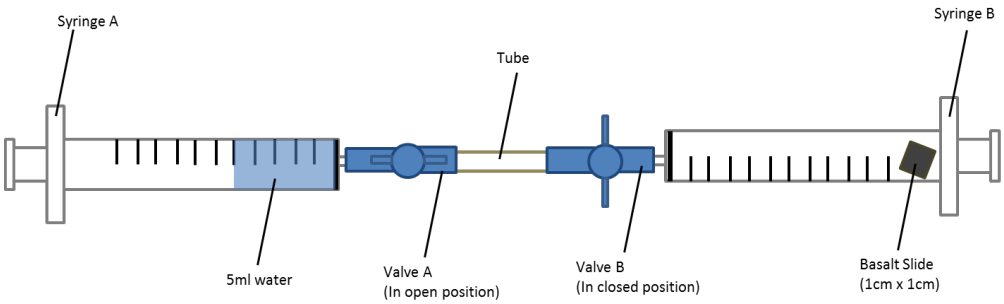

Figure 55: Experiemental set up for parabolic flight, the Two Syringe System.

Once back in the Novespace facility, the cells from the 'A' Syringes were plated out onto R2A agar around Bunsen flames for sterility, as the Novespace laboratories did not have laminar flow hoods. The cells in the PBS that were drawn back into Syringe A after 20 seconds, were serially diluted and plated onto R2A. The basalt slides from Syringe B were placed into containers with fresh PBS, and vortexed to free the remaining desiccated bacteria. These were then serially diluted and plated, and the cell counts from each TSS were compared, giving a ratio that was turned into a percentage.

Results and Discussion

There were no differences that were strong enough to to suggest a clear pattern.

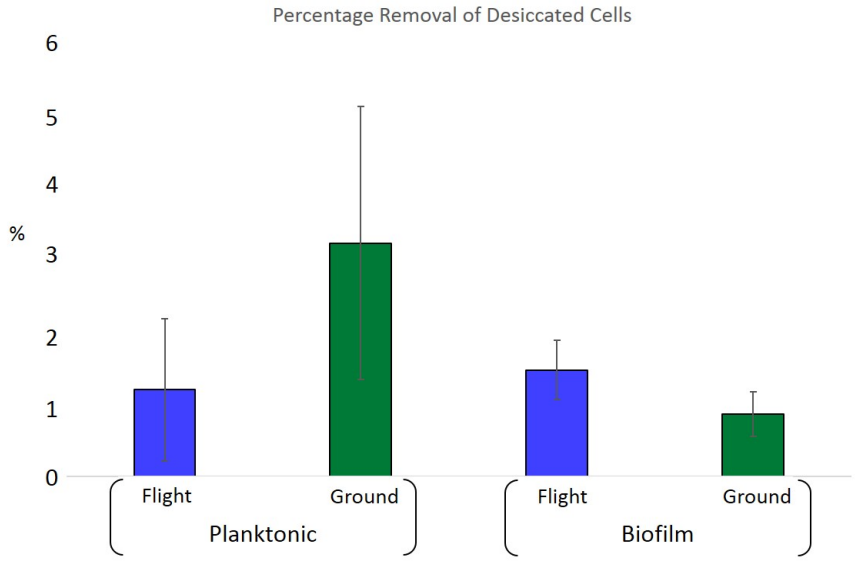

Figure 56: Ratio of desiccated cells disturbed from the surface of the rock by the injection of liquid in different gravity conditions. Bars on the left represent desiccated planktonic cells, bars on the right represent desiccated biofilms.

Rehydrating the bacteria desiccated onto the samples in different gravity regimes did not significantly affect the number of cells washed off the basalt, P=0.343. This is most likely due to turbulence as a mixing force independent of gravity, however it will be worth noting during the analysis of the BioRock experiment that up to 2.5% of the desiccated bacteria on the surface of the rock may be washed from the rock during nutrient solution injection, and unlike the terrestrial controls, these cells will be unlikely return to the basalt surface to contribute to nutrient injection.
Four different experimentalists were brought in to depress the plungers on different flights, in an effort to deliberately bring in more human variation. This was because at the time of the parabolic experimental design, the nutrient solution injection stage of the ISS experimental set-up was due to be introduced by the astronauts. The experimental design for the hard-ware has since been upgraded, and now the plungers will be depressed mechanically by the instrumentation.
If the experiment was to be repeated, the use of a fixative would be included, so that the cells could be processed in the Edinburgh laboratories, where there is access to a laminar flow hood and a sonicator; the latter being a more reliable way of detaching biofilm cells from rock.

Conclusion

The different gravity conditions are unlikely to affect the number of cells washed from the rock by the injection of liquid media into the BMRs, as in a container the dimensions of the BMRs, turbulence will act as a mixing force that is not dependent on gravity. When comparing terrestrial and reduced gravity samples during BioRock post-flight analysis, it will be important to remember that cells washed off the rock at 1 x g will be much more likely to make their way back to the basalt surface, potentially contributing to biofilm biomass, than 10 x g.

5.8 ICP-MS of Rare Earth Elements

5.8.1 Introduction

The previous experiments in this chapter deal with testing the suitability of the model organisms and the experimental hardware for the purposes of the BioRock experiment. Some of the methods employed to assess the success of growth will also be employed during the post-flight analysis of the BioRock samples when they return from exposure to microgravity, specifically the methodologies relating to the Confocal Laser Scanning Microscopy. This method will mainly be used to answer the first of the two questions that BioRock aims to answer, about changes to the biofilm biomass and structure after exposure to reduced gravity. The second question is specifically concerning the change in elemental release rates associated with microbe-mineral interactions during exposure to reduced gravity. The measurement of weathered products will be performed using Inductively Coupled Plasma - Mass Spectroscopy (ICP-MS). In order to assess the efficacy of this method for the desired purpose, and to ascertain some preliminary baseline data, basaltic weathering experiments were performed on the three model organisms.

Early attempts at discerning biotic and a-biotic weathering patterns proved difficult in the case of all the case of *Sphingomonas desiccabilis* and basalt.
Certain elements become bound in the EPS after being leached from the rock, so it is important to try and extract as much of the biofilm from the basalt as possible before the slide is discarded. However, the best methods for detaching the biofilm from the rock can also be disruptive to the rock surface, inducing further leaching that is unrelated to the experimental parameters. Vortexing carried to much risk of breaking up the rock, so repeated exposure to sonication at 50Hz and 60 Hz was employed. Sonication was also performed on abiotic samples for the same amount of time to reduce variation.
Once the EPS has been separated from the rock, it must be broken down completely to make a clear solution for the ICP-MS, and initially this was attempted through filtration after the introduction of nitric acid. The results we retrieved from the first experiments were misleading and displayed no pattern, with the

values varying dramatically between replicates. The use of stronger concentrations of nitric acid, added heat, and sonication to separate the bonds holding the leached elements to the organic molecules did not succeed, and so ashing protocols were introduced (see section 3.5).
Even after instigating ashing protocols to free the inorganic elements that had been taken up by cells or had adhered to the surface of the cells, attempts to use more bio-available elements (e.g. Potassium and aluminium) yielded erratic results. The heavier elements (U, Th) and the rare earth elements (La, Pr, Nd, Sm, Eu, Dy, Er , Yb) are more chemically stable [159] and less biologically available than some of the more common elements. These showed more consistent results within triplicates, and were consequently chosen as more reliable indicators for the weathering rates.

5.8.2 Preparations for ICP-MS

Sphingomonas desiccabilis, Cupriavidis metallidurans, and *Bacillus subtilis* were grown up overnight from frozen stock solutions, with 25μl of each culture aliquoted into separate vials containing 25ml of R2A (100%). Each culture was then brought to a similar concentration, using optical density as a measure of cell density. The starting culture for *S.desiccabilis* was 0.176Abs, 0.185 for *C.metallidurans*, and 0.167 for *B. subtilis*.
Samples were set up in 6-well plates; 50ml of 50%R2A, 5μl of culture, and basalt slides 1 x 1 x 0.4cm (see Fig. 57).

Only three wells out of 6 were used, as a precaution against cross-contamination. The wells were covered in breathable multiwell membranes and wrapped in parafilm to reduce evaporation. They were left to form biofilms for three weeks at room temperature (22^{o}C).
After three weeks, the media was removed from each well with a sterile 1ml pipette and placed in individual 50ml falcon tubes; over three weeks the average loss of liquid, despite precautions, was 1.5ml. The basalt slide was also transferred using sterile tweezers, and the falcon tubes were sonicated for 4 minutes at 50Hz, and again for 4 minutes at 60Hz, to extract as much of the biofilm from the basalt as possible. Previous attempts at preparing samples for ICP-MS included a step of vortexing the falcon tubes, but this step carried the risk of breaking up the basalt slides and releasing additional minerals into the liquid and skewing the mineral release rates.
Basalt slides were then removed, and the media was transferred to sterile glass vials, placed in the furnace for ashing, and re-suspended in nitric acid.

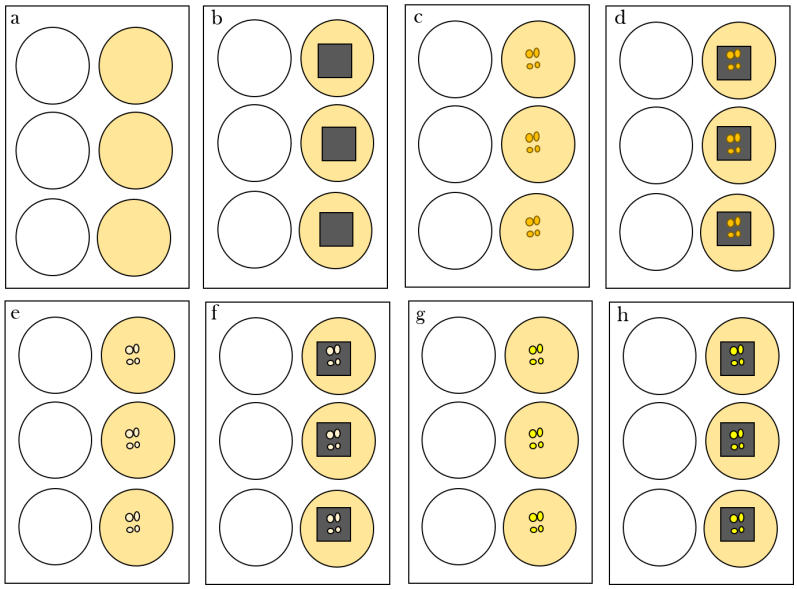

Figure 57: Experimental set-up for ICP-MS experiment. Six well plates containing: a) 50% R2A, b) 50% R2A and basalt slides, c) *S.desiccabilis* in 50% R2A, d) *S.desiccabilis* in 50% R2A and basalt slides, e)*C.metallidurans* in 50% R2A, f) *C.metallidurans* in 50% R2A and basalt slides, g)*B. subtilis* in 50% R2A, h)*B. subtilis* in 50% R2A and basalt slides.

5.8.3 Results

Elemental leaching from the basalt was observed in all the biotic and abiotic conditions of the experiment, with the biotic samples showing consistently higher levels of leaching than the abiotic controls. Of all the REEs, neodymium was released from the rock in the highest values. Lanthanum, which did not show up in the XRF, was found to have the second highest values, followed by praseodymium, samarium, and dysprosium, which all occupy the same range of release rates.
In all of the elements tested apart from ytterbium, thorium, and uranium, samples inoculated with *Cupriavidus metallidurans* showed the greatest increase in weathering rates, although the value for erbium *Sphingomonas desiccabilis* was only 0.01ppb lower than *C. metallidurans* (see Fig. 58).
Bacillus subtilis appeared to have more of an effect on weathering rates than *Sphingomonas desiccabilis* in the elements from lanthanum to samarium. This was also the case with Uranium, which it weathered more successfully than *S.desiccabilis* and *C. metallidurans*, with t-Tests (assuming equal variance) supporting this with values of P=0.027 and P=0.021 respectively in their comparisons with *B. subtilis*. The t-Test between *C.metallidurans* and *S.desiccabilis* for Uranium showed no significance, with a P value of 0.8. B.subtilis was the only

biotic condition to garner a significant increase in uranium weathering compared to the abiotic sample, with P = 0.04.
Ytterbium showed a significant rise in leaching in the presence of *Sphingomonas desiccabilis* compared to abiotic leaching (P= 0.018), and *S.desiccabilis* leaching was also significantly higher than the leaching in the presence of *B.subtilis* (P=0.045). All other elements, though following the pattern of higher elemental release in the presence of biology, gave low confidence values in terms of the significance between bacterial species, with P>0.05.

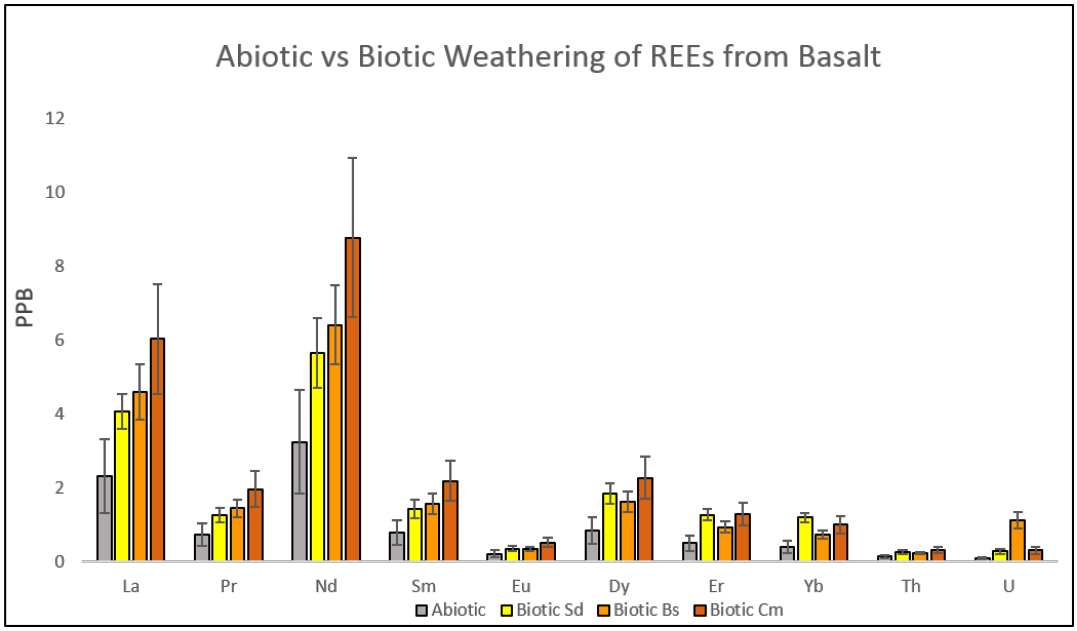

Figure 58: Comparison of the average REE elemental release rates from the abiotic and biotic weathering experiments. Abbreviations: PPB = Parts Per Billion, REE = Rare Earth Elements, Sd = *Sphingomonas desiccabilis*, Bs = *Bacillus subtilis*, Cm = *Cupriavidus metallidurans*. Colour coding for abiotic samples is high to low from red to pink, the biotic samples show slight variations, but generally follow the same trend.

The leaching followed the same pattern in almost all cases across the elements, (see the colour coded table in Fig. 59), with the highest abiotic leaching rates also being the highest rates for the respective bacteria. The exceptions were in the case of Pr and Er with *S. desiccabilis*, and with both U and Th with *B. subtilis* and *C.metallidurans*.

Values in ppb from the four weathering conditions:				
	Abiotic	*S.d.*	*B.s.*	*C.m.*
Nd	3.236726	5.604872	6.395147	8.751937
La	2.31104	4.023532	4.56557	6.00674
Dy	0.845584	1.83366	1.627709	2.265707
Sm	0.788577	1.419644	1.566352	2.182141
Pr	0.72897	1.252427	1.441409	1.956726
Er	0.500485	1.269894	0.932886	1.279392
Yb	0.405616	1.190137	0.729176	0.989847
Eu	0.215256	0.353092	0.337387	0.512907
U	0.085633	0.269178	-4.1322	-0.15647
Th	0.072423	0.233257	0.212167	0.28046

Figure 59: A table of the average REE elemental release rates from the abiotic and biotic weathering experiments, colour coded to indicate highest values (red) to lowest values (indigo and pink). Abbreviations: PPB = Parts Per Billion, REE = Rare Earth Elements, Sd = *Sphingomonas desiccabilis*, Bs = *Bacillus subtilis*, Cm = *Cupriavidus metallidurans*

5.8.4 Discussion

The null hypothesis was that the rate of mineral leaching would stay constant in the presence of the test organisms. While the t-Tests show there is too much variation within the results to confidently reject the null hypothesis, the pattern of accelerated leaching in the presence of biology is consistent across all of the measured elements. The variation within the results may be a result of materials lost on ignition during the ashing process, or a reflection of the variability of the elements within the basalt slides.

Of all the Rare Earth Elements, neodymium was leached from the basalt in the highest quantities. This correlates with the XRF data (see section 4.2.2), which found that Nd was present in the rock in concentrations of 9.5ppm. Lanthanum, showed the second highest elemental release rates, across all conditions. However La did not show up in the XRF, nor did any of the other REEs tested, with the exception of uranium, which was the second least abundantly leached element for the abiotic and *S.desiccabilis* conditions, and the least leached element for *B.subtilis* and *C.metallidurans*.

C.metallidurans was the most successful biological accelerant to the mineral weathering. This is possibly due to the species' adaptations to heavy metal toxicity, the absence of which may slow down growth in the other two species[160]. In the presence of certain leached elements, bacteria may require increased energy

expenditure on up-regulating protein production for the purposes of pumping harmful metals from the cell[161][162], which would negatively impact their doubling rate, and their ability to produce EPS and other biofilm essential proteins and products that could contribute to weathering.
The consistency with which the elemental leaching pattern is echoed by all the different organisms supports the idea that the use of the rare earth elements to determine overall biological leaching patterns has merit. Consequently, this method has been adopted to quantify the mineral release rates from the BioRock experiment once it has been flown and returned to Earth.

5.9 Conclusions

Bacillus subtilis and *Cupriavidus metallidurans* are well characterised organisms with stress tolerance mechanisms and DNA repair mechanisms[148], [149]. They have also been the subject of multiple space-flight experiements [150], [60], [151], [61]. Experiments with *Sphingomonas desiccabilis* have shown that it can match these organisms in suitability for space-flight, at least as far as surviving the procedures and potentially stressful conditions to deliver it to and from the ISS. The experiments have also shown that the materials and dimensions of the experimental hardware will not interfere with the geomicrobial activity of the bacteria, and that post-flight analysis using CLSM and ICP-MS will allow qualitative and quantitative data to be collected about architectural changes in biofilm formation, and mineral release rates.
The experiments conducted in this chapter have allowed for the progression of the BioRock experiment through the Critical Design Review to its assignment to Increment 59 on the ISS.

6 The Effects of Hypergravity on Biofilms and Biomining

6.1 Introduction

The effects of gravity are negligible at the scale of an individual bacterium, but its effects on the environment within which a bacterium operates can lead to changes in both behaviour and gene expression. In the previous chapter gravity conditions that are lower than the terrestrial 1 x g were considered, but in striving to understand the ways in which exposure to lower gravity alters the routine Earth-bound operations of our model organism, the impact of increased gravity was seen as a necessary step to build a more complete picture of gravity's role and effects on living systems.

While gravity is a near constant on Earth, when considering environmental parameters of potential off-world habitats, gravity is a variable that must also be included. Many of the potentially habitable environments in our solar system where efforts are coalescing in the search for life have a weaker gravitational field than Earth, such as Mars, Europa, Enceladus. It is known that beyond the solar system, many 'Earth-like' planets, which are candidates in the search for life, have stronger gravitational fields, though this proportion of larger planets is due in part to the greater ease with which larger bodies can be found by current detection techniques. The research may also hold some relevance when considering the habitability of exoplanets, although even the largest exoplanets are unlikely to have gravity environments as high as the ones being tested here, as the larger the planet - the further the surface is from the centre of gravity.

Most experiments at hyperaccelerations have focused on survival, and most of these survival experiments were performed in nutrient limited phosphate buffered solutions at 4^{o}C, which would not be conducive to microbial proliferation even at 1 x g [83].

Studies that have examined growth behaviour at simulated hypergravity have all focused on the behaviour and metabolic activities of planktonic cells. In 1991, Bouloc and D'Ari found no differences between the growth and energy metabolism of their *E.coli* in the control cultures and cultures grown at 3 x g and 5 x g - nor did they find any differences in their space-flight samples [84]. Brown *et al.*, studied *E.coli* again ten years later, looking at gravitational forces an order of magnitude greater. After 171 hours of growth at 50 x g, they found a 33% reduction in population numbers, and a 29% reduction metabolism efficiency [85]. Deguchi *et al.* (2011) showed *P. denitrificans* surviving and replicating at 403,627 x g, the upper limit of the centrifuge[90], but not the upper limit of the organism. Population growth was inhibited, but population growth still occurred, leading the authors to speculate that as cell density increased it helped to offset the pres-

sure increase, allowing some continued population growth, albeit reduced. The authors took this to suggest that the habitability of extraterrestrial environments is not limited by gravity.
These experiments on planktonic prokaryotes have raised some interesting questions about how the other side of gravity, hyper rather than hypo, can affect living cells. However, planktonic cells are only one part of the story when considering bacterial life, as the majority of bacterial cells in the wild exist in cooperative biofilms. Biofilms are begun by single cells, and how the effect of hypergravity on the single cell affects the formation and the development of a mature biofilm has not been examined. Additionally, while a single cell is too small to directly feel gravity's effects, a biofilm may grow to a size where gravity's effects do begin to compete with forces on the micron scale, e.g.- viscous drag, chemical energies, electrical forces, polymerisation. This in turn may have an effect on the structure and architecture of the biofilm, along with its efficiency. As no studies have been done to date on biofilms under hypergravity, this chapter is focused on answering basic fundamental questions.
Namely:
• Can biofilms grow in gravity environments greater than 1 x g?
• Are there any differences in biofilms expression at hypergravity?
• How does hypergravity affect the ability of geomicrobial biofilms to access nutrients from a substrate?

6.2 Planktonic growth at hypergravity

In order to be able to compare *Sphingomonas desiccabilis* to other reported microorganism behaviour under hypergravity, some planktonic experiments were run to see if the same trends were observed. It also enabled a preliminary assessment of *S. desiccabilis*'s susceptibility to hypergravity. Cells were spun in R2A nutrient solution for 24 hours at both 10 x g and 100 x g. Final growth was measured using both optical density at 600nm, and colony forming units on R2A agar.

6.2.1 Preparation

Cells were grow up over night, 25μl from glycerol stocks into 25ml of sterile R2A. The overnight culture was then diluted with another 20ml of sterile R2A, bringing the total culture to the correct volume for all replicates. The optical density of the starting culture was 0.098Abs recorded using a spectrometer at 600nm, calibrated with sterile R2A. Eight glass vials were autoclaved, and 5ml of the culture solution was pipetted into each of them, four for 1 x g controls and four to be spun in the Denley BS400 centrifuge at 10 x g. The experiment was

later repeated for confirmation, with a starting culture of 0.049Abs. The radius of the rotating centrifuge arms is 150mm, and in order to replicate 10 x g the vials were spun at 240rpm (see section 6.5.4 for the equation used to work out G force from RPM and arm radius). The 10 x g vials and the 1 x g vials were left for 24 hours and then brought to the laminar flow hood for manipulation within a sterile environment. One ml from each vial was placed in a cuvette for optical density measurements. A further 100μl was also removed from each vial to be serially diluted in 900μl of R2A and plated out for counts of colony forming units.

6.2.2 Results and Discussion

The results confirmed a difference in growth at 1 x g and at 10 x g, with cells replicating slower in the simulated 10 x g environment. In order to confirm this, the test was repeated, this time with a lower starting culture of 0.049Abs, (see Fig. 60).

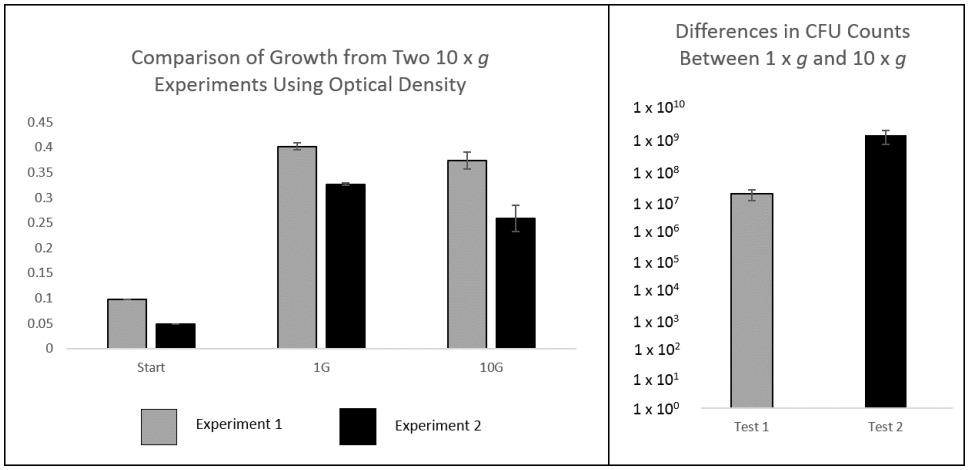

Figure 60: The bar chart on the left shows optical density absorbance, measured at 600nm, after 24 hours of exposure to different gravity conditions. Grey bars representing the averaged readings of the four repeats from the first experiment, and the black bars representing the averaged readings from the four repeats of the second experiment. The chart on the right shows was constructed from the colony forming units data, and show the extent to which 1 x g cell density outnumbered that of the 10 x g spun cultures.

The repeated experiment confirmed the findings of the first experiment, with greater differences observed between the two gravity conditions when inoculated with a lower cell count. While this does conform with general planktonic response to hypergravity, Bouloc and D'Ari (1991) and Brown*et al* (1999) who ran hypergravity experiments on *E.coli*, found any effect only began to manifest at higher

gravity conditions than 10 x g [84] [87].
The experiment was then conducted at 100 x g, with a starting culture of 0.057Abs. After 24 hours, the cells/ml grew to 10^5 in both cases, although under higher gravity, the 100 x g cells grew to higher numbers by a 43.08% increase. A two tailed t-test with unequal variance gave a P-value of 0.0001, however the range was still larger in the hypergravity samples, with a 1 x g standard error of 41, 600, versus the 100 x g standard error of 736,600 (see Fig. 61). As the test was only conducted for 24 hours, it is not clear whether this is related to a shortening of the lag phase in the 100 x g condition, or whether despite previous expectations from previous results and literature, the population of *S. desiccabilis* benefited from the higher gravity. A repeat of the experiments, after 48 hours, may reveal that the 1 x g populations had overtaken the 100 x g counts. The experiment could also be conducted with the bacteria exposed to interruptions in the hypergravity, so that with measurements taken at different time points could answer this question more fully.

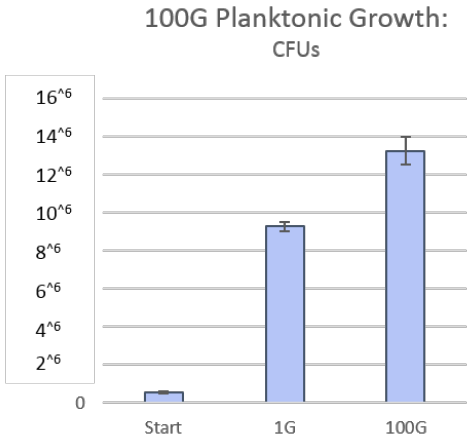

Figure 61: Colony forming units of the *S.desiccabilis.* start culture at 0h, and the 1 x g control cultures, and the 100 x g cultures after 24h.

6.3 Preliminary Hyper-Gravity Biofilm Growth Experiments

A preliminary experiment was conducted on a BS400 Denley centrifuge for three weeks, with four basalt slides at 10 x g and four controls at 1 x g. Samples were stained with Sypro ruby and examined with the confocal microscope, which showed areas of the rock which were much more extensively covered with biofilm than any of the 1 x g controls - or any of the previous experiments conducted on basalt (see Fig. 62).

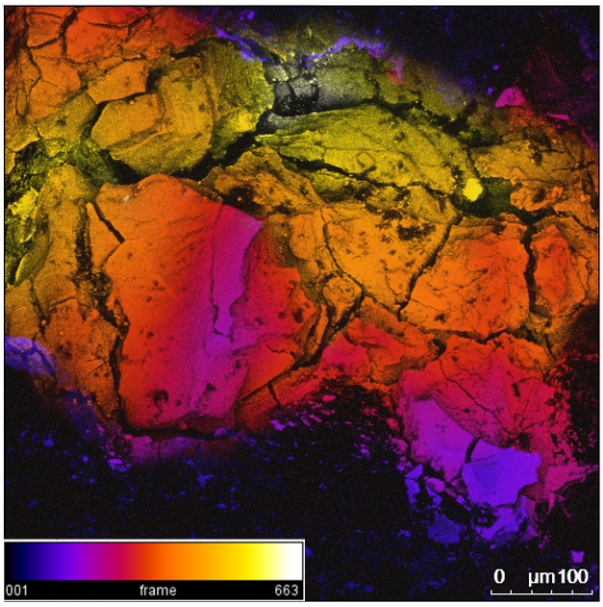

Figure 62: Temporal hyperstack of 663 layers of *S.desiccabilis.* biofilm grown at 10 x *g* on basalt.

This justified further investigations into biofilm growth at hypergravity, as it ran counter to planktonic data and assumptions about bacterial growth at hypergravity.

6.4 Three week 10 x *g* Experiment on Different Substrates

As rock and rock analogue surfaces are uneven and porous, it proves difficult to reliably quantify the thickness of biofilms that grow upon them. As mentioned in Chapters 4 and 6, different factors such as surface area, and hydrophobicity affect attachment at the mineral surface, confusing the single variable being tested here. To provide a surface with the least number of variables, 0.2μm polycarbonate isopore membranes were chosen as a substrate. These were also used for the first biofilm microgravity experiments in 2001 by McLean *et al.*[163]. To provide an intermediary step between general and geomicrobial biofilms, and reduce variables in the nutritional and physical properties of the minerals which make up the basalt, quartz sintered discs were selected as an additional substrate. Basalt was selected again as the substrate to examine the microbe-mineral interactions of *Sphingomonas desiccabilis* in altered gravity conditions, as the two have now been well characterised together, and basalt remains one of the most common rock types in the rocky planets.

6.5 Methodology

In order to investigate biofilm growth at hypergravity, three different substrates of different complexities were used (see Fig. 63). All preparations took place in sterile conditions inside the laminar flow hood, with autoclaved or pre-sterilised materials.

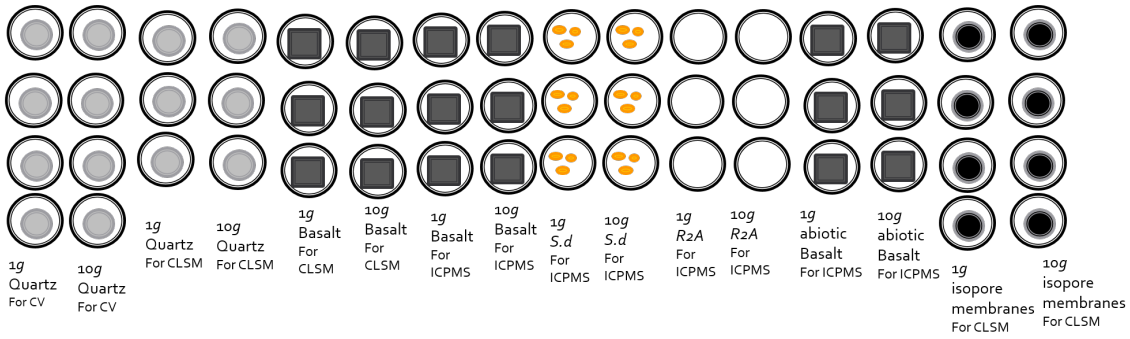

Figure 63: Experimental set-up for 10 x g spin and 1 x g control. From left to right: Four quartz sintered discs per gravity (g)condition, for crystal violet biomass assay (CV); three quartz discs per g condition for Confocal Laser Scanning Microscopy (CLSM) imaging of biofilm; three basalt slides per g condition for CLSM; three basalt slides per g condition for Inductively Coupled Mass Spectrometry (ICP-MS), and the biotic and abiotic controls; and four isopore membranes per g condition for CLSM.

6.5.1 Isopore Membranes

In order to minimise the number of variables present on the micron scale with a mixed-mineral surface, a set of substrates that were as uniform as possible were chosen to accompany the other samples in the centrifuge. These uniform samples consisted of 35mm diameter R2A agar plates, with 0.22μm polycarbonate isopore membranes.
Previous preliminary experiments had confirmed that *Sphingomonas desiccabilis* biofilms would form on such a homogenous surface, which were detectable through the confocal microscope.

R2A agar was made up and balanced to pH 7.2 (see appendix for recipe). After being autoclaved, it was poured into mini petri-dishes to form 35mm diameter agar-plates. Eight polycarbonate isopore membrane filters (0.2μm GTPB, from Merck Millipore Ltd.) were transferred, one into each mini agar-plate, and 100μl of R2A and *S. desiccabilis* at an optical density of 0.030A was added to each plate. Four of the mini agar plates were loaded into the centrifuge bucket, and

the other four were wrapped in a padded container for transport to the University of Dundee.
After three weeks incubation in their relative gravity conditions, the isopore membranes were brought back to the University of Edinburgh. The membranes were transferred to six well plates containing Triton X 1% and PBS, and Sypro Ruby stain and left for 30 minutes wrapped in tinfoil to prevent them from photobleaching. The samples were then washed twice in PBS, and stored in fresh PBS, ready for imaging with the CLSM.
There were four isopore membranes per condition, and each one was examined under the confocal microscope at a 20x magnification (dry), with four z-stacks built from randomly selected points across each sample.
After examining the rock under CLSM and building 3-Dimentional images of any biofilms found, FIJI (Image J) software was used to analyse the data. Temporal hyperstacks provided a top-down image of the composite 3-D image, using colour coding to indicate depth. Using the 'z-axis profile' tool, it was possible to assign numbers to the amount of biomass on each slice of the 3-dimensional image built by the CLSM. The intensity of the brightness of each layer of the z-stack is quantified, brightness corresponding to the amount of fluorescent dye held by proteins; while it is not possible to assign biomass values in terms of weight or mass, it allows an accurate representation of the corresponding amounts of biological matter present on each stack.

6.5.2 Sintered Quartz Discs

Sintered quartz discs have been used as endolithic analogues in previous studies looking at habitability [164], and so these were also included in the 10 x g three week Dundee spin, to provide a heterogeneous surface of a homogenous material. Fourteen sintered quartz discs were autoclaved and placed individually in 35mm diameter mini-petri dishes with sterile tweezers, and inoculated with 3ml of R2A nutrient solution and *S.desiccabilis* at an optical density of 0.030A. Seven of these were placed in the centrifuge bucket for spinning at 10 x g; the other seven were stored in the same environmental conditions but without the artificial hypergravity.
For analysis after incubation and hyper-acceleration, three quartz discs per condition were kept for CLSM, and prepared in the same way as the isopore membranes (see above).
The remaining four per condition were prepared for crystal violet assay. This involved removing the liquid culture and adding 5ml of 0.04% crystal violet solution. These were left for 30 minutes and then washed twice with PBS. A 33% acetic acid in millipore water solution was then introduced to the petri dishes, 5ml per sample, which was left in for twenty minutes. Then 1ml from each sample was

transferred into cuvettes, for optical density readings at 550nm, calibrated with the acetic acid in millipore water mix. Four fresh sterile isopore membranes were also placed in new mini petri dishes, and treated with crystal violet as above, so the background crystal violet absorbed by the quartz could be subtracted from the final optical density measurements.

6.5.3 Basalt Slides

Eighteen basalt squares were cut from the mother-rock and sanded to size, 1 x 1 x 0.4cm, (see Chapter 4 for more details), and autoclaved prior to the experiment. Each one was then placed in sterile mini petri-dishes with sterile tweezers. Half of these were then placed in the centrifuge bucket, for spinning at 10 x g, while the other half were packaged separately for storage at 1 x g in the centrifuge room in Dundee.
After spinning and return to Edinburgh, three per gravity condition were set aside for confocal microscopy, while another three were set aside for pre-ICP-MS processing, along with 3 sterile basalt slides per gravity condition, and the associated required controls of R2A only, and R2A with *Sphingomonas desiccabilis*.
Samples were prepared for CLSM using 1% Triton X 100 in PBS with Sypro Ruby stain at a 5:1 ratio, left for half an hour, then rinsed twice with PBS, placed in fresh PBS, and covered with tin-foil to prevent them from photo-bleaching. Biofilms were examined at 200x and 400x magnification.
The ashing protocol was the same as 5.0.2; briefly: The basalt slides and solution were transferred to 50ml falcon tubes and sonicated for 4 minutes at 50Hz, and again for 4 minutes at 60Hz. The basalt slides were removed, and the media was transferred to sterile glass vials and placed in the furnace for 100^{o}C for two hours, and then 450^{o}C for five hours to burn off the organic elements. These were then left overnight to cool. Two drops of 50% nitric acid were added to each vial, swirled, and left for an hour to dissolve the ash. The solution was transferred into sterile 15ml falcon tubes, and a further 5ml of 2% nitric acid was added.
As well as the rare Earth elements (REEs), Mg, Al, Fe, and Sr were also quantified; they had been shown to leach with more reliability than some of the other elements at 1 x g, albeit with less consistency than the REEs.

6.5.4 Centrifugation

Samples were transported by bus, train, and foot to and from the Fulton Building of Dundee University's, School of Science and Engineering; meaning all samples underwent some turbulence during the journey. Each sample should have experienced the same degree of mixing as a result of being transported in the same box.

Once in Dundee, the 1 x g controls were placed on a shelf 1m from the centrifuge. The 10 x g samples were placed in the centrifuge bucket (see Fig. 64).

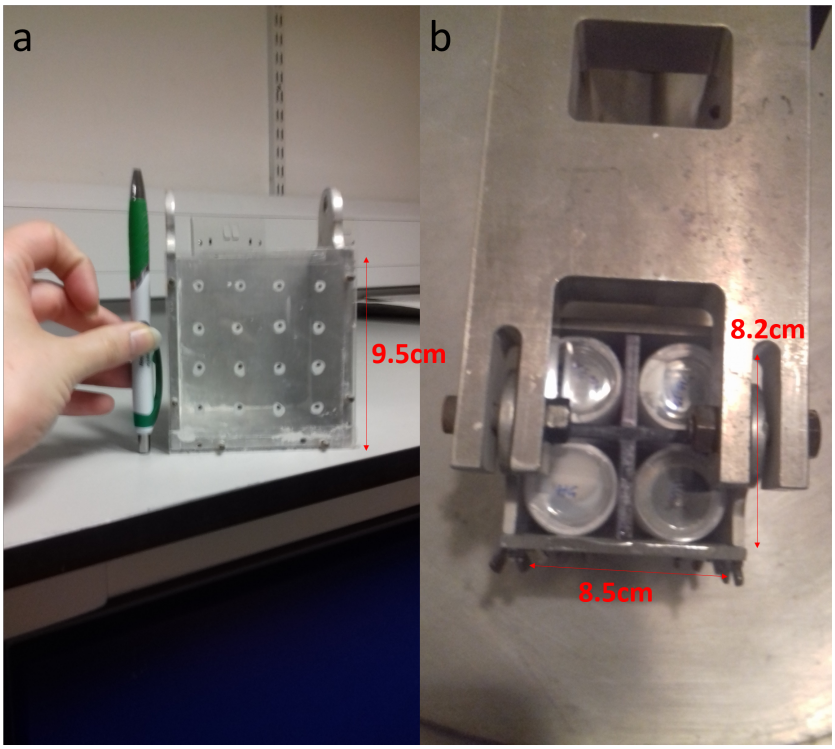

Figure 64: The centrifuge bucket with scale, a) the bucket when empty, b) the bucket with samples, from above, affixed to centrifuge arm .

The small scale geo-technical centrifuge had a rotating arm 25cm long (see Fig. 65). Consequently, using (3), it was calculated that 189rpm be used to simulate 10 x g. The centrifuge was bolted to the floor for stability.

$$Gforce = 1.12 \times \ r \ \times \frac{RPM^2}{1000} \tag{3}$$

Spinning started at 17:00pm, and took 5 minutes to reach full speed. There was three hours between inoculation in Edinburgh and exposure to 10 x g in Dundee.

After three weeks of spinning, samples were collected and returned to Edinburgh University by public transport. The samples were kept overnight in a refrigerated room at 4^oC until analysis was possible, which began the following day.

Figure 65: The centrifuge a) from above, with scale, and b) from a distance.

6.6 Results

6.6.1 Isopore Membranes

Twelve isopore membranes were placed on 35mm R2A agar plates, and inoculated with 100μl of *Sphingomonas desiccabilis*, from a culture grown up overnight and diluted with fresh R2A to an optical density of 0.03Abs at 600nm. Six of the plates were placed in the centrifuge bucket and spun at 10 x g for three weeks, while the other six were kept in the same environmental conditions at 1 x g for the same amount of time. The membranes were prepared for confocal microscopy by moving them from the agar surface to individual wells in a six well plate, and adding 1ml of 1% Triton X 100 and 200μl of Sypro Ruby at a 1 x concentration. Membranes were examined at 100x and 200x magnification. Three control membranes, which had been placed on 35mm R2A agar plates but without inoculation, were also treated in the same way and examined under the microscope to ensure visual cues for biofilms were correctly identified.
Membranes of both gravity conditions showed biofilm growth across the entire

surface of the membrane. The biofilms were distributed uniformly across the surface of the membrane, (see Fig. 66) and points were selected at random to take the z-stacks measurements.

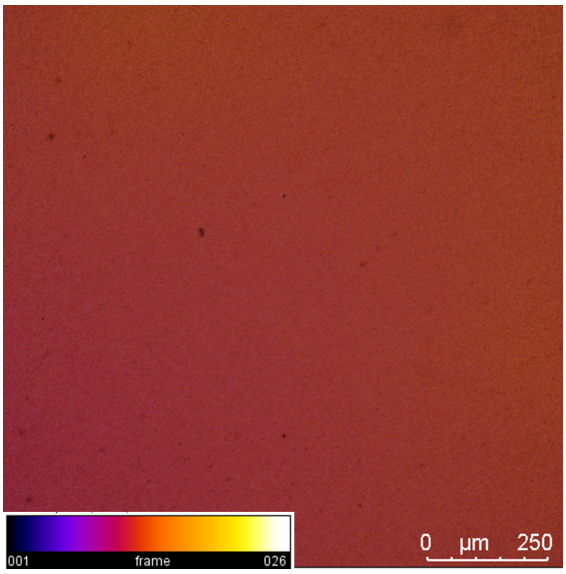

Figure 66: A temporal hyperstack of the biofilm on an isopore membrane, representatively homogeneous and level.

The z-stacks were then processed on FIJI, using the 'z-axis profile' tool, which measures the brightness of each layer of the z-stack, with brightness corresponding to the amount of fluorescent dye held by proteins. The curves differed consistently when looking at the 10 x g samples compared to the 1 x g samples, with the higher gravity curves being wider, suggesting there was more biomass attached to the membrane (see Fig. 67).

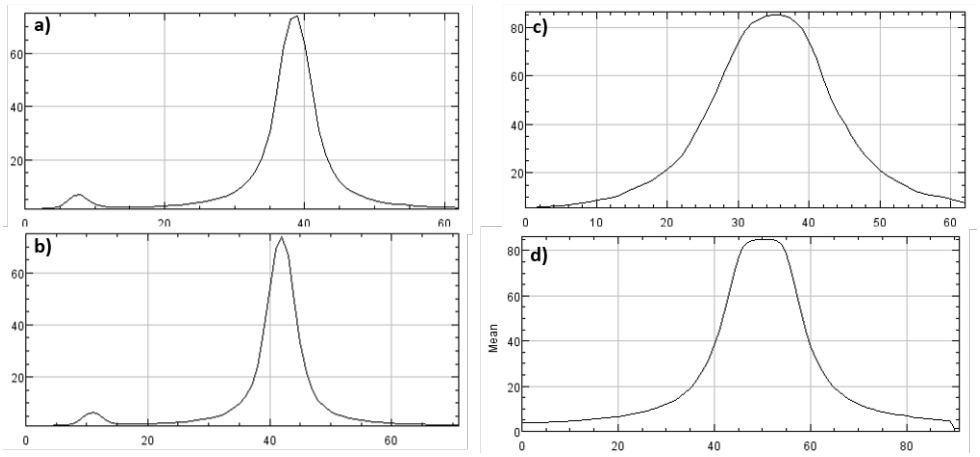

Figure 67: a)-b) 1 x g z-axis profile, showing the thinner peaks compared to c)-d) peaks of the 10 x g membranes, which are more rounded, indicating greater biomass.

Taking the average width of each curve, using the Full Width at Half Maximum (FWHM) as a consistent parameter, it was possible to assign numbers to the amount of biofilm biomass on each level of the 3 dimensional image built by the CLSM (see Fig. 68). The results showed that the membranes which had been spun at 10 x g after inoculation had thicker biomass attached to the surface than the 1 x g membranes (see 69).

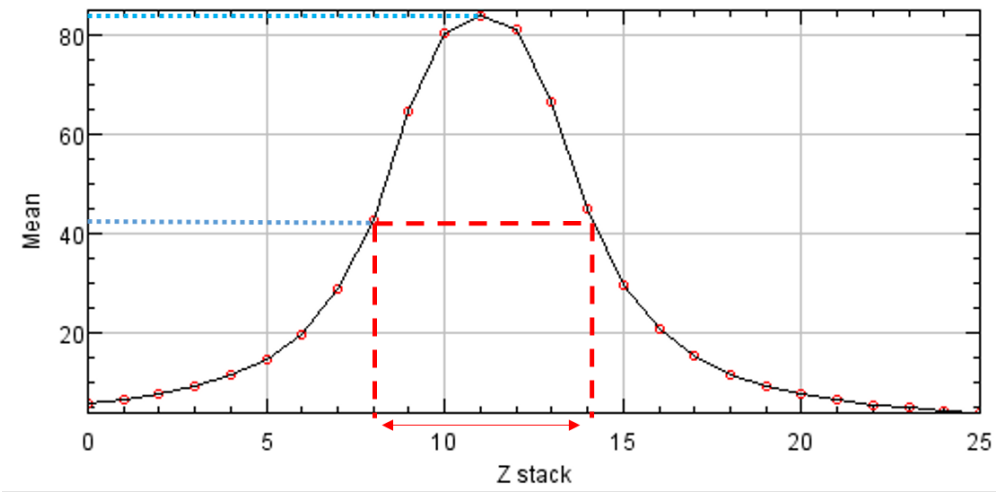

Figure 68: The Z-axis profile, showing the brightness corresponding to biomass at each level of the Z-stack, with lines showing how the calculation of the thickness of the biomass was established for numerical comparison using the full width half maximum for consistancy.

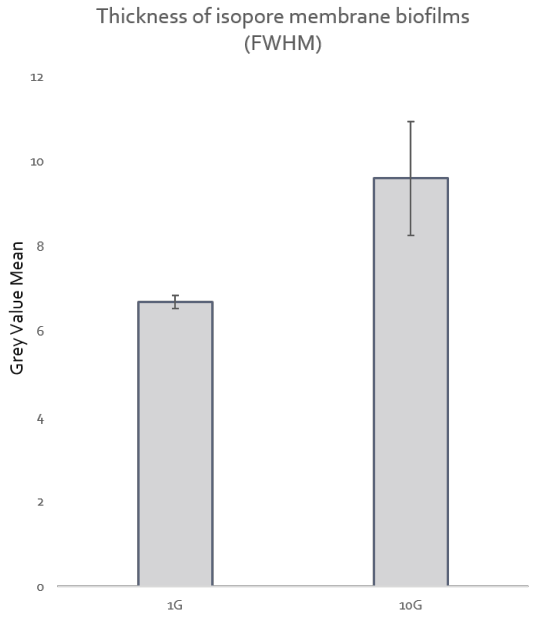

Figure 69: The average relative thickness of the biofilms grown at 1 x *g* and 10 x *g* on the isopore membranes, as calculated from the distance across the full width half maximum. Error bars represent standard error.

Once the z-axis profiles of the two gravity conditions and the controls had been transformed into numerical data, the data showed an increase in biomass of 43.3%. A single factor ANOVA test was run on the two samples and the blanks, giving a P-value of 0.0226, which allows us to reject the null hypothesis that the observed difference was a result of chance rather than the higher gravity.

6.6.2 Confocal Microscopy of Sintered Quartz Discs

Fourteen sintered discs were inoculated with 3ml of *S.desiccabilis* in R2A, at an optical density of 0.03Abs, 600nm. Half of these were spun at 10 x *g*, while the other half were kept under terrestrial gravity conditions. Three per condition were randomly selected and put aside for confocal microscopy, and the remaining four underwent analysis via a crystal violet assay to quantify biomass.

The quartz discs were prepared for CLSM using 1% Triton X 100 in PBS with Sypro Ruby stain in a 5:1 ratio. Examinations at 200x and 400x magnifications showed very little growth on the quartz substrate in either gravity condition. There were few visible colonies on the sintered discs (see Fig. 70), and those that were observed were also small in size compared to biofilms grown on other

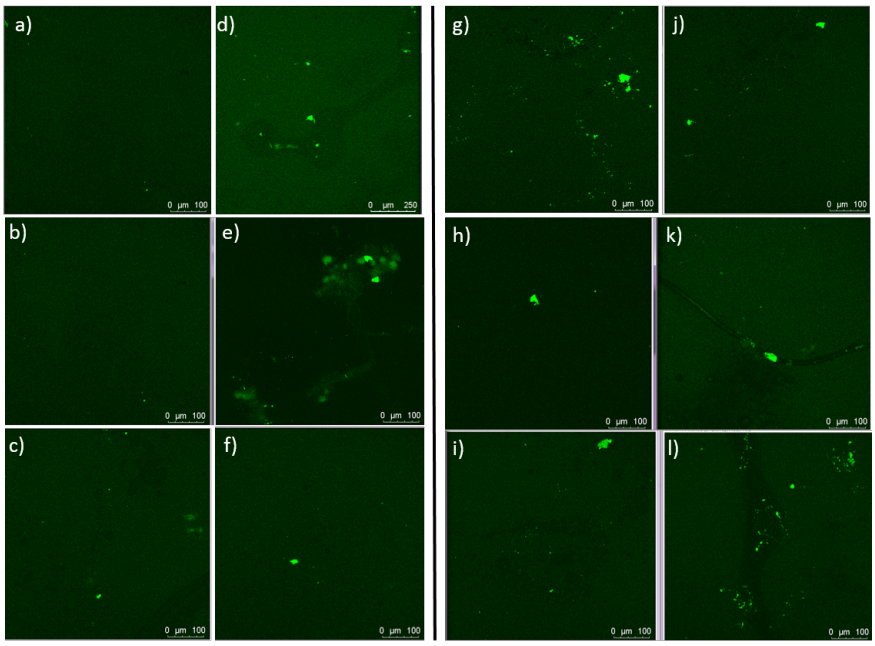

Figure 70: a)-f): *Sphingomonas desiccabilis* micro-colonies growing on quartz sintered discs at 1 x *g*; g)-i): *S.desiccabilis* micro-colonies growing on quartz sintered discs at 10 x *g*. After three weeks, none of the samples appear to have developed any mature biofilms.

substrates in other experiments for a period of three weeks. The findings in Chapter 4 may go some way towards explaining this.

6.6.3 Crystal Violet of Sintered Quartz Discs

As might be expected from the images built on the CLSM, the optical density measurements from the crystal violet assay were low across all the sintered disc samples, ranging from 0.022 - 0.04Abs for the 1 x *g* samples, and from 0.024 - 0.055Abs for the 10 x *g* samples. While the results were higher on average by 0.01Abs for the 10 x *g* samples (see Fig. 71), a two-tailed T-test assuming equal variance gave a P-value of 0.274. It is not possible to say with confidence that the observed difference is a result of the higher gravity environment.

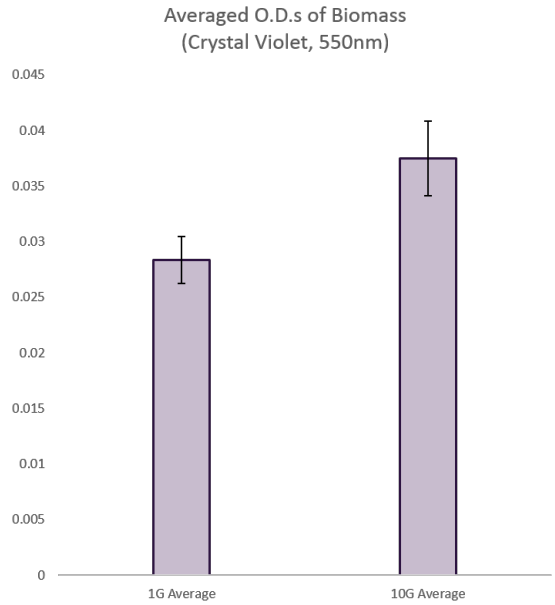

Figure 71: The average 550nm optical densities of the crystal violet from the quartz sintered discs, representing total biofilm biomass at 1 x *g* and 10 x *g*. Error bars represent standard error.

6.6.4 Confocal Microscopy on Basalt Slides

Biofilms grown on the 10 x *g* samples were consistently larger and more voluminous than biofilms growing on the basalt in the 1 x *g* environment. The same analysis that was run to quantify the width of the biofilms on the isopore membranes could not work on the heterogeneous surface of the basalt, however, by using the z-axis profile to give a numerical value for the Grey Mean Value(GMVs) of each stack, it was possible to build a semi-quantitative picture of the amount of biomass present in the area by the total brightness of the fluorescing dye, corresponding to the amount of protein present. This gives an indication of a combination of percentage area cover and density. Values for the 10 x *g* samples showed higher GMVs than the 1 x *g* samples, indicating the biofilm coverage was distributed more widely across most of the occupied z-stacks (see Figs 72 and 73). The graphs show that the terrestrial gravity basalts were generally of a depth of 100-150 z-stacks, with one at 200 z-stacks, and another two around 400 stacks, while a greater number of the 10 x *g* biofilms reached over 200 stacks. None of the mean grey values for the 1 x *g* biofilms rose above 4, while six of the ten hypergravity biofilms rose above 4, with the two highest GMVs at 8.6 and 9.

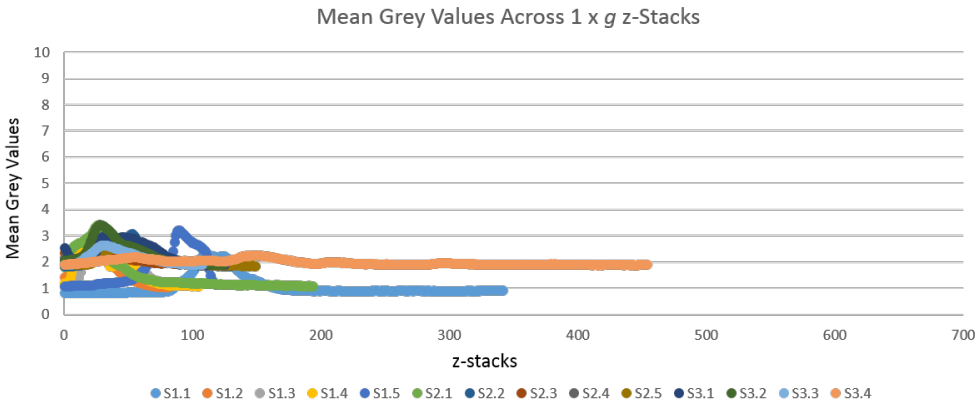

Figure 72: Scatter graph showing amount of fluorescing proteins per layer of z-axis stack in the 1 x *g* basalt biofilms. The y-axis is Grey Mean Value, indicating area coverage/biofilm width, and the x-axis represents each level of the z-stack, indicating depth/biofilm thickness.

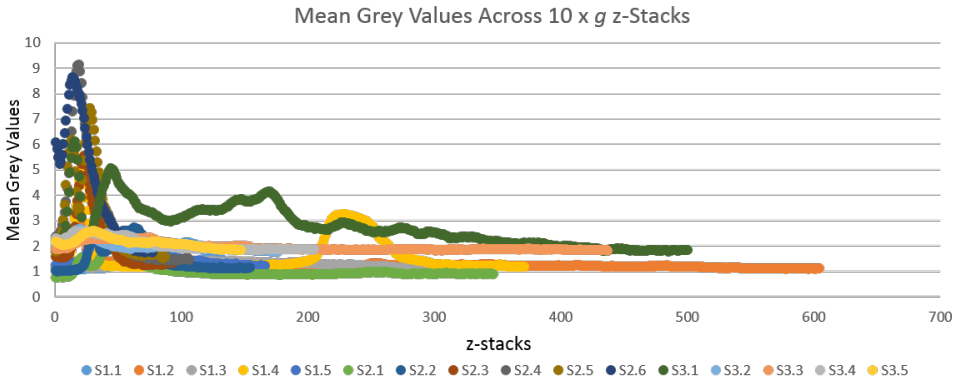

Figure 73: Scatter graph showing amount of fluorescing proteins per layer of z-axis stack in the 10 x *g* basalt biofilms. The y-axis is Grey Mean Value, indicating area coverage/biofilm width, and the x-axis represents each level of the z-stack, indicating depth/biofilm thickness.

For imaging purposes, the two largest biofilms from each gravity condition have been selected to demonstrate the differences observed in the biofilms all across the basalt, at a similar scale. Looking at Figure 74, which shows the 10 x *g* *biofilm growth,* it is possible to see that across a similar scale and number of z-axis stacks, there is conspicuously more biomass than Figure 75, which shows the 1 x *g* biofilms.

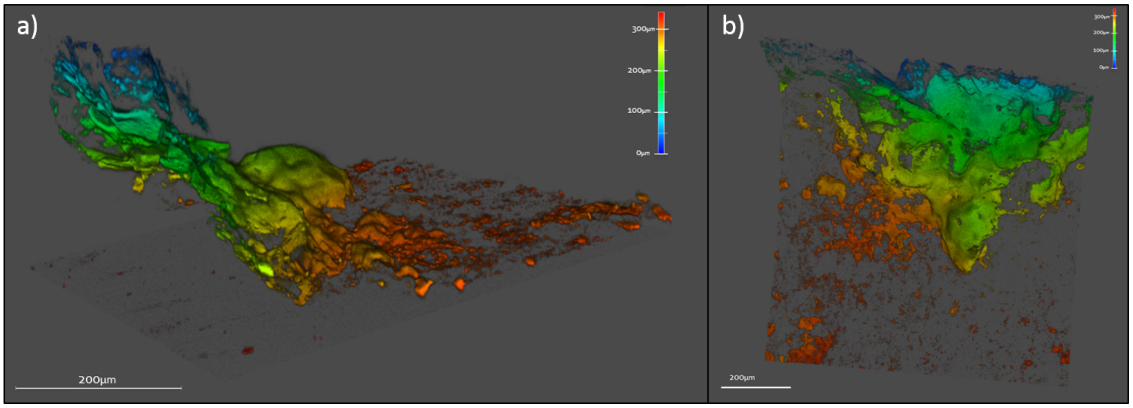

Figure 74: 3D representations of 400 layers of *S.desiccabilis.* biofilm grown at 10 x *g* on basalt. a) Laterally, b) Top-down.

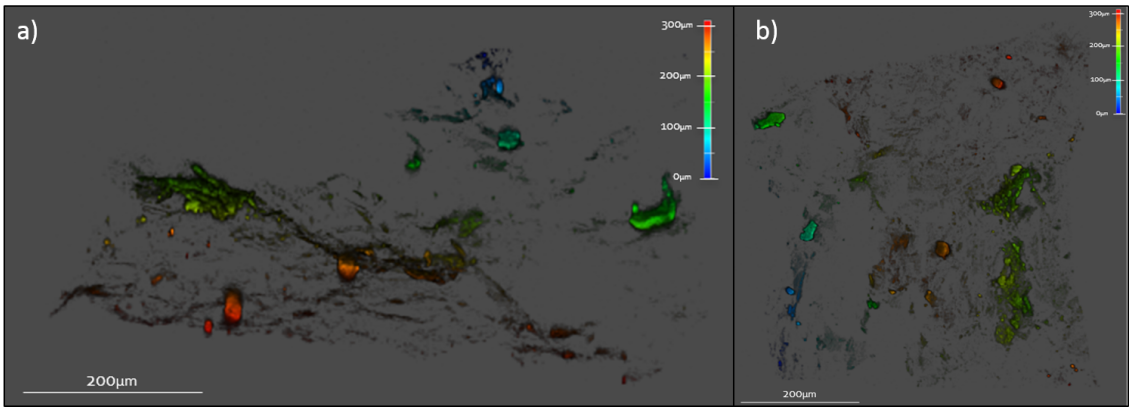

Figure 75: 3D representations of 400 layers of *S.desiccabilis.* biofilm grown at 1 x *g* on basalt. a) Laterally, b) Top-down.

6.6.5 ICP-MS of Elements Leached from Basalt at 1 x *g* and 10 x *g*

Sphingomonas desiccabilis was grown on basalt slides for three weeks to assess the difference between biotic and abiotic leaching at 1 x*g* and 10 x *g*.

Mg, Al, Fe, and Sr

Magnesium was high in all of the conditions, due to the composition of the R2A, but within both gravity conditions it was highest in the biotic weathering samples, suggesting that the presence of *Sphingomonas desiccabilis* expedited the release of Mg from the basalt substrate. Abiotic weathering was higher at 10 x *g*, ranging from 1850 – 2866 ppb, versus 1450 – 1599 ppb at 1 x *g* (see Table 13).

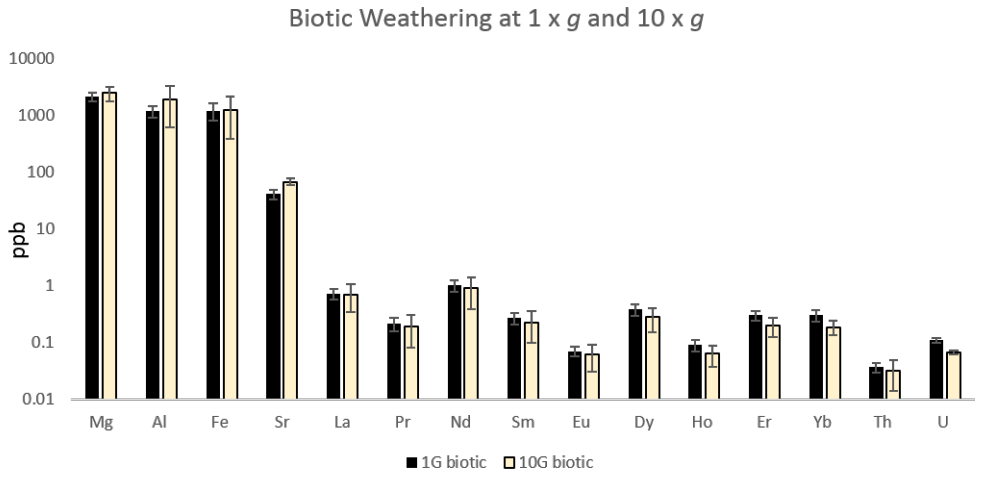

Figure 76: Bar chart with logarithmic y-axis, showing mineral concentration in parts per billion from biotic weathering samples at 1 x *g* and 10 x *g*.

For aluminium, the averages of both biotic and abiotic weathering rates were higher at 10 x *g* than at 1 x *g* for aluminium release, however the range of results within conditions was also greater. 10 x *g* abiotic Al weathering release ranged from 217.5 - 499 ppb, averaging at 938.3 ppb, while 1 x *g* abiotic weathering release ranged from 365.4 – 1774 ppb, averaging at 393.6 ppb. The differences within the results for abiotic weathering at 1 x *g* were 281.5 ppb, and within the 10 x *g* abiotic weathering were 1408 ppb.
For biotic weathering, 10 x *g* released on average 763 ppb more Al than at 1 x *g*, but the range within the results was greater by 2775 ppb, extending from 392.5 – 4576 ppb compared to 749.6 – 1662 ppb for the 1 x*g* samples.
Al concentrations were an order of magnitude lower in the controls without basalt, and the ranges were more consistent, indicating that the higher concentrations in the abiotic and biotic weathering were due to leaching from the rock. This was true of all the other elements measured, with the exception of Mg.

The average iron concentrations were higher in the 10 x *g* samples than the 1 x *g* samples, and the range of values were once again greater at 10 x *g* than at 1 x *g*. Biotic release of iron at 10 x *g* ranged from 337.4 – 2971 ppb, versus a more constrained range of 516.4 – 1868 ppb for 1 x *g*. The abiotic average was also higher at 10 x *g* than at 1 x *g*, although the upper and lower values were more extreme for the 10 x *g* results than the 1 x *g* result: 271.5 – 461 ppb at 1 x g, and 263.8 – 1724 ppb at 10 x *g*.

The highest values for strontium were in the tens of parts per billion one to two

orders of magnitude lower than Mg, Al and Fe. The lowest strontium values were in the R2A samples, and there was a rise in the values of Sr when *Shingomonas desiccabilis* was included, however ANOVA analysis of the R2A and *S. desiccabilis* results showed these differences could not be deemed significant (P=0.082), though it might indicate that *S.desiccabilis* uses Sr for some of its cellular components. The strontium average for abiotic weathering was lower at 10 x *g* (28.9 ppb) than at 1 x *g* (35.6ppb), however, the highest and lowest values of the abiotic weathering at 10 x *g* (4.7 – 50.7 ppb) were more extreme than the highest and lowest value of the abiotic weathering at 1 x *g* (30.85 – 42.47 ppb). Biotic weathering was also higher at 10 x *g*, with an average of 67.07 ppb, and a range of 56.11 – 85.05 ppb, compared to the 1 x *g* biotic average of 40.97 ppb, and a range of 26.16 – 55.97 ppb. While the ranges do not overlap, a two-tailed t-Test assuming equal variance showed that the differences were not significant.

Rare Earth Elements

Values for Lanthanum, and all of the rare earth elements measured, were two orders of magnitude lower than the values of Sr. Values for abiotic weathering were higher at 10 x *g* (0.43 ppb) than 1 x *g* (0.29 ppb), again with a greater range at 10 x *g* (0.25 – 0.61 ppb) than at 1 x *g* (0.23 – 0.38 ppb). Biotic weathering averages were similar at 1 x *g* (0.72 ppb) and 10 x g (0.7 ppb), but once again 10 x *g* had a greater range of La concentrations (0.396 – 1.41 ppb), than 1 x *g* (0.5 – 1.04 ppb).

Praseodymium release was higher in the biotic samples than the abiotic samples, and the biotic release values were similar in both gravity conditions. Abiotic praseodymium release was lower at 1 x *g*, averaging at 0.078 ppb, ranging from 0.06 – 0.1 ppb, while 10 x *g* abiotic release averaged at 0.12 ppb, with a range of 0.07 – 0.19 ppb.

Biotic Pr release was slightly lower at 10 x *g*, with an average concentration of 0.19 ppb compared to the 1 x *g* average of 0.21 ppb. The range of concentrations was greater at 10 x *g* (0.072 – 0.42 ppb) than at 1 x *g* (01.5 – 0.31 ppb).

Neodymium concentrations were higher overall in the samples where biotic leaching occurred. 1 x *g* abiotic weathering had a short range, from 0.296 – 0.454 ppb, averaging at 0.359 ppb, while the 10 x *g* abiotic weathering rates ranged from 0.309 – 0.844 ppb, averaging at 0.513 ppb. The average of the 1 x *g* biotic leaching was slightly higher than at 10 x *g*, with 1 ppb versus 0.89 ppb measured, but the range of the 10 x *g* weathering was more extensive, with values of 0.34 – 1.91 ppb in contrast to the 1 x *g* range of 0.72 – 1.48 ppb.

Values for Samarium followed the same pattern as Neodymium, with higher overall elemental counts in the biologically assisted weathering, and a greater range of results in the 10 x *g* conditions. 1 x *g* abiotic weathering averaged at 0.09 ppb,

ranging from 0.08 – 0.12 ppb, while 10 x g abtioic weathering averaged at 0.128 ppb, and ranged from 0.07 – 0.22 ppb. Biotic weathering was higher at 1 x g with an average of 0.27 ppb against 0.22ppb for the 10 x g condition. The values for 10 x g extended above and below the 1 x g concentrations, with a range of 0.087 – 0.477 ppb versus 0.197 – 0.391 ppb at 1 x g.

Table 13: Avarage Biotic and Abiotic Elemental Release Rates

Element	**1 x g**		**10 x g**	
	Abiotic Average	**Biotic Average**	**Abiotic Average**	**Biotic Average**
Mg	1521	2128.67	2391.3	2482
Al	393.6	1169.53	938.3	1932.5
Fe	381.93	1211.47	843.57	1242.17
Sr	35.64	40.98	28.97	67.07
La	0.286	0.7198	0.43	0.7012
Pr	0.0772	0.2118	0.1175	0.194
Nd	0.3589	1.0013	0.5125	0.8959
Sm	0.0913	0.2681	0.128	0.2237
Eu	0.0222	0.0702	0.0304	0.061
Dy	0.1143	0.378	0.145	0.278
Ho	0.027	0.0905	0.0311	0.063
Er	0.0908	0.299	0.095	0.1961
Yb	0.088	0.3035	0.0871	0.1864
Th	0.0198	0.0366	0.026	0.031
U	0.056	0.109	0.068	0.067

Values for Europium followed the same pattern as La, Pr, Nd, and Sm, with higher overall elemental counts in the biotic weathering, and a greater range of results in the 10 x g conditions. 1 x g abiotic weathering averaged at 0.02 ppb, ranging from 0.019 – 0.026 ppb, while 10 x g abtioic weathering averaged at 0.03 ppb, and ranged from 0.018 – 0.05 ppb. Biotic weathering was higher at 1 x g with an average of 0.07 ppb compared to 0.06ppb at 10 x g. The values for 10 x g exceeded the 1 x g concentrations, with a range of 0.03 – 0.12 ppb versus 0.05 – 0.098 ppb at 1 x g.

Dysprosium release rates mirror the other REEs so far, with higher values in the biotic weathering over the abiotic weathering, and a wider range of results in the 10 x g conditions. 1 x g abiotic weathering averaged at 0.011 ppb, ranging

from 0.01 – 0.14 ppb, while 10 x *g* abtioic weathering averaged at 0.145 ppb, and ranged from 0.09 – 0.23 ppb. Biotic weathering was higher at 1 x *g* with an average of 0.38 ppb compared to 0.28 ppb at 10 x *g*. The range in values for 10 x *g* was slightly wider than the values recorded for 1 x *g*, with concentrations of 0.14 – 0.53 ppb at 10 x *g* versus 0.29 – 0.54 ppb at 1 x *g*.

The mineral release rates of Holmium follow the same pattern as the previous REEs, with biotic rates exceeding abiotic rates, the 1 x *g* biotic weathering was higher than the 10 x *g* biotic weathering, and the 10 x *g* variation was greater than the 1 x *g* variation. 1 x *g* abiotic weathering averaged at 0.027 ppb, with a range of 0.0242 – 0.032ppb, while 10 x *g* release rates averaged at 0.031 ppb, ranging from 0.018 – 0.049 ppb. Biotic released averaged at 0.09 ppb for 1 x *g*, ranging from 0.07 – 0.13 ppb, while the 10 x *g* average was 0.063 ppb, with high and low values of 0.03 – 0.11 ppb.

Erbium also follows the same pattern as the previous REEs, with higher biotic weathering rates, 1 x *g* biotic weathering surpassing 10 x *g* biotic weathering, and greater variation in the 10 x *g* conditions. Abiotic weathering at 1 x *g* averaged at 0.09 ppb, ranging from 0.08 – 0.11 ppb, and at 10 x *g* the average was 0.095 ppb, with a range of 0.05 – 0.14 ppb. Biotic weathering at 1 x *g* averaged 0.3 ppb, with a range of 0.23 – 0.42 ppb; the 10 x *g* average was 0.2 ppb, ranging from 0.11 – 0.34. The upper value at 10 x *g* is lower, but the range is still more extensive, with a difference of 0.22 ppb rather than 0.19 ppb between the 1 x *g* values.

Ytterbium bucks the trend of the previous REEs (see Fig. 77), as the 1 x *g* biotic samples have the most variation , rather than the 10 x *g* biotic samples(0.212ppb versus 0.18ppb). In other respects Yb results do not deviate from the other REEs, with biotic results yielding greater elemental release rates, and the 1 x *g* biotic leaching values remaining higher than the 10 x *g* values. The average abiotic mineral concentration at 1 x *g* is 0.88ppb, ranging from 0.076 – 0.106 ppb, and a 10 x *g* average of 0.87ppb, ranging from 0.05 – 0.13ppb. Biotic weathering at 1 x *g* averaged at 0.3 ppb, ranging from 0.23 – 0.44ppb, while 10 x *g* averaged at 0.19ppb, ranging from 0.12 – 0.29ppb.

Thorium, while not an REE, also displays the same patterns in leachings as the majority of the REEs measured, with higher biotic elemental release, greater variation at 10 x *g*, and a higher average value for biotic weathering at 1 x *g* compared to 10 x *g*. The average abiotic mineral concentration for Th at 1 x *g* was 0.02ppb, ranging from 0.016 – 0.03ppb, and at 10 x *g* the average was 0.026ppb, ranging from 0.017 – 0.032ppb. Biotic weathering at 1 x *g* averaged 0.037ppb, ranging from 0.029-0.05ppb, while 10 x *g* averaged at 0.031ppb, ranging from 0.012 – 0.066ppb.

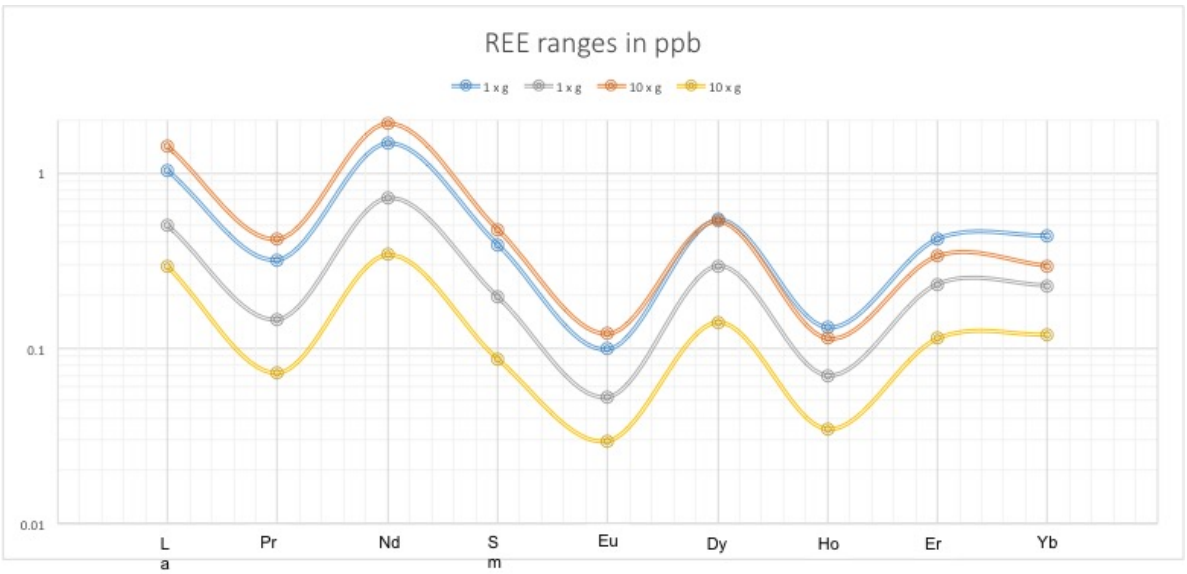

Figure 77: The upper and lower extremes of biotic leaching recorded for the rare earth elements.

Uranium proved to be the only element recorded that did show a significant difference in biotic weathering between the two gravity conditions (P=0.015). As with the other heavier elements, the higher concentration was from the samples in the 1 x g condition. Abiotic weathering was higher in the 10 x g condition, with an average of 0.68ppb, ranging from 0.025 – 0.132ppb, while abiotic weathering at 1 x g gave an average of 0.056ppb, and a range of 0.04 – 0.07ppb. Biotic weathering averaged at 0.109 for 1 x g, 0.047ppb greater than the 10 x g average of 0.075ppb. The biotic range at 1 x g was also greater than the range at 10 x g, unlike most of the other elements apart from Yb. The 1 x g biotic values ranged from 0.09 – 0.12ppb, and the 10 x g values ranged from 0.06 – 0.07ppb.

Statistical Analysis

Two-tailed T-tests were run on all of the minerals, comparing abiotic release rates in the two gravity conditions, and comparing biotic release rates in the two gravity conditions. F-test were run prior to the t-Tests to establish the equality of variances, and the appropriate t-Test was selected for each data set. In all cases, excepting uranium, the t-Tests confirmed the null-hypothesis that the 10 x g gravity environment had no significant effect on the elemental release rates (see Table 14).

Table 14: Two-Tailed t-Test P-Values Behind Accepting the Null-Hypothesis that there is No Significant Difference Between Weathering Rates of the Two Gravity Conditions

Element	Abiotic P-Value	Biotic P-Value
Mg	0.1	0.676
Al	0.28	0.603
Fe	0.414	0.976
Sr	0.104	0.104
La	0.269	0.965
Pr	0.896	0.336
Nd	0.427	0.863
Sm	0.481	0.773
Eu	0.572	0.796
Dy	0.535	0.551
Ho	0.684	0.442
Er	0.89	0.331
Yb	0.976	0.252
Th	0.315	0.8
U	0.727	0.015

It was also noted, when comparing values across replicates, that on the whole elemental release rates were higher in certain samples than others. Showing highest and lowest values are generally consistent across replicates, especially the heavier and rare earth elements (see Fig. 78).

6.7 Discussion

Biofilm growth on different substrates at 1 x g and 10 x g were compared to establish whether there were any differences in growth. Mineral release rates from basalt were also investigated under the two gravity conditions. Isopore membranes were used as a homogenous flat surface, so that biomass could be reliably imaged and measured. Quartz discs were used to provide a heterogenous surface structure with homogenous surface chemistry. Basalt slides were used to investigate the effects of hypergravity on a genuine rock, one that had already been categorised with *Sphingomonas desiccabilis* (see Chapters 4 and 5). The biofilms were uniform and flat across the entire surface of the isopore membranes when examined through the confocal microscope, which was in keeping with expectations of non-motile biofilm growth on a homogeneous flat surface. Through using

Biotic and Abiotic Leaching Within Replicates

Sample	Mg	Al	Fe	Sr	La	Pr	Nd	Sm	Eu	Dy	Ho	Er	Yb	Th	U
7	1599	464.3	413.3	33.59	0.3751	0.1022	0.4548	0.1158	0.02637	0.1415	0.03226	0.1114	0.1057	0.02502	0.07128
8	1514	499	271.5	30.85	0.2519	0.06732	0.3261	0.0799	0.02099	0.1017	0.02418	0.08214	0.08171	0.0185	0.05314
9	1450	217.5	461	42.47	0.2301	0.06197	0.2959	0.07832	0.01924	0.09964	0.02435	0.07899	0.0764	0.01599	0.04244
10	2198	1097	1250	41.09	0.62	0.1704	0.8094	0.2166	0.05952	0.3009	0.07066	0.2438	0.2428	0.03082	0.1142
11	2688	1662	1868	55.67	1.036	0.3191	1.476	0.3911	0.09855	0.5391	0.1311	0.4201	0.4397	0.05046	0.1217
12	1500	749.6	516.4	26.16	0.5035	0.1458	0.7184	0.1967	0.05259	0.294	0.06987	0.2322	0.2279	0.02861	0.0914
19	2866	1774	1724	31.6	0.6125	0.1851	0.8438	0.2185	0.05468	0.2302	0.04889	0.1437	0.1304	0.03276	0.04791
20	1850	365.4	263.8	50.69	0.4257	0.09779	0.3846	0.0915	0.01801	0.1143	0.02696	0.08682	0.0789	0.01733	0.1315
21	2458	675.5	542.9	4.616	0.2535	0.06974	0.3092	0.07393	0.0186	0.09037	0.01759	0.05432	0.05211	0.02756	0.02502
22	3892	4576	2971	60.08	1.414	0.4191	1.913	0.4766	0.1206	0.5296	0.1134	0.3357	0.2949	0.06602	0.07455
23	1788	392.5	337.4	85.02	0.396	0.09064	0.4344	0.1078	0.03243	0.1638	0.04074	0.139	0.1448	0.01673	0.06833
24	1766	829	418.1	56.11	0.2937	0.07222	0.3404	0.08682	0.02953	0.1405	0.03447	0.1135	0.1194	0.01166	0.05727

Legend:

1G abiotic	1G biotic	10G abiotic	10G biotic
Highest	Highest	Highest	Highest
Middle	Middle	Middle	Middle
Lowest	Lowest	Lowest	Lowest

Figure 78: Biotic and abiotic leaching values per replicate, across all selected elements; with each replicate colour coded to show highest and lowest values for given element in the given condition. *N.B.* Table shows samples 7 - 24, samples 1 - 6 were controls.

FIJI (Image J), it was possible to use software analysis to measure differences in morphologies of the biofilms. On uneven rock substrates the 'z-axis profile' is a jumble of peaks and troughs, but with the homogeneous surface of the membrane, and the correspondingly smooth surface of the biofilm, there was only a single bell curve on each profile, which represented the biofilm growing on both sides of the membrane. The Grey Mean Value, indicating the amount of dye fluorescing, represents the amount of protein present at each layer of the z-stack. The thinner the biofilm, the narrower the curve that describes it, as the biomass occupies fewer layers of the z-stack; a thicker biofilm allows a larger 3D image to be constructed, which takes up additional z-axis layers, and is consequently represented by a wider curve (see Fig. 67. Despite lower cell numbers – or at the very least slower growth – in the planktonic cultures at 10 x g, the P-value(0.0226) from the Analysis of Variance between abiotic and biotic 1 x g and 10 x g membrane fluorescence indicates that the increase in the thickness of the biofilms at 10 x g is not due merely to chance.
As with the increased biofilm biomass noted in microgravity experiments, it is suggested that this increase in biomass is a result of the stress exerted on the microbes by the change in environment, leading to certain genes and proteins being up- and down- regulated. In addition, increases in sedimentation pressures will cause more of the non-motile bacteria to find their way to the rock surface, perhaps aiding in success with initial attachment.

There was also a greater variation in the thickness of the hyper-gravity biofilms

compared to the terrestrial g biofilms, with the range at 1 x g being 2.7 layers, and the 10 x g variation in thickness being 14.3 layers. This increase in variation supports the idea that the biofilms forming on the 10 x g membranes were expressing different genes as a response to stress. Different bacteria replicating within the cultures would respond differently to the stress, based on their own specific genes and mutations, and these differences would propagate within the increasing micro-colony/biofilm populations over time. Under 1 x g conditions, without stress, such differences would not be driven to manifest so visibly in the population.

On the sintered quartz discs, the crystal violet showed there was only a small difference between the 1 x g and 10 x g samples. Further examination under CLSM then showed that there were only a few small biofilms, which appeared more like microcolonies than full biofilms. *S.desiccabilis* had limited growth on the quartz discs, which may account for the low optical density readings from the crystal violet assay. The justification for choosing the sintered discs was to find a chemically homogeneous but heterogeneously surfaced rock analogue, to provide an intermediary step between the membrane and the basalt which could provide insight should there be drastic differences between the membrane and basalt results. If the experiment were to be repeated, it would behove the researcher to find a textured substrate with more nutritional value for the bacteria in question. However, as the same effect - an increase in growth - was observed in both the standard biofilms and the geomicrobiological biofilms, such an intermediary substrate was not necessary.

The biofilms on the basalt slides, when imaged under the confocal microscope, yielded similar results to the preliminary experiments, namely, some biofilms were of a similar size to the 1 x g controls, and some were much more extensive. It is worth noting that due to selection bias, biofilms smaller than the 1 x g would not have been imaged, but we know from other quantitative tests that some of the biofilms at 10 x g did not exhibit increased population numbers.
Morphologically, there were a number of biofilms grown in high-gravity that were not extensive in depth, but which were extensive in area coverage, whereas 1 x g *Sphingomonas desiccabilis* biofilms typically only cover a small area of but can sometimes grow to some depth. Some of the 10 x g biofilms were extensive in both area coverage and depth (see Fig. 74 and Sample 3.1 on Fig.73). This, along with the isopore membrane data, suggests that there is a genetic component present in some of the cells which allow them to respond to the stress of hyperacceleration by growing faster, or creating copious amounts of EPS.
It is worth noting that the 10 x g biofilms were also more extensive than any of the biofilms imaged during the rest of the research for this thesis, including the 30^{o}C biofilms grown 20% nutrient solution in section 5.3.2.

The elemental release rates appear to follow two separate trends. The elements at the lighter end of the spectrum, Mg, Al, Fe and Sr, which are biologically useful, and which occur in the basalt in higher concentrations than the REEs, showed the highest overall increase in concentrations, for both the biotically and abiotically induced weathering. While not statistically significant, the release rates were higher for the 10 x g biotic samples compared to the abiotic samples. The rare Earth elements and the heavier Th and U, which are inert in respect to biology, and which make up a smaller proportion of the basalt, exhibited a different tendency. The highest average concentration of leaching for each element took place in the 1 x g gravity biotic condition, although in almost all cases, the highest and lowest recorded values were from the 10 x g environment. Variation was higher at 10 x g in all of the results bar Uranium. It was also generally noted that higher and lower readings were generally consistent within samples (see Fig 78). This could indicate that some of the variation is due to different mineral seams within the basalt slides, but also indicates that the biofilm growth was more successful in some samples than others.

One possible theory that could explain the increased variation in mineral release rates, as well as the varied but overall higher biomass in the biofilms, is along similar lines to the explanation proffered for the population crash before the exponential phase observed in the Deguchi planktonic experiments[90]. As the variation is greater at 10 x g, this may be indicative of the stressors acting on the bacteria in the higher gravity triggering different genetic responses in the primary microcolonies that go on to form the mature biofilms. Not all the bacteria that seed the initial microcolonies will successfully up-regulate the stress response genes which may account for the increased growth. This success or struggle in response to the stress will perpetuate down the descendants of the original bacteria, resulting in a greater overall variation than in the base-line gravity environment, which the bacteria have evolved in.

Despite the presence of greater biomass in the higher gravity regime, bioleaching cannot be said to have increased significantly. Perhaps this is indicative that the biomass is mostly extra mucous rather than an increase in cell numbers, or perhaps the increased sedimentation caused by the hydrodynamics of hypergravity concentrates all of the nutrients in the R2A solution at the rock surface, reducing the need to expend energy on up-regulating the genes required for active weathering. he abiotic leeching results were higher at 10 x g, than the 1 x g abiotic samples, in all cases except with strontium. This is perhaps because of altered fluid dynamics, but when considered against the lower biotic leaching at 10 x g than 1 x g, could suggest that the presence of the biology inhibited leaching under hypergravity.

Future Work

A repeat of the experiment at 100 x g and higher would allow a further insight

into the relationship of gravity to biofilm formation. This experiment has shown that the effects of gravity on biofilm growth and repression are non-linear, and to categorise the relationship further, higher gravity environments need to be explored. This bioleaching aspect of this experiment could also be elucidated by a repeat at 100 x g, as the results were suggestive of trends but inconclusive, and a higher gravity environment could exacerbate and highlight patterns that were too subtle to definitively identify at 10 x g.
A repeat of the 10 x g experiment and a new 100 x g tests with a genetics component would also be beneficial, to inform the community on up- and down-regulation of genes and proteins at hyper-gravity, and a comparison with the genes that are differentially regulated at microgravity would be of interest, to see if they share similarities or if a different phenomenon governs the response to hyper-gravity. If some of the same genes which govern the increase of growth at microgravity are also up-regulated in hypergravity, then hypergravity experiments could offer a cheaper alternative for experiments on biofilm growth and suppression as a response to microgravity.
Repeats would also allow further quantification of the colloidal and capsular EPS carbohydrate and protein composition, to shed light on how the biofilm is changing in response to the stress of hypergravity. This research also has the potential to lead to beneficial results for industries that use Sphingomonad biofilm products, such as the food, pharmaceutical, and petroleum industries (see section 2.6). If greater quantities of EPS are produced in conditions of hypergravity, it could speed the production of useful bioproducts.

6.8 Conclusion

Experiments with planktonic bacteria at hypergravity have shown that while lag time is shortened, total population growth is stunted. Two 24 hour planktonic growth experiments with *Sphingomonas desiccabilis* at 10 x g showed the same pattern, although one experiment at 100 x g did suggest otherwise, casting some doubt onto the efficacy on a single time point for assessing growth kinetics. With planktonic bacteria from the literature, 10 x g experiments on *E.coli* did not reveal altered growth kinetics[87], but the results in this chapter indicate that 10 x g appears to be enough of a change as to influence the growth of *S.desiccabilis*.

The same pattern of reduced growth at higher gravities did not appear with the biofilm experiments. Instead, the inoculated isopore membranes and basalt slides exposed to three weeks iof 10 x g had a number of thick extensive biofilms, which were considerably larger than the largest of the 1 x g biofilms. This suggests the relationship of gravity to biofilm growth is non-linear, and the stress of hypergravity may accelerate and benefit biofilm growth, up to a point which is yet to be determined. Variation was higher at 10 x g in all the permutations of the

experiments, apart from the planktonic counts.
The results from the inductively coupled plasma mass spectroscopy indicated that the greater biomass observed at 10 x g did not lead to increased bioweathering. Further investigations at 10 x g, to categorise the difference in biofilm constitution would reveal much about the changes that are taking place. Further experiments at 100 x g and higher would allow for a more complete picture to be built of the effects of hypergravity on biofilm formation and mineral release rates.

7 Conclusions

7.1 Introduction

In this thesis, the forces affecting biofilm attachment and formation were explored, as well as the effects of gravity on either side of the terrestrial gravity environment the bacteria have evolved in. This chapter provides a summary of the specific conclusions presented at the end of each results chapter.

7.2 The Forces Affecting Mineral Attachment

The literature on the forces governing biofilm formation did not all agree on the extent to which the XDLVO forces (electrostatic repulsion, polar charge, Lifshitz-van der Waals forces) dictated the suitability of a material for biofilm adherence, and of which forces would dominate over the others. The research presented in Chapter 4 indicates that with complex surfaces such as those presented by bacterial cells and mineral interfaces, adherence is less easily characterised than experiments with colloids have suggested previously. This was in keeping with the medical research community's findings with host-pathogen cell to cell biofilm adherence and formation.
The factors investigated here were surface porosity, electrophoretic mobility, hydrophobicity, and stereochemical structure - as a determination of nutritional value. Of these, porosity - representing surface texture - appeared to have the most significant effect; any of the minerals with a surface porosity of less than 0.02% had very little biomass, regardless of their other physical properties. The factor which appeared to dominate mineral attachment preference after porosity had passed 0.02%, was the nutritional benefit provided by each mineral.
Hydrophobicity and surface tensions, the two XDVLO forces being tested here, appeared to have the least effect. Quartz and olivine had the least amount of biomass; they represented the two smoothest surfaces, but shared no other similar characteristics. Orthoclase was the most amenable mineral for colonisation by *Sphingomonas desiccabilis*. Chemically, orthoclase is identical to microcline, but it terms of porosity it was an order of magnitude more porous than microcline. Nutritionally, it was perceived to contain the most biologically advantageous elements of the three minerals that were not excluded from successful colonisation by limitations in surface structure as determined by porosity.
The research was conducted in an attempt to assess to what extent XDVLO theory could accurately describe the mineral attachment preference, and concluded that other physical and biological factors - namely increased Gibbs' free energy and kink sites, and bacterial appendages - played a more important role in the

complex process of microbial adhesion to mineral surfaces.

7.3 Model Organism Characterisation in Preparation for BioRock

Experiments have previously shown increased growth rates and population numbers in bacterial biofilms exposed to microgravity. An experiment is being launched to the International Space Station (ISS) in 2019 to learn how geomicrobial biofilms will be altered by micro- and Martian- gravity, and how this will affect their geomicrobial processes. Two well characterised organisms and one relatively new organism, which are known to have mineral weathering capabilities, are being flown on basalt samples to the Kubik centrifuge on board the ISS.
In Chapter 5, to ensure that the uncharacterised organism *Sphingomonas desiccabilis* was a suitable model organism for the space-flight experiment, and that reasonable conclusions could be drawn about the effects of microgravity, experiments were conducted to better understand the bacteria. Specifically; to learn about the duration of its desiccation tolerance, establish the optimum nutrient concentrations to encourage biofilm growth, and to identify some of the genes that code for its responses.
It was determined that *S.desiccabilis* populations that were dried down onto the basalt surfaces would still contain enough viable cells after one month to repopulate new liquid media. This should allow enough elasticity to weather delays in launching to the ISS without compromising the experiment.
Experiments with nutrient solution concentration showed that lower concentrations were positively correlated to biofilm growth and negatively correlated to planktonic growth. With the R2A media, the most biomass was observed in the 20% R2A : nanopore water, followed by the 50% R2A dilution, and finally the 100%. As one of the current theories is that the higher populations in microgravity are a result of nutrient limitations, the 50% R2A solution was selected for the BioRock experiment, due to concerns that a 20% solution on top of the altered liquid mixing regimes may limit the nutrients too far.
In addition, a whole gene sequence was performed on *Sphingomonas desiccabilis*. Genes were found for biofilm formation, and other Sphingomonads known to possess the same genes were identified, in an attempt to place *S. desiccabilis* in greater context within the four Sphingomonad genera. Of the extracellular polysaccharide (EPS) genes identified, *S. desiccabilis* appeared to have the most in common with *Sphingobium japonicum*. Genes associated with temperature and osmotic shock and DNA repair, which will be partly responsible for the organism's desiccation tolerance, were also identified.

7.4 Experimental Hardware Growth Experiments in Preparation for ISS Microgravity Experiments

Chapter 5 also details experiments that were conducted to test and refine the experimental hardware for the BioRock experiment. In order to create biomining reactors (BMRs) that would be suitable for both the requirements of BioRock, and for the restricted conditions onboard the ISS and in the Kubik centrifuges, preliminary experiments to determine the suitability of different dimensions were performed. Bioreactors with different distances between the sample and O_2 membranes, different sizes of O_2 membranes, different volumes of nutrient solution, and different gravity vectors (up vs. down) were tested. The results showed that as long as all the requirements for growth were met, the specific dimensions would not critically alter the growth behaviour of the bacteria.

Experiments were conducted on the materials that were then selected for the construction of the new BMRs to ensure that none of them exhibited bactericidal properties. Growth was not inhibited in the presence of any of the materials, and so the BMRs were built and delivered for further testing.

Growth tests in the finalised reactors, which ultimately had a larger membrane effective area than any of the preliminary experiments, showed that conditions for *Sphingomonas desiccabilis* growth were even more favourably met by the new experimental hardware, with higher final populations after three weeks.

Parabolic flight experiments were also conducted to study the initiating step of the reduced gravity experiment, where nutrient solution is injected into the chambers with the basalt and the desiccated bacteria. As liquid mixing dynamics behave differently in reduced gravity, the research was to establish whether the injection of the nutrient solution at μg would result in different levels of bacteria being washed from the surface of the basalt, and affecting final biofilm biomass counts. The experiment showed that the turbulence of the injection action overcame any mixing limitations from the microgravity.

The final stage of the experiment involves the injection of a fixative into the BMR to halt metabolism and growth. The selection of fixatives for use onboard the ISS is limited, and both RNAlater and Notoxhisto were both tested before selecting the Notoxhisto, which worked within desired parameters at both 4^oC and 8^oC, the latter being the upper temperature limit the cold stowage unit had been recorded to deviate to.

Experiments were also conducted to ensure the proposed post-flight analysis techniques would result in measurements that could confirm or disprove the BioRock hypotheses. Images taken with the confocal laser scanning microscope (CLSM) at different temperatures and nutrient conditions showed enhanced growth at higher temperatures and lower nutrient solutions, and reduced growth in lower temperatures and higher nutrient conditions. This corresponded with predictions, and was supported by crystal violet biofilm biomass data. Inductively coupled plasma

mass spectroscopy (ICP-MS) analysis was run on liquid samples that contained the products of biotic and abiotic weathering experiments. Results showed a trend towards increased mineral weathering in the presence of each of the three different model organisms, but the results were not statistically supported, and so further investigation is required.
In conducting ICPMS experiments, it was possible to refine the protocol to include an ashing step to preserve a greater number of the weathered elements that would otherwise remain bonded to the cellular components of the bacteria and escape analysis in the spectrometer. It was also determined that rare earth elements (REEs) were the elements that gave the most stable and consistent results across repeats, leading to the decision that these should act as the indicators of overall weathering activity on the rock matrix for BioRock and future weathering experiments.

7.5 Hypergravity Growth of Planktonic *Sphingomonas desiccabilis*

Previous experiments have been conducted on planktonic bacteria, and the results had shown that at accelerations greater than 20 x g lower populations begin to manifest[86]. *E.coli* grown at 10 x g and under, no altered growth kinetics have been observed [87][84]. This suggests that there is a threshold between 10 and 20 x g where the macro condition of gravity begins to make itself felt upon the cell on a microscopic level, due to altered fluid dynamics.
In Chapter 6, experiments with *Sphingomonas desiccabilis* were conducted to establish how this organism responds to the stress of hypergravity in its planktonic state, to place it in context with the current literature before testing biofilms for the first time. Two planktonic growth experiments - reported in section 6.2 - on *Sphingomonas desiccabilis* at 10 x g did show lower numbers of growth compared to the 1 x g controls. However, a later iteration of the same experiment at 100 x g contradicted this by having higher population counts in the high gravity condition compared to the control.
One hypothesis is that in the higher gravity condition the lag phase was shortened, as was found by Brown (1999), and that if measurements had been taken later, the 1 x g populations would have overtaken the higher g populations. This could be tested with a repeat over a longer time scale, or with a modified experimental set up so that exposure to higher gravity is interrupted for measurements at multiple time points.

7.6 *Sphingomonas desiccabilis* Biofilm Growth at Hypergravity

To date, no investigations have been reported on biofilm growth at hypergravity. For gravitational microbiology studies, hypergravity represents a significantly easier condition to replicate than microgravity, and could open a new perspective into the relationships of the macro-scale force of gravity on micron-scale living microorganisms.
Chapter 6 details biofilm growth experiments conducted on the chemically and structurally homogenous surfaces of isopore membranes, on the chemically homogenous but structurally heterogenous surfaces of sintered quartz discs, and on the chemically and structurally heterogenous surfaces of basalt slides. Confocal laser scanning microscopy was used to image and qualify the biofilms, and through the use of ImageJ's FIJI software, it was possible to use the images to extract useful numerical data.
In all cases, apart from the sintered quartz discs, where growth was limited in all conditions, the highest observed biofilm growth was in the 10 x g condition. The flat surface of the isopore membrane allowed for quantification of the different biofilm biomass based on the number of fluorescing stacks on either side of the polycarbonate membrane, and showed an average increase in biomass of 43.3% at 10 x g. Biofilm growth on the basalt slides also exceeded that of the 1 x g controls, with 60% of the measured biofilms exceeding the upper limits of the 1 x g biofilm coverage. As well as informing us about the biological responses to different gravity conditions, hyperacceleration could also be used in industry to increase and accelerate the yield of certain EPS products, such as gellan.

7.7 Bioleaching of Basalt by *Sphingomonas desiccabilis* at Hypergravity

Assessing mineral release rates at higher gravity conditions will be useful for comparing to the microgravity results from BioRock. In addition, it has the potential to shed light on the biotic processes happening at the mineral surface. The Inductively Coupled Plasma Mass Spectroscopy (ICP-MS) results in Chapter 6 did not detect a difference in rare earth element (REEs) release rates from basalt at 1 x g and 10 x g, despite the production of more EPS in the higher gravity condition, as is also described in Chapter 6. Further experiments in higher gravity environments could reveal at what point increased acceleration results in increased or decreased weathering rates.

7.8 Final comments

The forces around microbial attachment leading to biofilm formation on mineral surfaces were investigated, examining the micro-scale forces that occupy the scale of bacteria under terrestrial gravity conditions. The findings in this thesis support those from the medical journals that suggest that the dynamic and complex surfaces of cell membranes bring too many other factors to bear, and that these factors dominate over the XDVLO forces that govern interactions of more simple colloidal particles. Consequently, future investigations into microbe-mineral interactions, whether at terrestrial or altered gravity conditions, can focus on characterising the most relevant parameters, suggested here as being surface texture/Gibbs free energy, the biological nutritional value of the exposed rock surface, and the bacterial appendages of the model organism.

Basalt was used for hypergravity experiment, along with *Sphingomonas desiccabilis*, and that data can now be used - along with the ground data - to compare with the results from the upcoming BioRock experiment to give a more comprehensive integrated view of geomicrobial growth and weathering across different gravity conditions. Biofilm biomass did increase in the higher gravity condition, suggesting that the relationship between gravity and biofilm formation is non-linear, that both reduced and increased gravitational environments will enhance biofilm biomass. This is consistent with the theory that the observed increase in bacterial growth is a stress response.

As well as clarifying the relationship between microbes, their processes, and gravity, hypergravity conditions through acceleration could be used in industry to increase and accelerate the yield of certain EPS products, such as gellan and useful catalysts.

Bacteria in biofilms have an advantage over planktonic bacteria. The research in this thesis suggests that certain conditions must be met; energy, nutrients, temperature and pressure, water, and a surface with some available Gibbs energy. If these conditions are met, biofilms will form and grow in spite of a myriad of stressors, including reduced and enhanced gravity.

8 Bibliography

References

[1] W. B. Whitman, D. C. Coleman, and W. J. Wiebe. Prokaryotes: the unseen majority. *Proceedings of the National Academy of Sciences*, 95(12):6578–6583, 1998.

[2] S. Kjelleberg and S. Molin. Is there a role for quorum sensing signals in bacterial biofilms? *Current Opinion in Microbiology*, 5(3):254–258, 2002.

[3] J. W. Costerton, Z. Lewandowski, D. E. Caldwell, D. R. Korber, and H. M. Lappin-Scott. Microbial biofilms. *Annual Reviews in Microbiology*, 49(1):711–745, 1995.

[4] T. R. Garrett, M. Bhakoo, and Z. Zhang. Bacterial adhesion and biofilms on surfaces. *Progress in Natural Science*, 18(9):1049–1056, 2008.

[5] Nicola R Stanley, Robert A Britton, Alan D Grossman, and Beth A Lazazzera. Identification of catabolite repression as a physiological regulator of biofilm formation by bacillus subtilis by use of dna microarrays. *Journal of Bacteriology*, 185(6):1951–1957, 2003.

[6] X. Zhang, P. L. Bishop, and M. J. Kupferle. Measurement of polysaccharides and proteins in biofilm extracellular polymers. *Water science and technology*, 37(4):345–348, 1998.

[7] C. D. Sifri. Quorum sensing: bacteria talk sense. *Clinical infectious diseases*, 47(8):1070–1076, 2008.

[8] W. G. Characklis and Marshal Kc. *Biofilms*. John Wiley and Sons, New York, 1990.

[9] R. J. Palmer and D. C. White. Developmental biology of biofilms: implications for treatment and control. *Trends in microbiology*, 5(11):435–440, 1997.

[10] L. Hall-Stoodley and P. Stoodley. Developmental regulation of microbial biofilms. *Current opinion in biotechnology*, 13(3):228–233, 2002.

[11] M. Hermansson. The dlvo theory in microbial adhesion. *Colloids and Surfaces B: Biointerfaces*, 14(1):105–119, 1999.

[12] Y. I. Chang and P. K. Chang. The role of hydration force on the stability of the suspension of saccharomyces cerevisiae application of the extended dlvo theory. *Colloids and Surfaces A: Physicochemical and Engineering Aspects*, 211(1):67–77, 2002.

[13] A. M. Gallardo-Moreno, M. L. Gonzalez-Martin, C. Perez-Giraldo, J. M. Bruque, and A. C. Gomez-Garc?a. The measurement temperature: an important factor relating physicochemical and adhesive properties of yeast cells to biomaterials. *Journal of colloid and interface science*, 271(2):351–358, 2004.

[14] Joana Azeredo, J Visser, and Rosário Oliveira. Exopolymers in bacterial adhesion: interpretation in terms of dlvo and xdlvo theories. *Colloids and Surfaces B: Biointerfaces*, 14(1-4):141–148, 1999.

[15] Michelle D Hoffman, Lauren I Zucker, Pamela JB Brown, David T Kysela, Yves V Brun, and Stephen C Jacobson. Timescales and frequencies of reversible and irreversible adhesion events of single bacterial cells. *Analytical chemistry*, 87(24):12032–12039, 2015.

[16] A. L. Olsson, H. C. Van der Mei, H. J. Busscher, and P. K. Sharma. Influence of cell surface appendages on the bacterium substratum interface measured real-time using qcm-d. *Langmuir*, 25(3):1627–1632, 2008.

[17] K. Sauer, A. K. Camper, G. D. Ehrlich, J. W. Costerton, and D. G. Davies. Pseudomonas aeruginosa displays multiple phenotypes during development as a biofilm. *Journal of bacteriology*, 184(4):1140–1154, 2002.

[18] C. Prigent-Combaret, O. Vidal, C. Dorel, and P. Lejeune. Abiotic surface sensing and biofilm-dependent regulation of gene expression in escherichia coli. *Journal of bacteriology*, 181(19):5993–6002, 1999.

[19] J Rogers, JV Lee, PJ Dennis, and CW Keevil. Continuous culture biofilm model for the survival and growth of legionella pneumophila and associated protozoa in potable water systems. *Health Related Water Microbiology*, pages 192–200, 1991.

[20] R. M. Donlan. Biofilms: microbial life on surfaces. *Emerging Infectious Diseases*, 8(9):881–90, 2002.

[21] Harald Horn and Susanne Lackner. Modeling of biofilm systems: a review. In *Productive Biofilms*, pages 53–76. Springer, 2014.

[22] Aoife Boyd and A áM Chakrabarty. Role of alginate lyase in cell detachment of pseudomonas aeruginosa. *Applied and environmental microbiology*, 60(7):2355–2359, 1994.

[23] P Gilbert, DJ Evans, and MRW Brown. Formation and dispersal of bacterial biofilms in vivo and in situ. *Journal of Applied Microbiology*, 74(S22), 1993.

[24] NJ Horan and CR Eccles. Purification and characterization of extracellular polysaccharide from activated sludges. *Water Research*, 20(11):1427–1432, 1986.

[25] I. W. Sutherland. Biofilm exopolysaccharides: a strong and sticky framework. *Microbiology*, 147(1):3–9, 2001.

[26] T. Tolker-Nielsen and S. Molin. Spatial organization of microbial biofilm communities. *Microbial ecology*, 40(2):75–84, 2000.

[27] MCM Van Loosdrecht, D Eikelboom, A Gjaltema, A Mulder, L Tijhuis, and JJ Heijnen. Biofilm structures. *Water Science and Technology*, 32(8):35–43, 1995.

[28] J. W. Wimpenny and R. Colasanti. A unifying hypothesis for the structure of microbial biofilms based on cellular automaton models. *FEMS Microbiology Ecology*, 22(1):1–16, 1997.

[29] D. Stoodley P. Y., DeBeer and Lewandowski Z. Liquid flow in biofilm systems. *Applied and environmental microbiology*, 60(8):2711–2716, 1994.

[30] D. Davies. Understanding biofilm resistance to antibacterial agents. *Nature reviews Drug discovery*, 2(2):114–122, 2003.

[31] Stoodley P. Roe F. Lewandowski Z. DeBeer, D. Effects of biofilm structures on oxygen distribution and mass transport. *Biotechnology and bioengineering*, 43(11):1131–1138, 1994.

[32] W. Kim, F. K. Tengra, Z. Young, J. Shong, N. Marchand, H. K. Chan, R. C. Pangule, M. Parra, J. S. Dordick, J. L. Plawsky, and C. H. Collins. Spaceflight promotes biofilm formation by pseudomonas aeruginosa. *PlosOne*, 8(4):e62437, 2013.

[33] James T Walker, Craig W Mackerness, Julie Rogers, and C William Keevil. Heterogeneous mosaic biofilm–a haven for waterborne pathogens. *Microbial biofilms*, pages 196–204, 1995.

[34] MR Fisk, R Popa, AR Smith, R Popa, and J Boone. Bacterial oxidation of iron in olivine: Implications for the subsurface biosphere, global chemical cycles, and life on mars. In *AGU Fall Meeting Abstracts*, 2011.

[35] Charles S Cockell, Matt Balme, John C Bridges, Alfonso Davila, and Susanne P Schwenzer. Uninhabited habitats on mars. *Icarus*, 217(1):184–193, 2012.

[36] David B Rowley. Rate of plate creation and destruction: 180 ma to present. *Geological Society of America Bulletin*, 114(8):927–933, 2002.

[37] Wolfgang Bach and Katrina J Edwards. Iron and sulfide oxidation within the basaltic ocean crust: implications for chemolithoautotrophic microbial biomass production. *Geochimica et Cosmochimica Acta*, 67(20):3871–3887, 2003.

[38] MJ Le Bas and Albert L Streckeisen. The iugs systematics of igneous rocks. *Journal of the Geological Society*, 148(5):825–833, 1991.

[39] Scott M McLennan. Sedimentary silica on mars. *Geology*, 31(4):315–318, 2003.

[40] Philip R Christensen, Joshua L Bandfield, James F Bell III, Noel Gorelick, Victoria E Hamilton, Anton Ivanov, Bruce M Jakosky, Hugh H Kieffer, Melissa D Lane, Michael C Malin, et al. Morphology and composition of the surface of mars: Mars odyssey themis results. *Science*, 300(5628):2056–2061, 2003.

[41] Philip R Christensen, Joshua L Bandfield, Vicky E Hamilton, Steve W Ruff, Hugh H Kieffer, Timothy N Titus, Michael C Malin, Richard V Morris, Melissa D Lane, RL Clark, et al. Mars global surveyor thermal emission spectrometer experiment: investigation description and surface science results. *Journal of Geophysical Research: Planets*, 106(E10):23823–23871, 2001.

[42] V Chevrier and PE Mathe. Mineralogy and evolution of the surface of mars: a review. *Planetary and Space Science*, 55(3):289–314, 2007.

[43] John P Grotzinger. Analysis of surface materials by the curiosity mars rover, 2013.

[44] Alex Ruzicka, Gregory A Snyder, and Lawrence A Taylor. Comparative geochemistry of basalts from the moon, earth, hed asteroid, and mars: Implications for the origin of the moon. *Geochimica et Cosmochimica Acta*, 65(6):979–997, 2001.

[45] Stéphane Uroz, Christophe Calvaruso, Marie-Pierre Turpault, and Pascale Frey-Klett. Mineral weathering by bacteria: ecology, actors and mechanisms. *Trends in microbiology*, 17(8):378–387, 2009.

[46] I Štyriaková, I Štyriak, and H Oberhänsli. Rock weathering by indigenous heterotrophic bacteria of bacillus spp. at different temperature: a laboratory experiment. *Mineralogy and Petrology*, 105(3-4):135–144, 2012.

[47] Aloke K Barman, Chandrika Varadachari, and Kunal Ghosh. Weathering of silicate minerals by organic acids. i. nature of cation solubilisation. *Geoderma*, 53(1-2):45–63, 1992.

[48] S. A.; Barker, W. W.; Welch and J.F. Banfield. Biogeochemical weathering of silicate minerals. In *Geomicrobiology: Interactions between microbes and minerals*, volume 35. Mineralogical Society of America, 1997.

[49] Owen W Duckworth, Martin M Akafia, Megan Y Andrews, and John R Bargar. Siderophore-promoted dissolution of chromium from hydroxide minerals. *Environmental Science: Processes & Impacts*, 16(6):1348–1359, 2014.

[50] Kevin G Knauss and Thomas J Wolery. The dissolution kinetics of quartz as a function of ph and time at 70 c. *Geochimica et Cosmochimica Acta*, 52(1):43–53, 1988.

[51] Patrick V Brady and John V Walther. Kinetics of quartz dissolution at low temperatures. *Chemical geology*, 82:253–264, 1990.

[52] Laura J Liermann, Birgitta E Kalinowski, Susan L Brantley, and James G Ferry. Role of bacterial siderophores in dissolution of hornblende. *Geochimica et Cosmochimica Acta*, 64(4):587–602, 2000.

[53] Agnieszka Włodarczyk, Robert Stasiuk, Aleksandra Skłodowska, and Renata Matlakowska. Extracellular compounds produced by bacterial consortium promoting elements mobilization from polymetallic kupferschiefer black shale (fore-sudetic monocline, poland). *Chemosphere*, 122:273–279, 2015.

[54] Alan T Stone. Reactions of extracellular organic ligands with dissolved metal ions and mineral surfaces. *Reviews in mineralogy and Geochemistry*, 35(1):309–344, 1997.

[55] JI Drever and LL Stillings. The role of organic acids in mineral weathering. *Colloids and Surfaces A: Physicochemical and Engineering Aspects*, 120(1-3):167–181, 1997.

[56] Geoffrey Michael Gadd. Metals, minerals and microbes: geomicrobiology and bioremediation. *Microbiology*, 156(3):609–643, 2010.

[57] Wuxing Liu, Xushi Xu, Xianghua Wu, Qiyin Yang, Yongming Luo, and Peter Christie. Decomposition of silicate minerals by bacillus mucilaginosus in liquid culture. *Environmental Geochemistry and Health*, 28(1-2):133–140, 2006.

[58] P Vandevivere, SA Welch, WJ Ullman, and DL Kirchman. Enhanced dissolution of silicate minerals by bacteria at near-neutral ph. *Microbial ecology*, 27(3):241–251, 1994.

[59] Engy Ahmed and Sara JM Holmström. Microbe–mineral interactions: The impact of surface attachment on mineral weathering and element selectivity by microorganisms. *Chemical Geology*, 403:13–23, 2015.

[60] MA Kacena, GA Merrell, B Manfredi, EE Smith, DM Klaus, and P Todd. Bacterial growth in space flight: logistic growth curve parameters for escherichia coli and bacillus subtilis. *Applied microbiology and biotechnology*, 51(2):229–234, 1999.

[61] N. M. E. J. Leys, L. Hendrickx, P. De Boever, S. Baatout, and M. Mergeay. Space flight effects on bacterial physiology. *Journal of biological regulators and homeostatic agents*, 18(2):193–199, 2004.

[62] Laurie Mauclaire and Marcel Egli. Effect of simulated microgravity on growth and production of exopolymeric substances of micrococcus luteus space and earth isolates. *FEMS Immunology & Medical Microbiology*, 59(3):350–356, 2010.

[63] E. C. Pollard. Theoretical studies on living systems in the absence of mechanical stress. *Journal of theoretical biology*, 8(1):113–123, 1965.

[64] Zheng J. Q. Cucinotta F. A. Wilson J. W. Horneck G Lindegren L. Melosh J. Rickman H. Valtonen M., Nurmi P. and C. Mileikowsky. Natural transfer of viable microbes in space from planets in extra-solar systems to a planet in our solar system and vice versa. *The Astrophysical Journal*, 690(1):210, 2009.

[65] CA Winter and JC Jones. The microgravity research experiments (micrex) data base. 2.

[66] Bastian E Rapp. *Microfluidics: Modeling, Mechanics and Mathematics*. William Andrew, 2016.

[67] G. Albrecht-Buehler. Possible mechanisms of indirect gravity sensing by cells. *Gravitational and Space Research*, 4(2):25–34, 1991.

[68] G. Horneck, D. M. Klaus, and R. L. Mancinelli. Space microbiology. *Microbiology and Molecular Biology Reviews*, 74(1):121–156, 2010.

[69] Markus Goldermann and Wolfgang Hanke. Ion channel are sensitive to gravity changes. *Microgravity science and technology*, 13(1):35, 2001.

[70] David Klaus, Steven Simske, Paul Todd, and Louis Stodieck. Investigation of space flight effects on escherichia coli and a proposed model of underlying physical mechanisms. *Microbiology*, 143(2):449–455, 1997.

[71] S. V. Lynch, K. Mukundakrishnan, M. R. Benoit, P. S. Ayyaswamy, and A. Matin. Escherichia coli biofilms formed under low-shear modeled microgravity in a ground-based system. *Applied and environmental microbiology*, 72(12):7701–7710, 2006.

[72] Nickerson C. A. Wilson J. W., Ott C. M. and others. Space flight alters bacterial gene expression and virulence and reveals a role for global regulator hfq. *Proceedings of the National Academy of Sciences*, 104(41):16299–16304, 2007.

[73] Aurélie Crabbé, Patrick De Boever, Rob Van Houdt, Hugo Moors, Max Mergeay, and Pierre Cornelis. Use of the rotating wall vessel technology to study the effect of shear stress on growth behaviour of pseudomonas aeruginosa pa01. *Environmental microbiology*, 10(8):2098–2110, 2008.

[74] Aurélie Crabbé, Michael J Schurr, Pieter Monsieurs, Lisa Morici, Jill Schurr, James W Wilson, C Mark Ott, George Tsaprailis, Duane L Pierson, Heidi Stefanyshyn-Piper, et al. Transcriptional and proteomic responses of pseudomonas aeruginosa pao1 to spaceflight conditions involve hfq regulation and reveal a role for oxygen. *Applied and Environmental Microbiology*, 77(4):1221–1230, 2011.

[75] A Be Nicholas, Aram Avila-Herrera, Jonathan E Allen, Nitin Singh, Aleksandra Checinska Sielaff, Crystal Jaing, and Kasthuri Venkateswaran. Whole metagenome profiles of particulates collected from the international space station. *Microbiome*, 5(1):81, 2017.

[76] ND Novikova. Review of the knowledge of microbial contamination of the russian manned spacecraft. *Microbial ecology*, 47(2):127–132, 2004.

[77] Natalia Novikova, Patrick De Boever, Svetlana Poddubko, Elena Deshevaya, Nikolai Polikarpov, Natalia Rakova, Ilse Coninx, and Max Mergeay. Survey of environmental biocontamination on board the international space station. *Research in microbiology*, 157(1):5–12, 2006.

[78] Alexander J; Vaishampayan Parag; White James R; Kumar Deepika; Stepanov Victor G; Fox George E; Nilsson Henrik R; Pierson Duane L; Perry Jay; Checinska, Aleksandra; Probst et al. Microbiomes of the dust particles collected from the international space station and spacecraft assembly facilities. *Microbiome*, 3, 2015.

[79] Alexander Probst, Rainer Facius, Reinhard Wirth, Marco Wolf, and Christine Moissl-Eichinger. Recovery of bacillus spore contaminants from rough surfaces: A challenge to cleanliness control of space missions. *Applied and environmental microbiology*, 2011.

[80] Cora S Thiel, Beatrice A Lauber, Jennifer Polzer, and Oliver Ullrich. Time course of cellular and molecular regulation in the immune system in altered gravity: Progressive damage or adaptation? *REACH-Reviews in Human Space Exploration*, 5:22–32, 2017.

[81] Luc van Heereveld, Jonathan Merrison, Per Nørnberg, and Kai Finster. Assessment of the forward contamination risk of mars by clean room isolates from space-craft assembly facilities through aeolian transport-a model study. *Origins of Life and Evolution of Biospheres*, 47(2):203–214, 2017.

[82] Michele Birmele, David Smith, Megan Morford, Luke Roberson, and Michael Roberts. Evaluation of an atpassay to quantify bacterial attachment to wetted surfaces in variable gravity conditions. In *42nd International Conference on Environmental Systems*, page 3508, 2012.

[83] Shigeru Deguchi and Koki Horikoshi. Expanding limits for life to a new dimension: Microbial growth at hypergravity. In *Polyextremophiles*, pages 467–481. Springer, 2013.

[84] Philippe Bouloc and Richard D'Ari. Escherichia coli metabolism in space. *Microbiology*, 137(12):2839–2843, 1991.

[85] Robert B Brown, D Klaus, and P Todd. Effects of space flight, clinorotation, and centrifugation on the substrate utilization efficiency of e. coli. *Microgravity science and technology*, 13(4):24–29, 2002.

[86] Yuko Kato, Yoshihiro Mogami, and Shoji A Baba. Responses to hypergravity in proliferation of paramecium tetraurelia. *Zoological science*, 20(11):1373–1380, 2003.

[87] Robert B. Brown. Clinostat and centrifuge growth kinetics of e.coli. Technical report, Department of Aerospace Engineering Sciences, University of Colorado, 1999.

[88] PO'B Montgomery. A relationship between growth and gravity in bacteria. *Aerosp. Med.*, 34:352–354, 1963.

[89] Naoto Yoshida, Takumi Minamimura, Terutoyo Yoshida, and Kihachiro Ogawa. Effect of hypergravitational stress on microbial cell viability. *Journal of bioscience and bioengineering*, 88(3):342–344, 1999.

[90] Shigeru Deguchi, Hirokazu Shimoshige, Mikiko Tsudome, Sada-atsu Mukai, Robert W Corkery, Susumu Ito, and Koki Horikoshi. Microbial growth at hyperaccelerations up to 403,627× g. *Proceedings of the National Academy of Sciences*, 108(19):7997–8002, 2011.

[91] G. S. N. Reddy and F. Garcia-Pichel. Sphingomonas mucosissima sp. nov. and sphingomonas desiccabilis sp. nov., from biological soil crusts in the colorado plateau, usa. *International journal of systematic and evolutionary microbiology*, 57(5):1028–1034, 2007.

[92] Gundlapally SN Reddy and Ferran Garcia-Pichel. Dyadobacter crusticola sp. nov., from biological soil crusts in the colorado plateau, usa, and an emended description of the genus dyadobacter chelius and triplett 2000. *International journal of systematic and evolutionary microbiology*, 55(3):1295–1299, 2005.

[93] Matthew A Bowker, SC Reed, J Belnap, and SL Phillips. Temporal variation in community composition, pigmentation, and fv/fm of desert cyanobacterial soil crusts. *Microbial Ecology*, 43(1):13–25, 2002.

[94] Robert D. Leighty. Colorado plateau physiographic province. *Contract Report. Defense Advanced Research Projects Agency (DOD)*, 2001.

[95] Eiko Yabuuchi, Ikuya Yano, Hiroshi Oyaizu, Yasuhiro Hashimoto, Takayuki Ezaki, and Hiroyuki Yamamoto. Proposals of sphingomonas paucimobilis gen. nov. and comb. nov., sphingomonas parapaucimobilis sp. nov., sphingomonas yanoikuyae sp. nov., sphingomonas adhaesiva sp. nov., sphingomonas capsulata comb, nov., and two genospecies of the genus sphingomonas. *Microbiology and immunology*, 34(2):99–119, 1990.

[96] Mariko Takeuchi, Koei Hamana, and Akira Hiraishi. Proposal of the genus sphingomonas sensu stricto and three new genera, sphingobium, novosphingobium and sphingopyxis, on the basis of phylogenetic and chemotaxonomic analyses. *International Journal of Systematic and Evolutionary Microbiology*, 51(4):1405–1417, 2001.

[97] M. F. Romine D. L. Balkwill, J. K. Fredrickson. Sphingomonas and related genera. In *The Prokaryotes: An Evolving Electronic Resource for the Microbiological Community*. Springer-Verlag, 2006.

[98] Hui Li, Xue Jiao, Yajie Sun, Shiwei Sun, Zhimei Feng, Wanlong Zhou, and Hu Zhu. The preparation and characterization of a novel sphingan wl from marine sphingomonas sp. wg. *Scientific reports*, 6:37899, 2016.

[99] Richard van Kranenburg, Ingeborg C Boels, Michiel Kleerebezem, and Willem M de Vos. Genetics and engineering of microbial exopolysaccharides for food: approaches for the production of existing and novel polysaccharides. *Current Opinion in Biotechnology*, 10(5):498–504, 1999.

[100] T Janikowski, D Velicogna, M Punt, and A Daugulis. Use of a two-phase partitioning bioreactor for degrading polycyclic aromatic hydrocarbons by a sphingomonas sp. *Applied microbiology and biotechnology*, 59(2-3):368–376, 2002.

[101] Keishi Senoo, Masaya Nishiyama, and Satoshi Matsumoto. Bioremediation of γ-hch-polluted field soil by inoculation with an aerobic γ-hch-decomposing bacterium (sphingomonas paucimobilis ss86). *Soil science and plant nutrition*, 42(1):11–19, 1996.

[102] Zhi Li, Hans-Jürgen Feiten, Dongliang Chang, Wouter A Duetz, Jan B van Beilen, and Bernard Witholt. Preparation of (r)-and (s)-n-protected 3-hydroxypyrrolidines by hydroxylation with sphingomonas sp. hxn-200, a highly active, regio-and stereoselective, and easy to handle biocatalyst. *The Journal of organic chemistry*, 66(25):8424–8430, 2001.

[103] Dongliang Chang, Hans-Jürgen Feiten, Karl-H Engesser, Jan B van Beilen, Bernard Witholt, and Zhi Li. Practical syntheses of n-substituted 3-hydroxyazetidines and 4-hydroxypiperidines by hydroxylation with sphingomonas sp. hxn-200. *Organic letters*, 4(11):1859–1862, 2002.

[104] Narendra B Vartak, Chi Chung Lin, Joseph M Cleary, Matthew J Fagan, and Milton H Saier Jr. Glucose metabolism in 'sphingomonas elodea': Pathway engineering via construction of a glucose-6-phosphate dehydrogenase insertion mutant. *Microbiology*, 141(9):2339–2350, 1995.

[105] Charles S Cockell. Synthetic geomicrobiology: engineering microbe–mineral interactions for space exploration and settlement. *International Journal of Astrobiology*, 10(4):315–324, 2011.

[106] Yongding Liu, Charles S Cockell, Gaohong Wang, Chunxiang Hu, Lanzhou Chen, and Roberto De Philippis. Control of lunar and martian dust—experimental insights from artificial and natural cyanobacterial and algal crusts in the desert of inner mongolia, china. *Astrobiology*, 8(1):75–86, 2008.

[107] C. S. Cockell. Geomicrobiology beyond earth: microbe-mineral interactions in space exploration and settlement. *Trends in microbiology*, 18(7):308–314, 2010.

[108] L. Hendrickx and M. Mergeay. From the deep sea to the stars: human life support through minimal communities. *Current Opinion in Microbiology*, 13(3):228–233, 2002.

[109] Bonnie P Dalton and Frank F Roberto. Lunar regolith biomining: workshop report. 2008.

[110] K. M. Lehto, H. J. Lehto, and E. A. Kanervo. Suitability of different photosynthetic organisms for an extraterrestrial biological life support system. *Research in microbiology*, 157(1):69–76, 2006.

[111] Karen Olsson-Francis and Charles S Cockell. Use of cyanobacteria for in-situ resource use in space applications. *Planetary and Space Science*, 58(10):1279–1285, 2010.

[112] Jeremy Walker and Céline Granjou. Melissa the minimal biosphere: Human life, waste and refuge in deep space. *futures*, 92:59–69, 2017.

[113] Tairo Oshima, Toshiyuki Moriya, Shinjiro Kanazawa, and Masamichi Yamashita. Proposal of hyperthermophilic aerobic composting bacteria and their enzymes in space agriculture. *Biological Sciences in Space*, 21(4):121–123, 2007.

[114] CE Krauss, M Horanyi, and S Robertson. Experimental evidence for electrostatic discharging of dust near the surface of mars. *New Journal of Physics*, 5(1):70, 2003.

[115] JE Colwell, S Batiste, M Horányi, S Robertson, and Steve Sture. Lunar surface: Dust dynamics and regolith mechanics. *Reviews of Geophysics*, 45(2), 2007.

[116] Judith N Latch, Raymond F Hamilton Jr, Andrij Holian, John T James, and Chiu-wing Lam. Toxicity of lunar and martian dust simulants to alveolar macrophages isolated from human volunteers. *Inhalation toxicology*, 20(2):157–165, 2008.

[117] Cyprien Verseux, Mickael Baqué, Kirsi Lehto, Jean-Pierre P de Vera, Lynn J Rothschild, and Daniela Billi. Sustainable life support on mars–the potential roles of cyanobacteria. *International Journal of Astrobiology*, 15(1):65–92, 2016.

[118] Lynn J Rothschild. Synthetic biology meets bioprinting: enabling technologies for humans on mars (and earth). *Biochemical Society Transactions*, 44(4):1158–1164, 2016.

[119] Finster K. Cockell C.S. Loudon C.M., Nicholson N. Biorock: new experiments and hardware to investigate microbe–mineral interactions in space. *International Journal of Astrobiology*, pages 1–11, 2017.

[120] Ruth E Wolf. What is icp-ms?

[121] Holler F. J. Crouch S. R. Skoog, D. A. Principles of instumental analysis. In *ELAN DRC-e Hardware guide (n.d.). PerkinElmer SCIEX*. Thomson Higher Education, 2007.

[122] Katsutoshi Hori and Shinya Matsumoto. Bacterial adhesion: from mechanism to control. *Biochemical Engineering Journal*, 48(3):424–434, 2010.

[123] CJ Van Oss, RJ Good, and MK Chaudhury. The role of van der waals forces and hydrogen bonds in "hydrophobic interactions" between biopolymers and low energy surfaces. *Journal of colloid and Interface Science*, 111(2):378–390, 1986.

[124] Yuehuei H An and Richard J Friedman. Concise review of mechanisms of bacterial adhesion to biomaterial surfaces. *Journal of biomedical materials research*, 43(3):338–348, 1998.

[125] Thomas Proft and EN Baker. Pili in gram-negative and gram-positive bacteria—structure, assembly and their role in disease. *Cellular and molecular life sciences*, 66(4):613, 2009.

[126] Cécile Berne, Adrien Ducret, Gail G Hardy, and Yves V Brun. Adhesins involved in attachment to abiotic surfaces by gram-negative bacteria. *Microbiology spectrum*, 3(4), 2015.

[127] Mladen Tomich, Paul J Planet, and David H Figurski. The tad locus: postcards from the widespread colonization island. *Nature Reviews Microbiology*, 5(5):363, 2007.

[128] Harry Y McSween, G Jeffrey Taylor, and Michael B Wyatt. Elemental composition of the martian crust. *Science*, 324(5928):736–739, 2009.

[129] Eric H Oelkers. General kinetic description of multioxide silicate mineral and glass dissolution. *Geochimica et Cosmochimica Acta*, 65(21):3703–3719, 2001.

[130] Domenik Wolff-Boenisch, Sigurdur R Gislason, and Eric H Oelkers. The effect of crystallinity on dissolution rates and co2 consumption capacity of silicates. *Geochimica et Cosmochimica Acta*, 70(4):858–870, 2006.

[131] Martha A Scholl, Aaron L Mills, Janet S Herman, and George M Hornberger. The influence of mineralogy and solution chemistry on the attachment of bacteria to representative aquifer materials. *Journal of Contaminant Hydrology*, 6(4):321–336, 1990.

[132] Karla D Krewulak and Hans J Vogel. Structural biology of bacterial iron uptake. *Biochimica et Biophysica Acta (BBA)-Biomembranes*, 1778(9):1781–1804, 2008.

[133] Charles S. Cockell. *Astrobiology: Understanding Life in the Universe*. Wiley-Blackwell, 2015.

[134] Kenneth Todar. Nutrition and growth of bacteria. 2013.

[135] Rogelio Garcidueñas Piña and Carlos Cervantes. Microbial interactions with aluminium. *Biometals*, 9(3):311–316, 1996.

[136] Wolfgang Epstein. The roles and regulation of potassium in bacteria. *Progress in nucleic acid research and molecular biology*, 75:293–320, 2003.

[137] RJ Smith. Calcium and bacteria. In *Advances in microbial physiology*, volume 37, pages 83–133. Elsevier, 1995.

[138] Masahiro Ito and Blanca Barquera. Sodium. its role in bacterial metabolism. *Binding, Transport and Storage of Metal Ions in Biological Cells*, 2:6, 2014.

[139] Safie Yaghoubi, Chad W Schwietert, and John P McCue. Biological roles of titanium. *Biological trace element research*, 78(1-3):205–217, 2000.

[140] Clays and minerals: Surface area and porosity, author=James Hutton Institute, The, url=http://www.claysandminerals.com/methods/surfacearea, journal=Claysandminerals.com, year=2011, publisher= the james hutton institute.

[141] J.F. Banfield and R.J. Hammers. Processes at minerals and surfaces with relevance to microorganisms and prebiotic synthesis. In *Geomicrobiology: Interactions between microbes and minerals*, volume 35. Mineralogical Society of America, 1997.

[142] Mike Lawrence and Yunhong Jiang. Porosity, pore size distribution, micro-structure. In *Bio-aggregates Based Building Materials*, pages 39–71. Springer, 2017.

[143] Derick G Brown and Peter R Jaffé. Effects of nonionic surfactants on the cell surface hydrophobicity and apparent hamaker constant of a sphingomonas sp. *Environmental science and technology*, 40(1):195–201, 2006.

[144] M. Hamadi., Ellouali. The relation between escherichia coli surface functional groups composition and their physicochemical properties. *Brazilian Journal of Microbiology*, 39(1):10–15, 2008.

[145] Thaveesri J. Verstraete W. Daffonchio, D. Contact angle measurement and cell hydrophobicity of granular sludge from upflow anaerobic sludge bed reactors. *Applied and environmental microbiology*, 61(10):3676–3680, 1995.

[146] Quere D de Gennes PG, Brochard-Wyart F. *Capillarity and Wetting Phenomena: drops, bubbles, pearls, waves*. Springer, New York, 2004.

[147] Bos-Rolf Poortinga, Albert T., Willem Norde, and Henk J Busscher. Electric double layer interactions in bacterial adhesion to surfaces. *Surface science reports*, 47(1):1–32, 2002.

[148] Paul J Janssen, Rob Van Houdt, Hugo Moors, Pieter Monsieurs, Nicolas Morin, Arlette Michaux, Mohammed A Benotmane, Natalie Leys, Tatiana Vallaeys, Alla Lapidus, et al. The complete genome sequence of cupriavidus metallidurans strain ch34, a master survivalist in harsh and anthropogenic environments. *PLoS One*, 5(5):e10433, 2010.

[149] Barbara Setlow and Peter Setlow. Role of dna repair in bacillus subtilis spore resistance. *Journal of Bacteriology*, 178(12):3486–3495, 1996.

[150] Elke Rabbow, Petra Rettberg, Simon Barczyk, Maria Bohmeier, Andre Parpart, Corinna Panitz, Gerda Horneck, Jürgen Burfeindt, Ferdinand Molter, Esther Jaramillo, et al. The astrobiological mission expose-r on board of the international space station. *International Journal of Astrobiology*, 14(1):3–16, 2015.

[151] Bo Byloos, Ilse Coninx, Olivier Van Hoey, Charles Cockell, Natasha Nicholson, Vyacheslav Ilyin, Rob Van Houdt, Nico Boon, and Natalie Leys. The impact of space flight on survival and interaction of cupriavidus metallidurans ch34 with basalt, a volcanic moon analog rock. *Frontiers in microbiology*, 8:671, 2017.

[152] Natalie Leys, Sarah Baatout, Caroline Rosier, Annik Dams, Catherine s'Heeren, Ruddy Wattiez, and Max Mergeay. The response of cupriavidus metallidurans ch34 to spaceflight in the international space station. *Antonie Van Leeuwenhoek*, 96(2):227, 2009.

[153] Debra W Jackson, Jerry W Simecka, and Tony Romeo. Catabolite repression of escherichia coli biofilm formation. *Journal of bacteriology*, 184(12):3406–3410, 2002.

[154] Nancy A Fujishige, Neel N Kapadia, Peter L De Hoff, and Ann M Hirsch. Investigations of rhizobium biofilm formation. *FEMS microbiology ecology*, 56(2):195–206, 2006.

[155] Naruya Saitou and Masatoshi Nei. The neighbor-joining method: a new method for reconstructing phylogenetic trees. *Molecular biology and evolution*, 4(4):406–425, 1987.

[156] Jan Gerwig, Taryn B Kiley, Katrin Gunka, Nicola Stanley-Wall, and Jörg Stülke. The protein tyrosine kinases epsb and ptka differentially affect biofilm formation in bacillus subtilis. *Microbiology*, 160(4):682–691, 2014.

[157] Hans-Jürgen Busse, Elke Hauser, and Peter Kämpfer. Description of two novel species, sphingomonas abaci sp. nov. and sphingomonas panni sp. nov. *International Journal of Systematic and Evolutionary Microbiology*, 55(6):2565–2569, 2005.

[158] Michele Balsamo, Ivana Barravecchia, Sara Mariotti, Alessandra Merenda, Chiara De Cesari, Marco Vukich, and Debora Angeloni. Molecular and cellular characterization of space flight effects on microvascular endothelial cell function–preparatorywork for the sfef project. *Microgravity science and technology*, 26(6):351–363, 2014.

[159] C. Guy, V. Daux, and J. Schott. Behaviour of rare earth elements during seawater/basalt interactions in the mururoa massif. *Chemical Geology*, 158(1):21–35, 1999.

[160] Karen OLSSON-FRANCIS, Rob Van Houdt, Max Mergeay, Natalie Leys, and Charles S Cockell. Microarray analysis of a microbe–mineral interaction. *Geobiology*, 8(5):446–456, 2010.

[161] Casey Catherine Bryce. Microbial stress in rock habitats. 2015.

[162] Pieter Monsieurs, Hugo Moors, Rob Van Houdt, Paul J Janssen, Ann Janssen, Ilse Coninx, Max Mergeay, and Natalie Leys. Heavy metal resistance in cupriavidus metallidurans ch34 is governed by an intricate transcriptional network. *Biometals*, 24(6):1133–1151, 2011.

[163] Robert JC McLean, John M Cassanto, Mary B Barnes, and Joseph H Koo. Bacterial biofilm formation under microgravity conditions. *FEMS Microbiology Letters*, 195(2):115–119, 2001.

[164] Charles S Cockell, Luke Hecht, Hanna Landenmark, Samuel J Payler, and Matthew Snape. Rapid colonization of artificial endolithic uninhabited habitats. *International Journal of Astrobiology*, pages 1–16, 2017.

9 Appendix A

R2A:

Table 15: Ingredients of R2A Nutrient Solution (100%) made up in 1L of Millipore Water

Component	Quantity in grams
Yeast extract	0.5
Proteose peptone	0.5
Casamino acids	0.5
Glucose	0.5
Soluble startch	0.5
Sodium pyruvate (110g/mol)	0.3
K_2HPO_4(174.2g/mol)	0.3
$MgSO_4$(120.366g/mol)	0.05

M9:

This media requires two stages of preparation:

Table 16: Ingredients of M9 Minimal Media (Step One) made up in 800ml of Millipore Water

Component	Quantity in grams
Na_2HPO_4 - $7H_2O$	64
KH_2PO_4	15g
NaCl	2.5
NH_4Cl	5

Stir until dissolved, and adjust to 1L with millipore water, and autoclave. Once autoclaved, add the next ingredients:

Table 17: Ingredients of M9 Minimal Media (Step Two) made up in 800ml of Millipore Water

Component	Quantity into Millipure H_2O	Quantity to Add to M9
Glucose	20g into 100ml	10ml
$MgSO_4$	0.24g into 2ml	2ml
$CaCl_2$ dihydrate	0.1g into 1ml	0.1ml

To adjust from 20% glucose to 50% and 5% glucose, replace glucose step in the table above with:

Table 18: Alternate Glucose Levels for M9

Percentage	Quantity into Millipure H_2O	Quantity to Add to M9
50%	50g into 100ml	10ml
5%	5g into 100ml	10ml

Table 19: Phosphate Buffered Solution (PBS)

Component	Quantity (in g)
NaCl	8
KCl	0.2
Na_2HPO_4	1.44
KH_2PO_4	0.24
$CaCl_2.2H_2O$	0.133
$MgCl_26H_20$	0.1

Mineral	% of Basalt
Albite	2.4
Anorthite	0.0
Microcline maximum	2.4
Orthoclase	0.7
Muscovite 1M	2.3
Oligoclase An16	3.2
Oligoclase An25	4.0
Andesine An50 C-1structure	14.8
Andesine An50 C1structure	4.1
Labradorite An65	29.9
Bytownite An85	4.0
Augite Px	13.8
Fayalite magnesian	6.6
Forsterite iron	3.0
Diopside iron	2.7
Microcline intermediate2	3.2
Microcline intermediate1	2.7

Figure 79: The full XRD analysis

10 Appendix B

Table 20: Zeta Potentials and Electrophoretic Mobility of *Sphingomonas desiccabilis*

Measurement	Voltage	Zeta Potential (mV)	Mobility (μm cm/Vs)
1	20	-34.3	-2.585
2	20	-28.9	-2.177
3	20	-31.4	-2.367
4	20	-36.9	-2.783
5	20	-30.1	-2.271
6	20	-33.8	-2.547
7	50	-30.2	-2.476
8	50	-30.2	-2.279
9	50	-33.8	-2.361
Average	N/A	-32.5	-2.427

11 Appendix C

Genes involved in Temperature and/or Osmotic Shock						
Label	Gene	Synonyms	Product	Roles	BioProcess	Product Type
SDES_v1_10393	ibpA	hslT, htpN	heat shock chaperone	5.5.2 : Temperature extremes ; 5.5.6 : Other stresses (mechanical, nutritional, oxidative)	Adaptations to atypical conditions ;	factor
SDES_v1_10849	clpP	lopP	ATP-dependent Clp protease proteolytic subunit (Endopeptidase Clp) (Caseinolytic protease) (Protease Ti) (Heat shock protein F21.5)	1.2.3 : proteins/peptides/glycopeptides ; 3.1.3.4 : proteases, cleavage of compounds ; 5.5.2 : temperature extremes	–	enzyme
SDES_v1_20077	groEL	mopA	chaperone Hsp60, peptide-dependent ATPase, heat shock protein	2.3.4 : chaperoning, folding ; 5.1 : cell division ;	–	factor
SDES_v1_20119	–	–	Heat shock protein DnaJ domain protein (fragment)	–	–	–
SDES_v1_20327	–	–	Cold-shock DNA-binding domain-containing protein	–	–	–
SDES_v1_30124	–	–	Cold-shock DNA-binding domain protein	–	–	–
SDES_v1_20612	otsA	pexA	trehalose-6-phosphate synthase	1.7.36 : Trehalose biosynthesis ; 5.5.1 : Osmotic pressure ;	Central intermediary metabolism ; Adaptations to atypical conditions ;	enzyme
SDES_v1_30146	dnaK	grpF, seg, lop, groPAB, groPC, groPF, grpC	chaperone Hsp70, co-chaperone with DnaJ	2.3.4 : Chaperoning, folding ; 5.1 : Cell division ; 5.5.1 : Osmotic pressure ; 7.1 : Cytoplasm ;	Protein folding and stabilization ; Cell division ;	factor
SDES_v1_30287	osmC	–	osmotically inducible, stress-inducible membrane protein	5.5.1 : Osmotic pressure ;	Adaptations to atypical conditions ;	membrane component
SDES_v1_40034	tufB	–	protein chain elongation factor EF-Tu, possible GTP-binding factor (duplicate of tufA)	2.3.2 : translation ; 5.5.1 : osmotic pressure ;	–	factor
SDES_v1_30146	dnaK	grpF, seg, lop, groPAB, groPC, groPF, grpC	chaperone Hsp70, co-chaperone with DnaJ	2.3.4 : Chaperoning, folding ; 5.1 : Cell division ; 5.5.1 : Osmotic pressure ; 7.1 : Cytoplasm ;	Protein folding and stabilization ; Cell division ;	factor
SDES_v1_30287	osmC	–	osmotically inducible, stress-inducible membrane protein	5.5.1 : Osmotic pressure ;	Adaptations to atypical conditions ;	membrane component
SDES_v1_40034	tufB	–	protein chain elongation factor EF-Tu, possible GTP-binding factor (duplicate of tufA)	2.3.2 : translation ; 5.5.1 : osmotic pressure ;	–	factor
SDES_v1_20262	–	–	Malto-oligosyltrehalose synthase	–	–	–
SDES_v1_20264	treZ	–	Malto-oligosyltrehalose trehalohydrolase	–	–	–
SDES_v1_20267	–	–	Trehalose synthase	–	–	–
SDES_v1_20610	otsB	–	Trehalose-phosphate phosphatase	–	–	–
SDES_v1_20612	otsA	pexA	trehalose-6-phosphate synthase	1.7.36 : Trehalose biosynthesis ; 5.5.1 : Osmotic pressure ;	Central intermediary metabolism ; Adaptations to atypical conditions ;	enzyme
SDES_v1_60061	–	–	Trehalose utilization	–	–	–

Figure 80: *Sphingomonas desiccabilis* genes that play a role in stress tolerance, found through the MaGe platform.

Genes Involved in DNA Repair						
Label	Gene	Synonyms	Product	Roles	BioProcess	Product Type
SDES_v1_10219	recA	lexB, srf, umuB, zab, recH, rnmB, tif, umuR	DNA strand exchange and recombination protein with protease and nuclease activity	2.1.3 : DNA recombination ; 2.1.4 : DNA repair ; 2.3.6 : Turnover, degradation ; 3.1.3.4 : Proteases, cleavage of compounds ; 5.8 : SOS response ; 7.1 : Cytoplasm.	DNA replication, recombination, and repair ; Degradation of proteins, peptides, and glycopeptides ; Protein interactions ; Adaptations to atypical conditions.	enzyme
SDES_v1_10622	uvrB	dar-1, dar-6	excinulease of nucleotide excision repair, DNA damage recognition component	1.2.2 : DNA ; 2.1.4 : DNA repair ; 2.1.5 : DNA degradation ; 5.6.1 : Radiation ; 5.8 : SOS response ; 7.1 : Cytoplasm.	DNA replication, recombination, and repair ; Degradation of DNA ; Detoxification ; Adaptations to atypical conditions.	cell process
SDES_v1_10982	radA	_	DNA repair protein RadA homolog	_	_	_
SDES_v1_11013	mutM	fpg	formamidopyrimidine/5-formyluracil/ 5-hydroxymethyluracil DNA glycosylase	2.1.4 : DNA repair ; 7.1 : Cytoplasm.	DNA replication, recombination, and repair.	enzyme
SDES_v1_11206	ada	_	fused DNA-binding transcriptional dual regulator ; O6-methylguanine-DNA methyltransferase	2.1.4 : DNA repair ; 2.2.2 : Transcription related ; 3.1.2.2 : Activator ; 3.1.2.3 : Repressor ; 3.3.1 : Operon (regulation of one operon) ; 7.1 : Cytoplasm.	DNA replication, recombination, and repair ; Transcription ; DNA interactions.	regulator
SDES_v1_11288	RadC	_	putative DNA repair protein RadC	_	_	_
SDES_v1_20452	recO	_	DNA repair protein RecO	_	_	_
SDES_v1_20590	recN	_	DNA repair protein RecN	_	_	_
SDES_v1_20718	xseB	yajE	exonuclease VII small subunit	1.2.2 : DNA ; 2.1.4 : DNA repair ; 2.1.5 : DNA degradation ; 7.1 : Cytoplasm.	DNA replication, recombination, and repair ; Degradation of DNA.	enzyme
SDES_v1_30138	uvrA	dar, dinE	ATPase and DNA damage recognition protein of nucleotide excision repair exci nuclease UvrABC	2.1.4 : DNA repair ; 5.6.1 : Radiation ; 5.8 : SOS response ; 7.1 : Cytoplasm.	DNA replication, recombination, and repair ; Detoxification ; Adaptations to atypical conditions.	enzyme
SDES_v1_30221	yggV	rdgB	dITP/XTP pyrophosphatase	2.1.4 : DNA repair ; 7.1 : Cytoplasm.	DNA replication, recombination, and repair.	enzyme
SDES_v1_50071	ruvB	_	holliday junction helicase, subunit B	2.1.3 : DNA recombination ; 2.1.4 : DNA repair ; 5.8 : SOS response.	_	enzyme
SDES_v1_80020	ligD	_	Multifunctional non-homologous end joining protein LigD [includes: 3'-phosphoesterase ; DNA ligase D ; DNA repair polymerase]	_	_	_
SDES_v1_80021	_	_	putative DNA repair protein Swit_3981	_	_	_

Figure 81: *Sphingomonas desiccabilis* genes that play a role in DNA repair, found through the MaGe platform.

Label	Gene	Synonyms	Product	Genes Involved in the Regulation of Efflux Pumps		
				Roles	BioProcess	Product Type
SDES_v1_10004	–	–	Multidrug resistance efflux pump	–	–	–
SDES_v1_10295	–	–	Efflux transporter, outer membrane factor (OMF) lipo, NodT family protein	–	–	–
SDES_v1_10301	–	–	Potassium efflux system KefA protein / Small-conductance mechanosensitive channel	–	–	–
SDES_v1_10417	–	–	putative efflux pump outer membrane protein	–	–	–
SDES_v1_10418	bepG	–	Efflux pump membrane transporter BepG	–	–	–
SDES_v1_10419	–	–	putative efflux pump periplasmic linker protein	–	–	–
SDES_v1_10424	–	–	Arabinose efflux permease family protein	–	–	–
SDES_v1_10472	arsB	arsF	arsenite/antimonite transporter	4.3.A.4 : The Arsenite-Antimonite (Ars) Efflux Family ; 4.S.19 : arsenite ; 5.6.2 : Detoxification (xenobiotic metabolism) ; 6.1 : Membrane ; 7.3 : Inner membrane.	Anions ; Detoxification.	transporter
SDES_v1_10538	acrB	acrE	multidrug efflux system protein	4.2.A.6 : The Resistance-Nodulation-Cell Division (RND) Superfamily ; 4.S.126 : multidrug ; 5.6.4 : Drug resistance/sensitivity ; 6.1 : Membrane ; 7.3 : Inner membrane.	Transport and binding proteins ; Toxin production and resistance.	transporter
SDES_v1_10539	acrA	Mb, lir, mbl, mtcA, sipB, nbsA	multidrug efflux system	4.2.A.6 : The Resistance-Nodulation-Cell Division (RND) Superfamily ; 4.S.126 : multidrug ; 5.6.4 : Drug resistance/sensitivity ; 6.1 : Membrane ; 7.3 : Inner membrane.	Transport and binding proteins ; Toxin production and resistance.	transporter
SDES_v1_10958	sugE	–	multidrug efflux system protein	4.2.A.7 : The Drug/Metabolite Transporter (DMT) Superfamily ; 5.6.2 : Detoxification (xenobiotic metabolism) ; 6.1 : Membrane ; 7.3 : Inner membrane.	Transport and binding proteins ; Detoxification.	transporter
SDES_v1_20173	–	–	cation efflux system protein (fragment)	–	–	–
SDES_v1_20284	–	–	Efflux transporter, RND family, MFP subunit	–	–	–
SDES_v1_20285	–	–	Efflux transporter, outer membrane factor (OMF) lipo, NodT family protein	–	–	–
SDES_v1_20567	–	–	Arabinose efflux permease family protein	–	–	–
SDES_v1_20719	–	–	RND efflux system outer membrane lipoprotein	–	–	–
SDES_v1_30068	–	–	Arabinose efflux permease family protein	–	–	–
SDES_v1_50041	acrD	yffA	aminoglycoside/multidrug efflux system	4.2.A.6 : The Resistance-Nodulation-Cell Division (RND) Superfamily ; 4.S.126 : multidrug ; 5.6.4 : Drug resistance/sensitivity ; 6.1 : Membrane ; 7.3 : Inner membrane.	Transport and binding proteins ; Toxin production and resistance.	transporter
SDES_v1_50042	acrA	Mb, lir, mbl, mtcA, sipB, nbsA	multidrug efflux system	4.2.A.6 : The Resistance-Nodulation-Cell Division (RND) Superfamily ; 4.S.126 : multidrug ; 5.6.4 : Drug resistance/sensitivity ; 6.1 : Membrane ; 7.3 : Inner membrane.	Transport and binding proteins ; Toxin production and resistance.	transporter
SDES_v1_50094	–	–	RND efflux system, outer membrane lipoprotein, NodT family	–	–	–
SDES_v1_50185	–	–	Efflux transporter, RND family, MFP subunit	–	–	–
SDES_v1_50224	–	–	MATE efflux family protein	–	–	–
SDES_v1_80023	fieF	–	Cation-efflux pump FieF	–	–	–

Figure 82: *Sphingomonas desiccabilis* genes that play a role in efflux pumps, found through the MaGe platform.

Pili Associated Genes		
Label	Gene	Product
SDES_v1_10970	_	Pilusassembly protein (fragment)
SDES_v1_10971	_	Flp pilusassembly protein, pilin Flp
SDES_v1_20489	tadC	Flp pilusassembly protein TadC
SDES_v1_20490	_	Flp pilusassembly protein TadB
SDES_v1_20491	_	Flp pilusassembly protein ATPase CpaE
SDES_v1_20492	_	Pilusbiogenesis CpaD family protein
SDES_v1_20494	_	Flp pilusassembly protein CpaB
SDES_v1_40308	_	Pilusassembly protein PilZ (fragment)

Figure 83: Pili Associated Genes